TECHNISCHE UNIVERSITÄT WIEN

Diploma thesis

Sintering of Mo-alloyed PM steels via the master alloy route

Carried out at the

Faculty of Technical Chemistry Institute of Chemical Technologies and Analytics TU Wien

Getreidemarkt 9/164-CT

1060 Wien

by

Aurel Dvorak, Bsc

[redacted]

under the supervision of

Associate Prof. Raquel De Oro Calderon, PhD, MSc

Eidesstattliche Erklärung

Ich erkläre an Eides statt, dass die vorliegende Arbeit nach den anerkannten Grundsätzen für wissenschaftliche Abhandlungen von mir selbstständig erstellt wurde. Alle verwendeten Hilfsmittel, insbesondere die zugrunde gelegte Literatur, sind in dieser Arbeit genannt und aufgelistet. Die aus den Quellen wörtlich entnommenen Stellen, sind als solche kenntlich gemacht.

Das Thema dieser Arbeit wurde von mir bisher weder im In- noch Ausland einem_r Beurteiler_in zur Begutachtung in irgendeiner Form als Prüfungsarbeit vorgelegt. Diese Arbeit stimmt mit der von den Begutachter_innen beurteilten Arbeit überein.

Ich nehme zur Kenntnis, dass die vorgelegte Arbeit mit geeigneten und dem derzeitigen Stand der Technik entsprechenden Mitteln (Plagiat-Erkennungssoftware) elektronisch-technisch überprüft wird. Dies stellt einerseits sicher, dass bei der Erstellung der vorgelegten Arbeit die hohen Qualitätsvorgaben im Rahmen der geltenden Regeln zur Sicherung guter wissenschaftlicher Praxis „Code of Conduct“ an der TU Wien eingehalten wurden. Zum anderen werden durch einen Abgleich mit anderen studentischen Abschlussarbeiten Verletzungen meines persönlichen Urheberrechts vermieden.

Ort und Datum	*Unterschrift*

Abstract

Sintered steels are used for complex, high precision components for high lot sizes. In contrast to classical steel production Ni, Cu and Mo are the most common alloying elements in sintered steels. They are used because of their compressibility and because of their non-sensitivity to O. But Cu and Ni are connected to environmental problems and price fluctuations. Therefore, there is an interest to use more environmentally friendly alternatives like Mn and Si. These O sensitive alloying elements need to be especially introduced into sintered steels. One way to introduce O sensitive alloying elements into sintered steels is the use of low melting master alloys (MA´s). In this alloying route, a ferrous base powder or a pre-alloyed powder is mixed with small amounts of MA´s, which contain the alloying elements. MA´s facilitate liquid phase sintering which allows comparably lower sintering temperatures and a good homogenization of alloying elements. In this work the effect of different base powders on sintered steels with low melting Mn-Si-MA´s was investigated. Furthermore, the possibility to introduce Mo admixed as a carbide (Mo_2C) into sintered steels combined with the same MA´s was investigated.

Two different Mn-Si-MA´s were investigated. First prepressed samples where those MA´s were combined with Mo- and Cr-pre-alloyed base powders (0,85 wt% Cr and Mo) were consolidated and their mechanical properties (density, hardness and impact energy) were tested. Then samples with a purely ferrous base powder and Mo admixed (0,5 wt% Mo) as Mo_2C with the same MA´s were mixed, pressed and consolidated and tested. In a last experiment, samples with a Mo-pre-alloyed base powder (0,45 wt% Mo) and the same MA´s were mixed, pressed, consolidated and tested. The microstructure of all samples was also characterized after etching with optical microscopy.

In the prepressed samples the ones with a Mo-pre-alloyed base powder showed a better combination of hardness and impact energy than the samples pre-alloyed with the same amount of Cr-pre-alloyed. There was no significant difference between the two used MA´s. A sintering temperature of 1250 °C yielded samples with better hardness and impact energy compared to samples sintered at 1140 °C after sinter hardening and tempering. It was possible to introduce Mo admixed as Mo_2C combined with the use of the investigated MA´s. The resulting samples showed similar hardness and impact energy values (up to 440 HV30 and impact energies up to 20 J/cm^2) as the prepressed samples with Mo in the sinter hardened and tempered condition. The samples sintered at 1250 °C showed better hardness, higher impact energies and more homogeneous microstructures compared to the samples sintered at 1140 and 1180 °C. Also, at the lower sintering temperatures undissolved component particles were found in the microstructures. Despite showing promising hardness values, the samples with a 0,45 wt% Mo-pre-alloyed base powder underwent grain boundary oxide formation. This resulted in very low impact energies.

The introduction of Mo as Mo_2C combined with low melting Mn-Si-MA´s in sintered steels was successful and yielded samples with comparable hardness and impact energy values to samples with pre-alloyed Mo. Due to a change in the measurement setup during the experiments, further investigations with Mo-admixed and Mo-pre-alloyed sintered steels combined with the investigated MA´s would be interesting. Also, a variation of the admixed

Mo content to study the impact on the resulting properties of the sintered steels should be conducted.

Kurzfassung

Sinterstähle werden für komplexe Bauteile mit hoher Präzision in hohen Stückzahlen verwendet. Im Gegensatz zur klassischen Stahlherstellung sind die wichtigsten Legierungselemente Ni, Cu und Mo. Diese werden aufgrund ihrer Komprimierbarkeit und O-unempfindlichkeit verwendet. Jedoch sind Cu und Ni mit Umweltproblemen und Preisfluktuationen verbunden. Deswegen besteht das Interesse umweltfreundlichere alternativen wie Mn und Si zu verwenden. Diese O-empfindlichen Legierungselement müssen speziell in Sinterstähle eingebracht werden. Eine Möglichkeit, um O-empfindliche Legierungselemente in Sinterstähle einzubringen ist die Verwendung von sogenannten Master Alloys (MA´s). In dieser Legierungsvariante wird ein Reineisen- oder vorliegiertes Basispulver mit kleinen Mengen an MA gemischt, welche die Legierungselemente enthalten. MA´s ermöglichen Flüssigphasensinterung was zu erniedrigten Sintertemperaturen und einer guten Verteilung der Legierungselemente führt. In dieser Arbeit wurde der Effekt verschiedener Basispulver in Sinterstählen mit niedrigschmelzenden Mn-Si-MA´s untersucht. Weiters wurde die Möglichkeit Mo zugemischt als Karbid (Mo_2C), in Kombination mit denselben MA´s, in Sinterstähle einzuführen untersucht.

Zwei verschiedene Mn-Si-MA´s wurden untersucht. Zuerst wurden vorgepresste Proben wo diese MA´s mit Mo- und Cr-vorlegierten Basispulvern (0,85 wt% Cr und Mo) kombiniert wurden konsolidiert und die mechanischen Eigenschaften der Proben (Dichte, Härte, Schlagzähigkeit) wurden getestet. Anschließend wurden Proben mit einem Reineisen-Basispulver und zugemischtem Mo (0,5 wt% Mo) als Mo_2C mit denselben MA´s gemischt, gepresst, konsolidiert und getestet. In einem letzten Experiment wurden Proben mit einem Mo-vorlegiertem Basispulver (0,45 wt% Mo) und denselben MA´s gemischt, gepresst, konsolidiert und getestet. Das Gefüge aller Proben wurde außerdem nach ätzen mittels Lichtmikroskop untersucht.

Bei den vorgepressten Proben zeigten die mit vorlegiertem Mo eine bessere Kombination aus Härte und Schlagzähigkeit als die Proben mit derselben Menge an vorlegiertem Cr. Es gab keine signifikanten Unterschiede zwischen den beiden MA`s. Eine Sintertemperatur von 1250 °C führte zu Proben mit besseren Härte- und Schlagzähigkeitswerten im gehärteten und angelassenen Zustand im Vergleich zu Proben, welche bei 1140 °C gesintert wurden. Es war möglich Mo als Mo_2C in Kombination mit den untersuchten MA´s zuzumischen. Die hergestellten Proben wiesen vergleichbare Härte- und Schlagzähigkeitswerte (bis zu 440 HV30 und Schagzähigkeitswerte bis zu 20 J/cm^2) zu den vorgepressten mit Mo Proben im gehärteten und angelassenen Zustand auf. Die Proben welche bei 1250 °C gesintert wurden zeigten höhere Härte, bessere Schlagzähigkeit und homogenere Gefüge im Vergleich zu den Proben welche bei 1140 und 1180 °C gesintert wurden. Außerdem wurden bei den niedrigeren Sintertemperaturen unaufgelöste Partikel in den Gefügen entdeckt. Trotz guten Härtewerten unterliefen die Proben mit 0,45 wt% Mo-vorlegiertem Basispulver Korngrenzenoxidbildung. Dies resultierte in sehr niedrigen Schlagzähigkeitswerten.

Die Einführung von Mo als Mo_2C kombiniert mit niedrigschmelzenden Mn-Si-MA´s in Sinterstähle war erfolgreich und führte zu Proben mit vergleichbaren Härte- und Schlagzähigkeitswerten wie bei Mo-vorlegierten Proben. Wegen einer Veränderung des der

Messungsparameter während der Experimente wäre es interessant weitere Untersuchungen mit Mo-zugemischten und Mo-vorlegierten Sinterstählen in Kombination mit den untersuchten MA´s durchzuführen. Des Weiteren sollte eine Variation des zugemischten Mo-Gehaltes und die Untersuchung der resultierenden Eigenschaften durchgeführt werden.

Acknowledgements

First and foremost, I would like to thank Raquel for giving me the opportunity for this work. I could not have asked for a more relaxed and confident environment to do my master thesis. Also thank you for the opportunity to continue our cooperation in a PhD, it is an honour for me!

I would also like to thank Herbert for providing help and very useful references and the chance to present my work outside of the university. It generally felt like having a second supervisor!

Thank you Christian for giving me the chance to start working at the university, without that, this work also would not have been possible!

It was an honour and more fun than I ever could have expected to start this work with you, Marko. Thank you!

I would love to thank everyone from the institute, I could always count on your help and input. Especially Lena, Nico, Beda and last but not least Basti, with whom I did virtually every lecture in this master. With you it was easy, fast and funny. Thanks!

Also, I have to single out Jan and Björn, who accompanied me in my studies from the very first day. We worked like brothers through the bachelor together and I am very happy and thankful that even after we went our separate ways in the master, I still consider you two as my best friends. I hope that this will also continue after our studies!

That I even came this far in life to do my master is attributed to one person and one person only, my mother. I would like to thank her with all my heart for always believing in me and taking me to where I am today. You made everything in my life possible and I love you so much, thank you from the bottom of my heart!

I would also like to thank my family, especially my sister Klara, my Grandparents Fritz and Christine and our newest addition Jean. Thank all of you for always being there for me and helping me through life!

And a very special thanks to my partner. Your appearance in my life coincided with the start of this work and I am grateful every day since that for your help and love!

Contents

1 Introduction and motivation

Master alloys (MA) as an alloying route for low alloyed powder metallurgy (PM) steels were introduced almost 50 years ago. In 1977 Zapf and Dalal used different MA-compositions like MCM (Mo-Cr-Mn), MVM (Mo-V-Mn) and MM (Mo-Mn) [1], [2], [3]. With this alloying route oxygen sensitive elements such as Si, Mn, Cr and V can be introduced into PM steels [1], [2], [3], [4], [5]. A MA is a powder which contains different alloying elements. In the context of PM steels, a MA is designed to be mixed with a (ferrous) base powder to achieve a specific chemical composition and mechanical properties. Newer developments led to design of MA´s, that promote the formation of a liquid phase during sintering therefore enhancing the homogenization of alloying elements in steels [4], [6], [7], [8], [9], [10], [11], [12].

Recent global developments promoted a constant increase in the price of the classical alloying elements for PM steels such as Cu and Ni. The increase combined with fluctuations in the prices of these elements [13], [14] show the need to substitute those elements in PM steels. Furthermore Cu interferes with the recycling of steel [15] and the toxicity of Ni [16] led to stricter usage restrictions by the European Council [17]. Also the demand for both elements has increased due to electromobility [18].

In this work the effect of different base powders on sintered steels with low melting Mn-Si-MA´s was investigated. Different pre-alloyed base powders with Mo and Cr were used in combination with two different MA´s containing the “unclassical” oxygen affine alloying elements Mn and Si. Furthermore, the impact of introducing of Mo admixed as Mo_2C into PM steels alloyed with MA´s on Mo-homogenization was investigated. Mo enhances hardenability and mechanical properties in steel [1], [19]. Mo was already used in the first MA´s in the 1970´s [1]. Even though it is an attractive alloying element, the problems with Mo are also the price fluctuations [20] and the high melting point of 2617 °C [21]. Due to the high melting point and the formation of carbides at intermediate temperatures sintering PM steels with admixed elemental Mo require high sintering temperatures above 1250 °C, where an eutectic phase is formed [22]. Also, the limited availability of Mo-MA´s or Mo-pre-alloyed base powders lead to a restricted flexibility.

Therefore, in this work the effect of different base powders and the introduction of Mo as a carbide (Mo_2C) combined with low melting Mn-Si-MA´s in PM steels was studied. The use of Mo_2C powder would mean more flexibility in the MA-PM-steel system and might require lower sintering temperatures. The aim of this work was to understand the effect of introducing Mo admixed as Mo_2C combined with the use of low melting MA´s on mechanical properties and microstructure in PM steels.

2 Theoretical background

2.1 Powder metallurgy

Powder metallurgy is the part of metallurgy that focuses on the production of metal powders and the production of parts made from such powders. These parts are shaped and consolidated, very often by sintering [23], [24]. The advantages of using PM can be economic or technical. For small parts produced in large lots with critical or complex geometric requirements the PM route is cheaper than conventional metallurgy. The PM route can produce microstructures with a "tailored" heterogeneity. In some cases, certain materials can only be produced by PM, for example hard metals [25], [26]. Powders for PM applications are usually produced by water or gas atomization [24]. A newer development is the ultra-high pressure water atomization (UHPWA) method, which allows to produce very fine powders (<25 µm) with a moderate oxygen content in a cost effective manner [27]. Compared to other PM forming techniques, like additive manufacturing, hot isostatic pressing (HIP) or metal injection molding (MIM), uniaxial pressing combined with sintering is used for parts of small to medium weight for large lot sizes. See Figure 1.

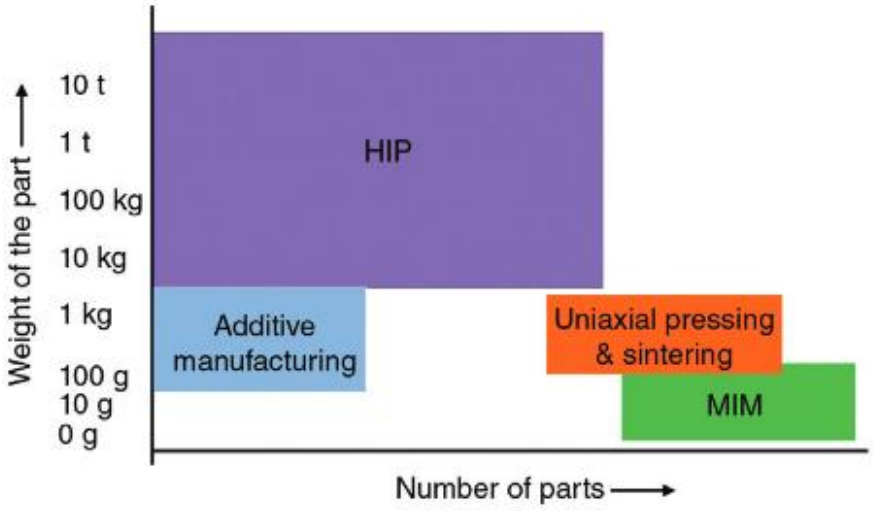

Figure 1: PM shaping techniques, according to [24]

2.1.1 Pressing

Pressing can be used to shape a powder or powder mixture. The simplest and most common way to produce PM parts is cold uniaxial pressing or die pressing. Powders that are filled in a die cavity are compacted by a punch, usually with a pressure between 400-1000 MPa. The powder particles are rearranged, interlocked and at high pressures cold welding can occur. The pressure cand be generated by mechanical or hydraulic presses. After compacting, the so-called green part is ejected from the cavity and cand be handled further due to its increased strength [25]. To reduce shear stresses during the ejecting process and increase compatibility a lubricant, usually a wax, is admixed to the powder [24].

2.1.2 Sintering and Liquid Phase Sintering

The thermal process that a PM part typically undergoes for its consolidation is called sintering. One definition by the ISO 3252:1999 is *"The thermal treatment of a powder or compact at a temperature below the melting point of the main constituent, for the purpose of increasing its strength by bonding together of the particles"* [23]. The temperature while sintering is usually 75-80% below the melting point [25]. For steels, where Fe is the main component, the sintering temperatures are between 1100-1350 °C. One characteristic of the sintering process is the transformation from single powder particles to a continuous material [28]. Sintering can lead to densification/shrinkage, but this is not desired for every material. There are different sintering mechanisms. While the driving force behind solid state sintering is the minimalization of energy by elimination of "defects" (the surface), liquid phase sintering (LPS) is a more complex mechanism. LPS requires a system with two constituents. While the major constituent has to stay solid during the whole sintering process, the minor constituent forms a liquid phase. The formation of the liquid phase can either occur due to melting of the minor constituent, or due to a reaction between the two constituents. The liquid phase enhances the velocity of the mass transport during sintering [24], [29]. With LPS densification during sintering can be achieved. Typical materials produced by LPS are high-speed steels, tool steels and hard metals. An important factor in LPS is the wetting behaviour of the formed liquid phase on the solid phase [25]. LPS can be classified by two different conditions of the liquid phase: persistent and transient:

Persistent liquid phase: the liquid and solid phase in equilibrium at the sintering temperature. This usually leads to full densification after sintering and is used for materials like hard metals, where full density is required [24], [30].

Transient liquid phase: at the sintering temperature only the solid phase is stable (if the overall material composition is considered). The liquid phase is usually formed due to a melting point below sintering temperature or by the formation of a lower melting eutectic phase. The transient liquid phase disappears during the sintering process and forms a solid solution with the solid phase. Fe-Cu-C is a typical system with transient liquid phase. In this system swelling occurs upon liquid phase formation. This swelling phenomenon combined with shrinkage in sintering processes, can be used to produce parts with net zero-dimensional change. Transient liquid phases often do not lead to densification, also due to the possible formation of secondary porosity [24], [29]. MA´s form those transient liquid phases during sintering [4], [5], [6], [31].

2.2 Steel

Steels are iron alloys, the most important alloying element in steels is typically C. The Din EN 10020 [32] defines that steels contain up to, but no more than 2,06 wt% C. Iron alloyed with more than 2,06 wt% C is considered cast iron. This specific limit was chosen, because it is the maximum solubility of C in Austenite or γ-Fe [33].

2.2.1 Microstructure

Steel is a special material as a wide range of microstructures and therefore properties can be obtained by different heat treatments and alloying elements. As C is the most important

alloying element in steels, the Fe-C phase diagram (see Figure 2), especially the range from 0 to 2,06 wt% C is intrinsically linked to steels. The occurring phases in steels, dependent on the temperature and carbon content are ferrite (α-Fe), austenite (γ-Fe), δ-ferrite (δ-Fe, similar to α-Fe at high temperatures) and cementite (Fe_3C) [33], [34]. Different alloying elements can stabilize austenite (Mn, Ni), ferrite (Si, Cr) or form carbides (Mo, Cr) when added in high amounts. Different arrangements of those phases are called microstructures. The transformation from austenite at lower temperatures into ferrite and cementite can lead to different microstructures. Slow cooling rates enhance diffusion-controlled transformations and lead to the formation of ferrite, cementite and pearlite. Fast cooling rates lead to shear-type transformations without diffusion and the resulting microstructures are martensite and bainite [33].

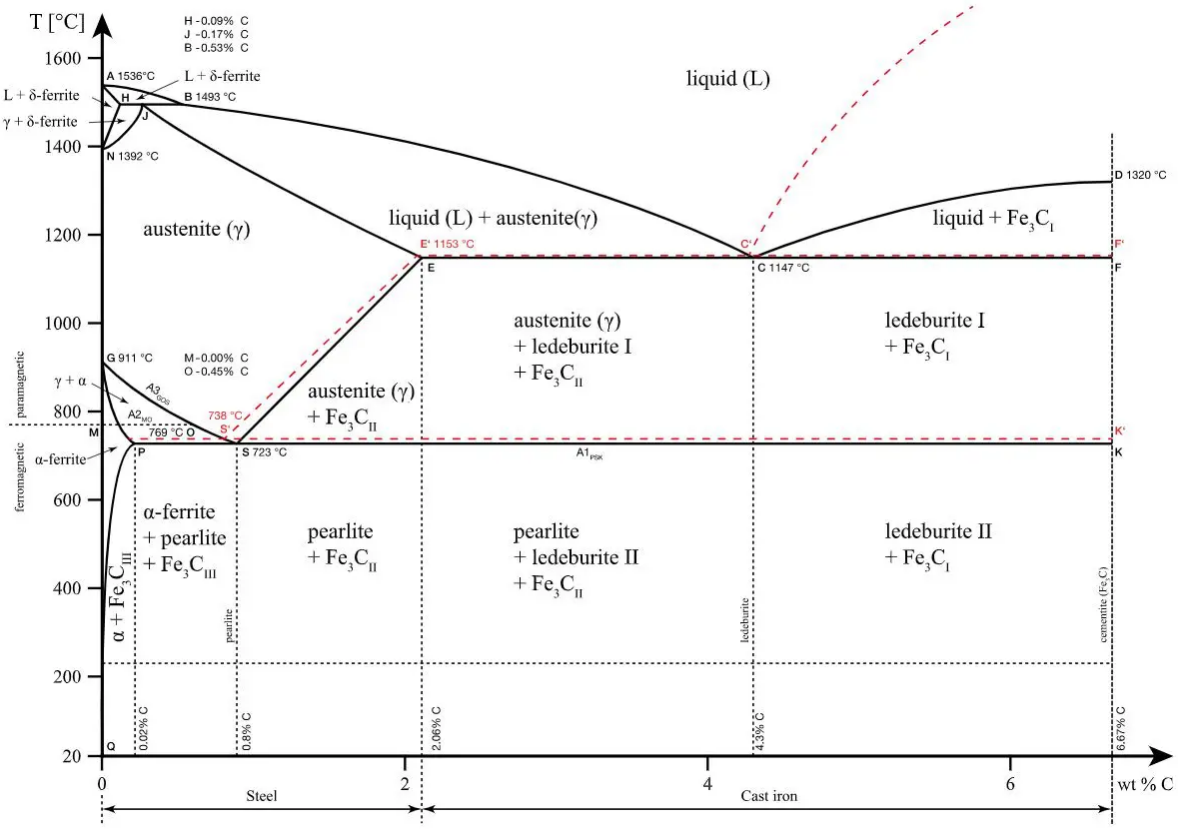

Figure 2: Fe-C phase diagram, according to [46]

Ferrite: α-Fe has a body-centered cubic space lattice. The transformation from the face-centered cubic space lattice in austenite into ferrite leads to a volume expansion. The density of ferrite is 7,87 g/cm³ [33]. Etching of ferritic microstructures effects the grainboundaries.

Cementite: Fe_3C is a metastable phase that forms when the solubility of C in austenite and ferrite is exceeded. It is hard and brittle, especially compared to ferrite and therefore plays an important role for strengthening and hardening steels [34]. It has a close density to ferrite of 7,70 g/cm³ [33].

Pearlite: Figure 2 shows that austenite with a carbon content of 0,77 wt% undergoes a eutectoid transformation into ferrite and cementite. The resulting microstructure is called perlite. It is composed of alternating lamellae of ferrite and cementite. Pearlite also forms

together with ferrite (proeutectoid) or cementite (hypereutectoid) [33]. An example of pearlite can be seen in Figure 3 [35].

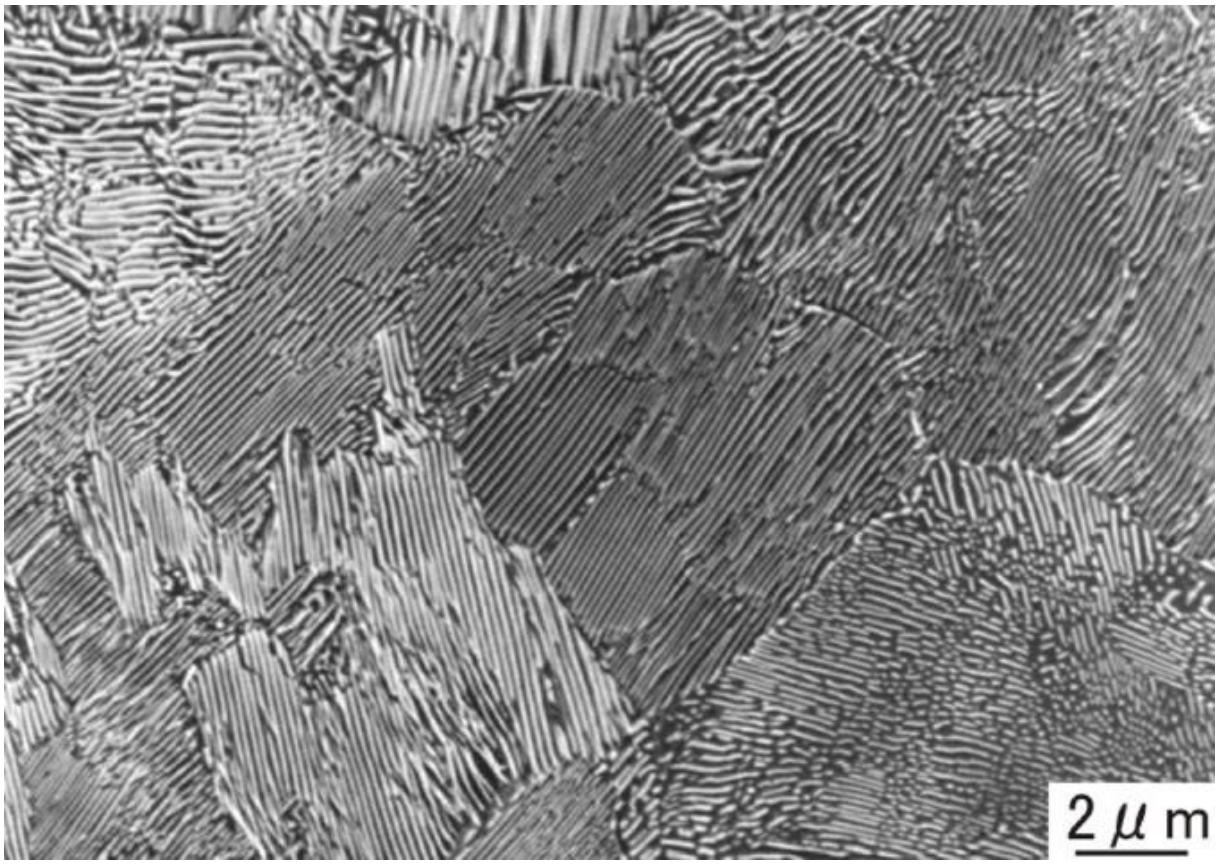

Figure 3: Pearlite, according to [47]

Martensite: To form this microstructure, the steels must be rapidly cooled or quenched. It is the hard microstructure associated with quenched steels. It is also not just a phenomenon found in steels. It can be found in metallic (Cu-Al, Au-Cd) and even ceramic (SiO_2 and ZrO_2). Martensite in steel is formed due to the allotropic change of the Fe from austenite to α-ferrite. Through the rapid cooling the diffusion of the C atoms, which are located in the octahedral sites of the body-centred cubic austenite, is completely suppressed. Therefore, the austenite does not transform into ferrite and cementite (pearlite) and the martensitic phase is formed via an instantaneous shear mechanism. Martensite is a body-centred tetragonal metastable phase where the C atoms in the octahedral interstitial sites. The higher the C content, the more the tetragonality of the martensite increases. Due to the shear mechanism the surface of martensite is tilted in comparison to the original austenitic region. In etched and polished samples the martensite crystals appear needle like [33]. An example of martensite can be seen in Figure 4 [35].

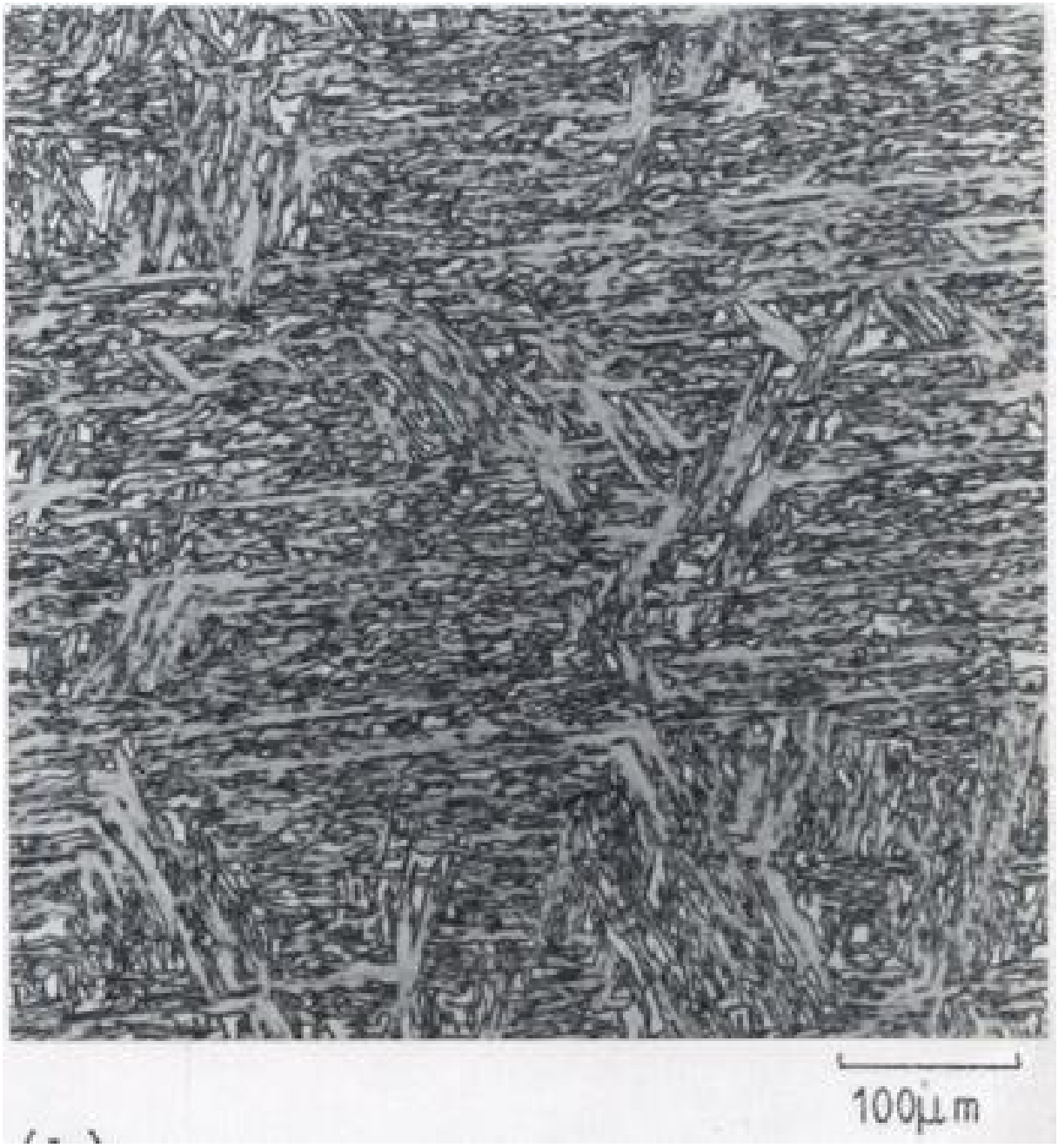

Figure 4: Martensite, according to [47]

Bainite: The formation of this microstructure is an intermediate between the diffusion mechanism of the pearlite formation and the shear mechanism of the martensite formation. It forms under continuous cooling or isothermal conditions. Bainite consists of cementite and ferrite, but unlike pearlite, both phases occur in nonlamellar arrays. The morphology of those arrays is highly dependent on the alloy composition and transformation temperature. The ferrite and cementite can occur in lath or plate form with dislocation structures, similar to martensite. Bainite can be classified morphologically into lower and higher bainite. Upper bainite forms at temperatures just below pearlite formation. A key identification for upper bainite are feathery clusters of ferrite laths. In polished and etched samples, it appears dark due to the rough, elongated carbide particles, which form between the ferrite laths. An example of upper bainite is shown in Figure 6 [33]. Lower bainite forms at temperatures close to the temperature where martensite starts to form, so at lower temperatures than upper

martensite. It also is harder than upper bainite [36]. Lower bainite also appears dark in polished and etched samples. It forms large plates. The carbides are formed within the plates, not between them like in upper bainite. They are also finer than in upper bainite [33]. An example of lower bainite is shown in Figure 7 [33]. The mechanism of the different bainite formation can be seen in Figure 5 [35].

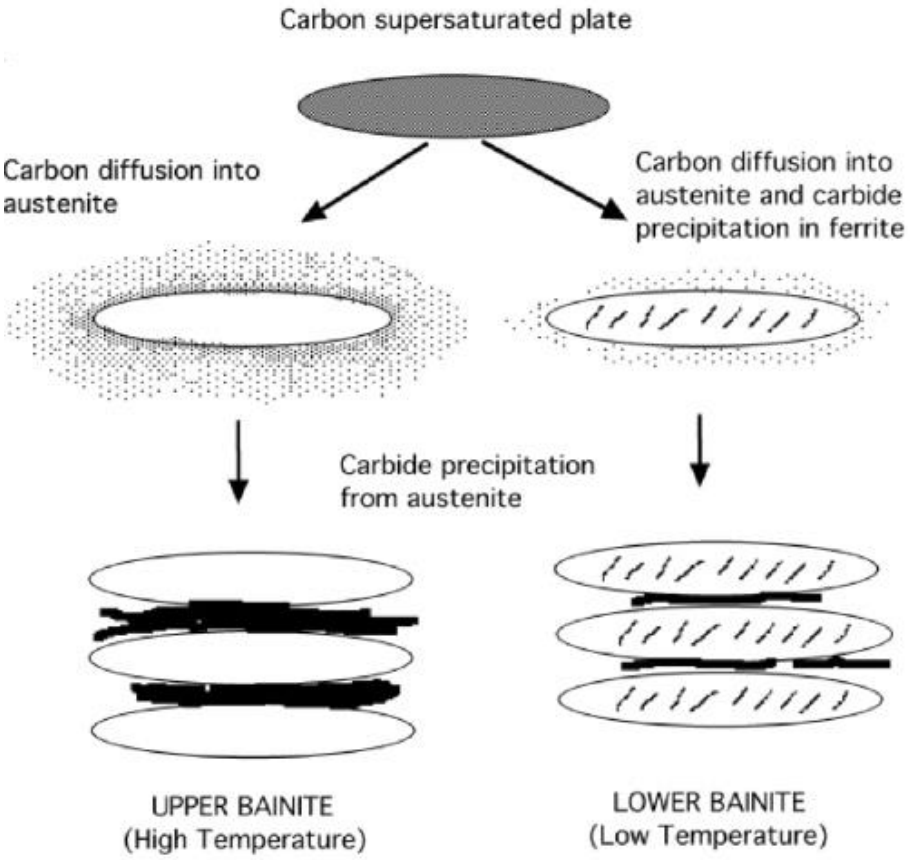

Figure 5: Bainite reaction mechanism, according to [47]

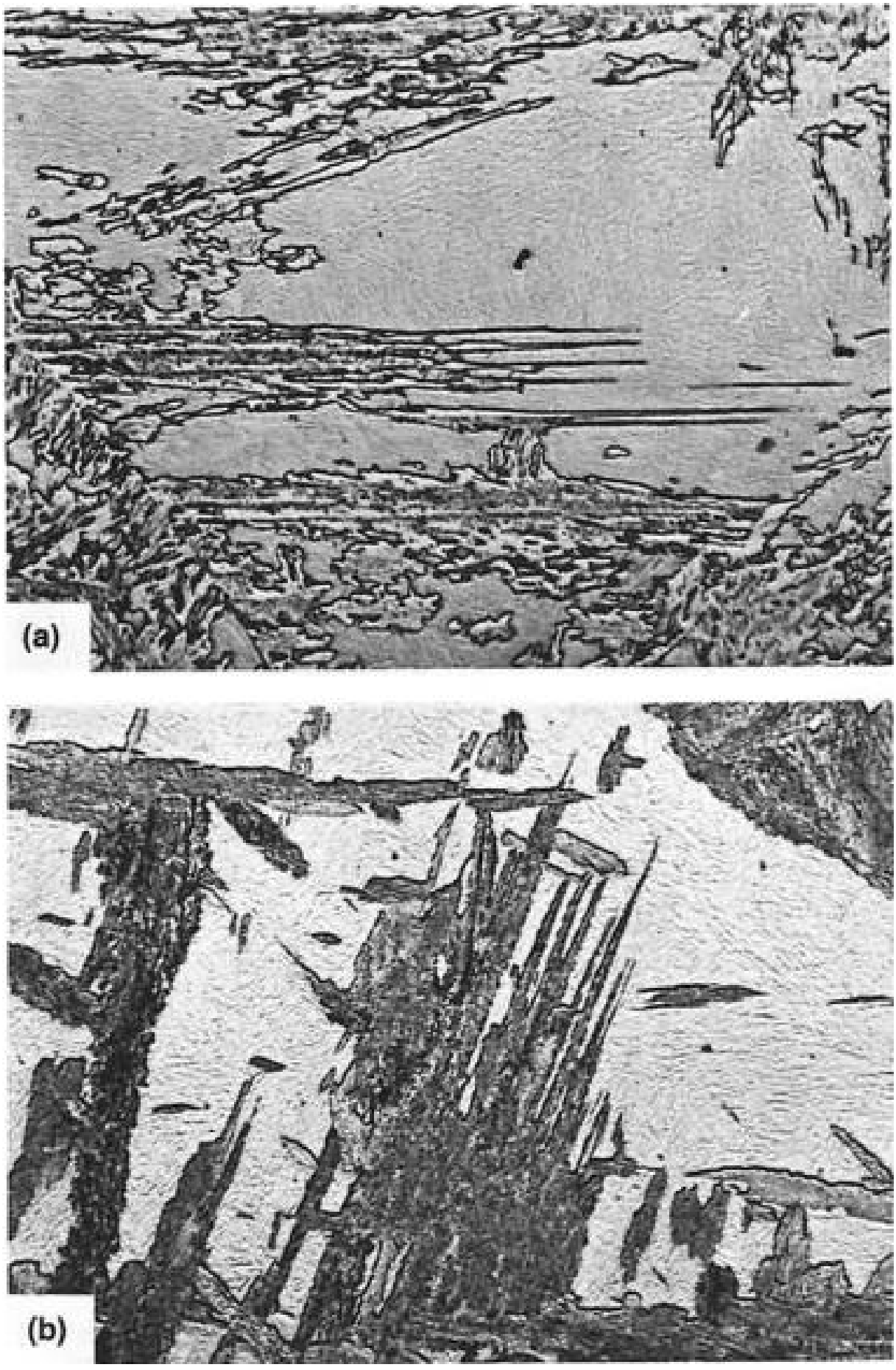

Figure 6: Upper bainite, according to [33]

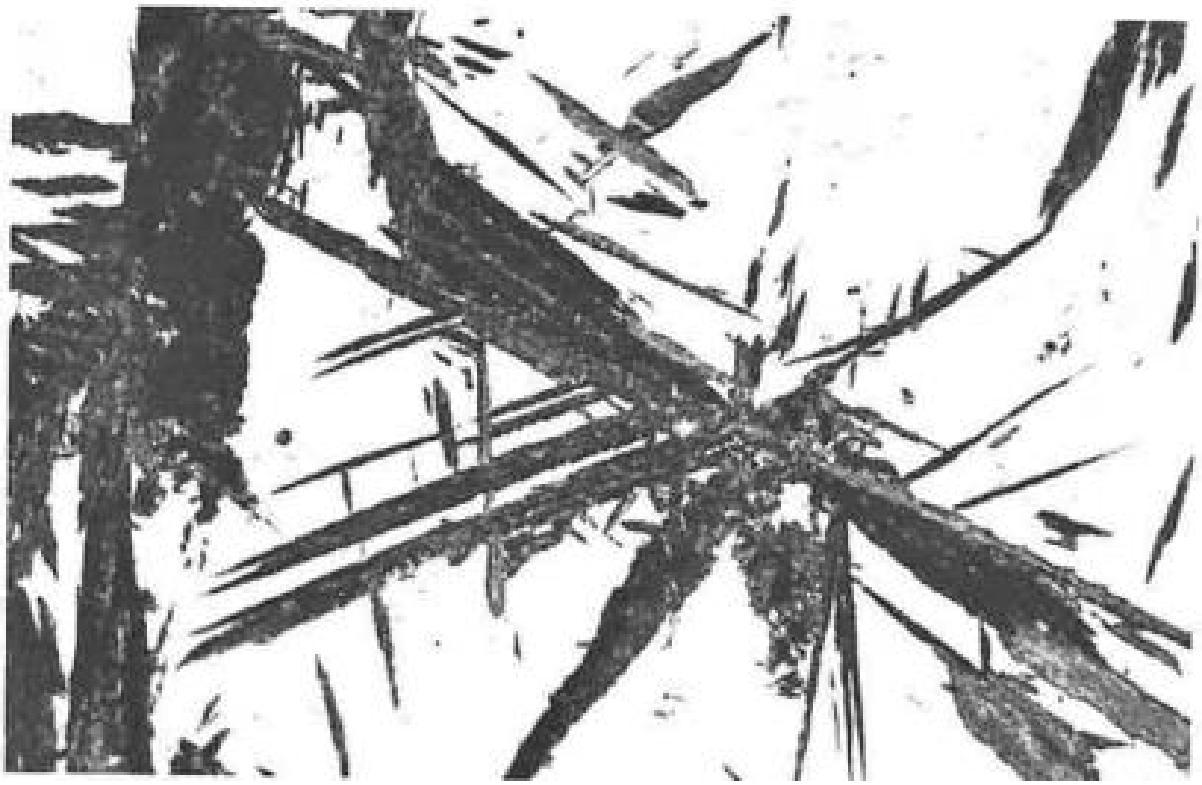

Figure 7: Lower bainite, according to [33]

The succession of the different microstructures relating to their hardness is plotted in Figure 8 [36]. The hardness-ranges for cold rolled pearlite, martensite and bainite can be seen in Figure 9 [37]. Hardenability of steels is the ability to form martensite during quenching [38].

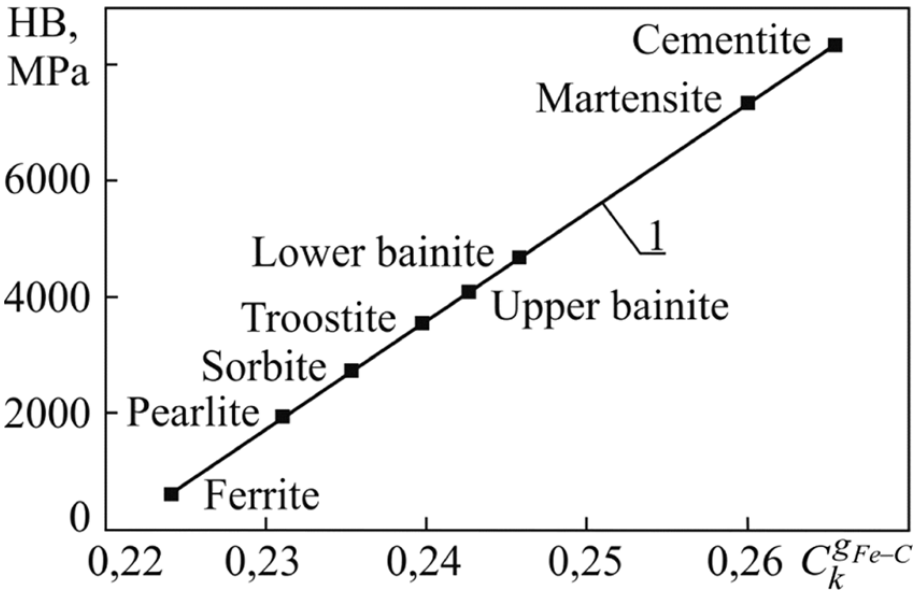

Figure 8: Hardness of different microstructures in eutectoid steel depending on the generalized Fe-C bonds covalence, according to [48]

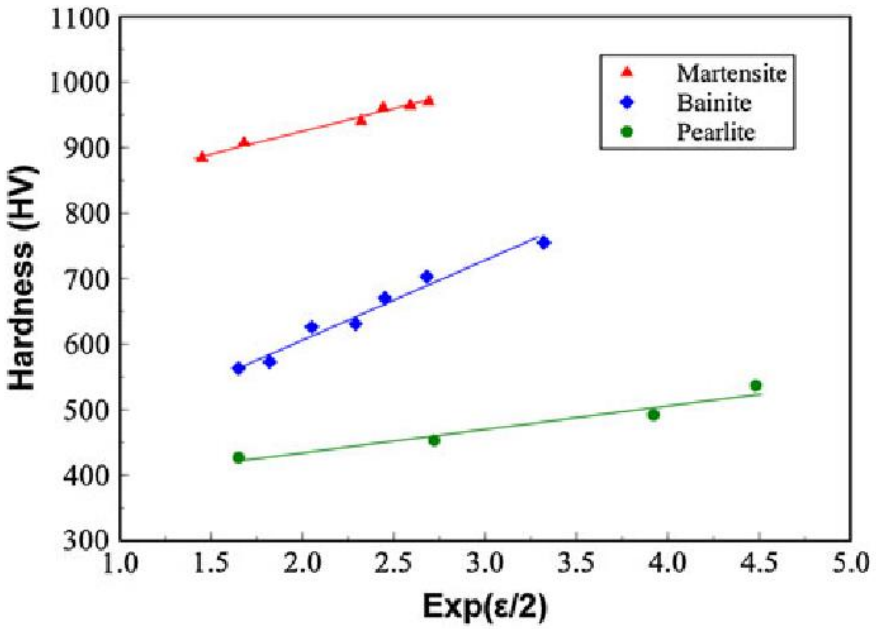

Figure 9: Hardness of microstructures in steels as a function of cold-rolling strain, according to [49]

2.2.2 Alloying elements

Typical alloying elements in classical steel production are C, Cr, Ni, Mn, Si and V. In PM steels the most important alloying elements are Ni, Cu and Mo. This is due to their good compressibility [39] they are not O sensitive. As discussed in 1 due to instable prices and other concerns there is a need to eliminate the dependency from the classical alloying elements (Cu, Ni) in sintered steels. Therefore, this work will focus on the alloying elements Mn, Si, Cr, (C) and Mo.

C: As already mentioned in 2.2.1, C is crucial for the formation of microstructures in steels. It forms cementite (Fe_3C), pearlite, martensite and bainite. The formation of those microstructures and the resulting properties depends on the carbon content and can be tailored by heat treatments. A higher C content facilitates microstructures with a higher strength and hardness, but also leads to a decrease in toughness and ductility [40]. C is an γ-Fe stabilizer and is soluble up to 2,06 wt% in γ-Fe [41]. In sintered steels C is the main reduction agent during sintering [25]. As oxides are reduced during the sintering process, the C content changes. Therefore, the C content that is admixed (nominal) and the C content after sintering (combined) is not identical and needs to be taken into account. C is usually admixed in the form of a fine graphite powder, which completely dissolves in the Fe after the α-γ transition [42].

Si: Si is a very common alloying element in conventional steel production. It strengthens α- Fe [40]. Si is an α-Fe stabilizer which increases material density. Tensile strength, hardness and hardenability are enhanced due to favoured martensite formation. In PM steels an a content of around 3 wt% Si is reported to be optimal [43], [44], [45], [46], [47]. Si is reported to promote the formation of adherent surface films on cast iron [19] and therefore is interesting for transient LPS because it enriches on the melt surface. This could promote the homogenization of alloying elements. The formation of grain boundary oxides can be

problematic. This phenomenon is enhanced by the presence of Mn [48]. Therefore the quality of the reducing atmosphere for sintered steels is critical [1], [43].

Mn: Mn is an γ-Fe stabilizer [40], [46] and acts as an deoxidizer due to its high oxygen affinity. It also strengthens steels and improves hardness, but to a smaller degree than C. It strongly enhances the hardenability in steels by enhancing martensite formation at even low cooling rates [46], [49], [50]. Due to its high vapor pressure Mn can sublimate below its melting point. This phenomenon hast two advantages during the sintering process: the fast homogenisation of Mn via gas phase transport and the formation of a protecting sintering atmosphere, which leads to an Mn loss [49], [51], [52]. Mn has an internal getter effect [53], which means that Mn can reduce Fe oxides in sintered steels during sintering [49], [51], [54]. As with Si, a high quality sintering atmosphere is crucial for Mn alloyed steels [51], [52], [54], [55]. Due the low price of Mn and ferromanganese it is a very attractive alloying element [18]. Introduction of Mn via MA in sintered steels has turned out to be a viable option [1], [4], [6], [44]

Cr: Like Si, Cr is an α-Fe stabilizer [41]. It increases corrosion resistance, hardenability, acts as a deoxidizer, improves high temperature strength and is a strong carbide former. For high temperature strengthening it is combined with Mo [40]. It reduces ductility [46] and also is able to perform an internal getter effect [53], [54]. Due to its higher oxygen affinity than Fe it is mainly used in pre-alloyed powders for pm steels and requires a clean sintering atmosphere [1], [8], [49]. Introduction of Cr for sintered steels the MA route reduces the oxygen affinity compared to admixed elemental Cr [8].

Mo: Like Si and Cr is an α-Fe stabilizer [56], [57]. It increases hardenability [1], [19], [40]and decreases C diffusion. This leads to retardation of pearlite formation [40], [57] and enables bainite formation at moderate cooling rates [40], [56]. Mo increases high temperature tensile and creep strength and reduces temper embrittlement [40]. Therefore used in fire-resistant steels [58]. It is reported to enhance mechanical properties, especially when combined with Cr and Ni [1], [19], [25]. Due to the lower oxygen affinity than Fe [59] Mo is commonly used and can be sintered under standard sintering conditions. When Mo is admixed as an elemental powder the grain size is critical. Mo, Fe and C form an eutectic phase above 1250 °C, therefore if the admixed Mo powder is to course, huge secondary pores can be formed [22]. Therefore the use of Mo-pre-alloyed powders is common in sintered steels [60]. Despite price fluctuations [20] Mo is an attractive alloying element which already was used in the development of the first MA´s [1].

Hardenability is a key factor for the mechanical properties in PM steels. The hardenability is the ability to form martensite during quenching [38] and described by the multiplying factor [61]. The higher the multiplying factor the better the hardenability. Figure 10 shows the influence of the discussed alloying elements in steels on the multiplying factor [33].

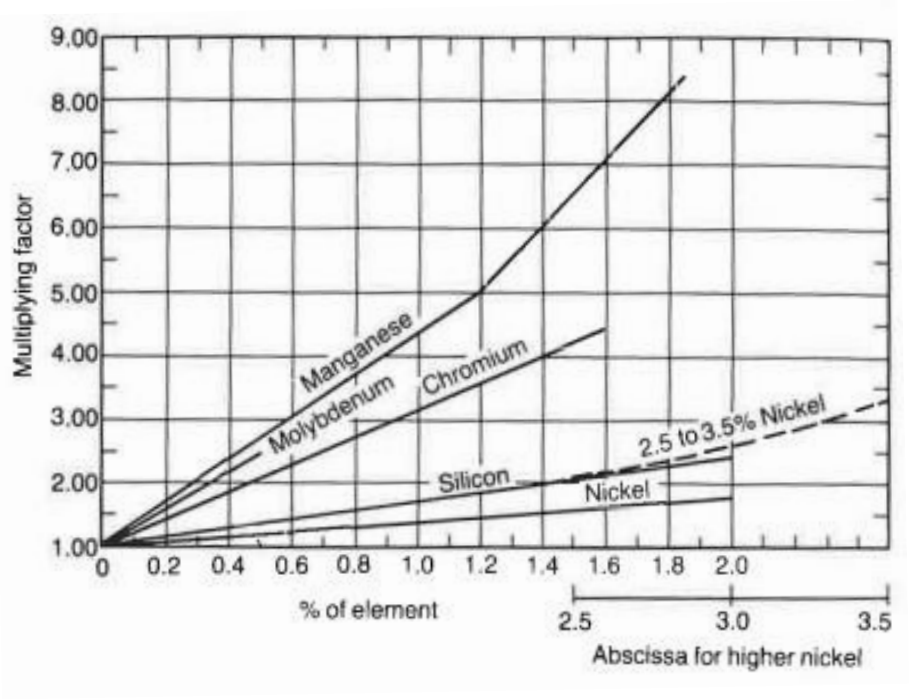

Figure 10: Relationship between alloying elements and multiplying factor (hardenability), according to [33]

2.3 PM steels

PM steels or sintered steels are steels that are produced via an PM route, classical by uniaxial pressing and sintering. In conventional steel manufacturing the Fe and alloying elements are melted, therefore the metals are in a liquid state, this is not necessarily true for PM steels. Typical alloying elements are Ni, Cu and Mo.

2.3.1 Introduction of alloying elements in PM steels

To introduce alloying elements in sintered steels there are 5 routes, which are shown in Figure 11 [62].

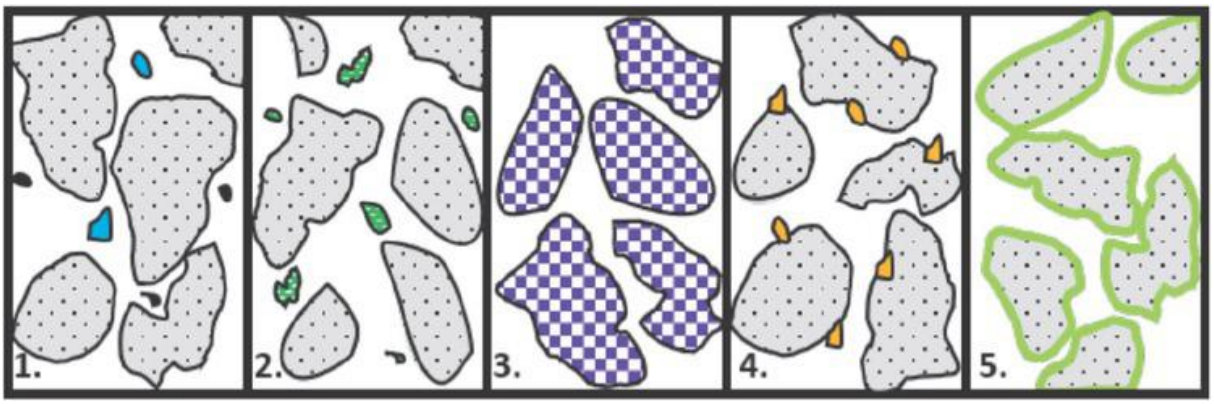

Figure 11: PM alloying routes: 1. elemental powders, 2. master alloy, 3. pre-alloying, 4. diffusion alloying, 5. Powder coating, according to [34]

A complete liquid state is not achieved in this way of alloying. Each of these alloying routes comes with their respective advantages and disadvantages.

Elemental powder mix: The mixing of elemental powders, usually metals, graphite and lubricants, is cheap, easy to realize and flexible [25]. Problems are that this route is not suitable for oxygen affine elements and agglomeration and segregation can appear [43]. Alternatively ferroalloys can be used as a more economic variant instead of the elemental powders [49], [63]. The flexibility of this process is unmatched by the other alloying routes.

Master alloys: Will be discussed separately in 2.3.2.

Pre-alloying: The alloying elements are added to the melted Fe before it is atomized into a powder. Therefore, it is suitable for elements with a high oxygen affinity like Cr and Mn [25]. Pre-alloyed base powders are not as compressible as pure ferrous base powders due to solid solution hardening [64]. Since only a limited number of compositions of pre-alloyed powders are available on the market it is not a flexible alloying route.

Diffusion alloying: A ferrous base powder is mixed with fine elemental powders like Cu or Ni and then heat treated to ensure diffusion between the powders. Segregation can be avoided with diffusion alloying. It can ensure either homogeneity or tailored heterogeneity. It is an expensive alloying route and mostly only available for Ni- and Cu-alloyed powders [1], [25], [65]. As with pre-alloyed base powders, diffusion alloying is not a flexible alloying route.

Powder coating: Coated powders are mostly used in the additive manufacturing process Laser powder bed fusion [66]. The application in sintered steels is uncommon.

After the classical processing route of mixing, PM steels are usually porous. Due to the high requirement to dimensional stability in PM parts a residual porosity of around 10% is unavoidable. This porosity causes limitations in mechanical properties [67], [68], see Figure 12 [25], [69]. Porosity also has advantages in sintered steel parts, such as weight and noise reduction in engine parts [70]. It also acts as a grain growth inhibitor [71] when the parts undergo a heat treatment.

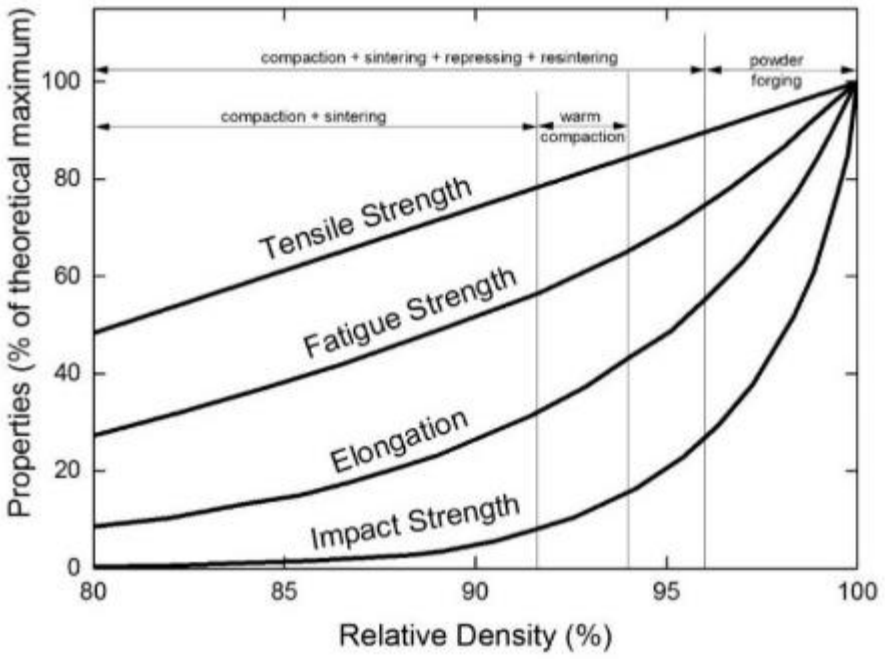

Figure 12: Relationship between relative Density and mechanical properties for PM steels [43], according to [25]

2.3.2 Master alloys

As already mentioned in 1 the first MA´s were introduced in the 1970´s [1]. It is an alloying route that allows to tailor specific properties in a final product. With the pre-alloyed MA powders it is possible to introduce oxygen sensitive alloying elements like Si, Cr, Mn and V [1], [4], [72], [73], [74] into sintered steels. By binding these elements chemically as carbides or solid solutions their chemical activity and therefore oxygen affinity is reduced. By adding MA´s in amounts of 2-6 wt% to base powders a high flexibility can be achieved. Also, if pure ferrous base powders are used the compressibility is improved compared to the route of using pre-alloyed powders. To achieve full chemical distribution of the melted MA through the solid base powder during the sintering, surface oxides on the base powder need to be reduced [75]. Especially for MA´s containing oxygen sensitive elements a clean and oxygen-free sintering atmosphere is needed. Due to the angular shape and the high hardness of early MA´s, [1] tool wear resulted and the interest in the concept stopped after the initial developments. The development of atomizing techniques [6], [31], [44], [76] and especially UHPWA [27] made the use and production of MA´s attractive. With UHPWA it is possible to produce small (<25 µm), rounded MA´s with alloying contents up to 50 wt% of oxygen sensitive elements and al low O content (<1 wt%). The combination of those factors makes the MA alloying route a viable and attractive option for the production of sintered steels.

3 Materials and experimental procedures

3.1 Powders

A variety of different powders were used in this work, an overview of all used powders is provided in Table 1. The morphology of the base powders, MA´s and the Mo source were characterized by scanning electron microscopy (SEM) and are shown in the following figures.

Table 1: Used Powders

Powder type	Commercial name	Description
Base powders	ASC 100.29	Iron powder; supplied by Höganäs AB; water atomized; high compressibility; C content <0,01 wt%; total O content 0,08 wt%; main fraction (70 %) particle size 45-150 µm; irregular morphology; see Figure 13; in this work referred to as "**Fe**"
	Astaloy CrS	Cr-pre-alloyed ferrous powder; 0;88 wt% Cr; 0,15 wt% Mo; 0,025 wt% C; supplied by Höganäs AB; water atomized; O content 0,24 wt% according to supplier; in this work referred to as "**Fe_0.85Cr_0.15Mo**"
	Astaloy 45 Mo	Mo-pre-alloyed ferrous powder; 0,45 wt% Mo; supplied by Höganäs AB; water atomized; O content 0,08 wt% according to supplier; irregular morphology and similar size distribution to Fe; see Figure 14; in this work referred to as "**Fe_0.45Mo**"
	Astaloy 85 Mo	Mo-pre-alloyed ferrous powder; 0,86 wt% Mo; 0,01 wt% C; supplied by Höganäs AB; water atomized; O content 0,07 wt% according to supplier; in this work referred to as "**Fe_0.85Mo**"
Master alloys	H166	Mn-Si-C-MA; composition Fe_33Mn_7.5Si_3.44C; manufactured by Atomising Systems Ltd.; UHPWA; O content 0,33 wt% (LECO TC400; hot gas extraction); elongated particles; particle size ~1-25 µm; morphology see Figure 15; in this work referred to as "**MA1**"
	H200 high ox	Mn-Si-C-MA; composition Fe_40Mn_9Si_1.5C; manufactured by Atomising Systems Ltd.; UHPWA; O content 1,37 wt% (LECO TC400; hot gas extraction); less elongated particles; high amount of very fine spherical particles (<5 µm); ; particle size ~1-25 µm; morphology see Figure 16; in this work referred to as "**MA2**"
Mo_2C	Mo_2C	Mo_2C powder; 0,94 wt% Mo; obtained from Treibacher AG; typically used for hard metal production; extremely fine particles; particle size ~1-3 µm; morphology see Figure 17; in this work referred to as "**Mo_2C**"
Graphite	UF4 96/97	Natural Graphite; manufactured by Graphit Kropfmühl GmbH; in this work referred to as "**C**"
Pressing aid	Hoechst Wachs C (HWC)	Ethylene disterylamide (EBS); $C_{38}H_{76}N_2O_2$; melting point 146 °C [77]. 0;6 wt% were calculated and admixed to finished powder mixes; in this work referred to as "**EBS**"

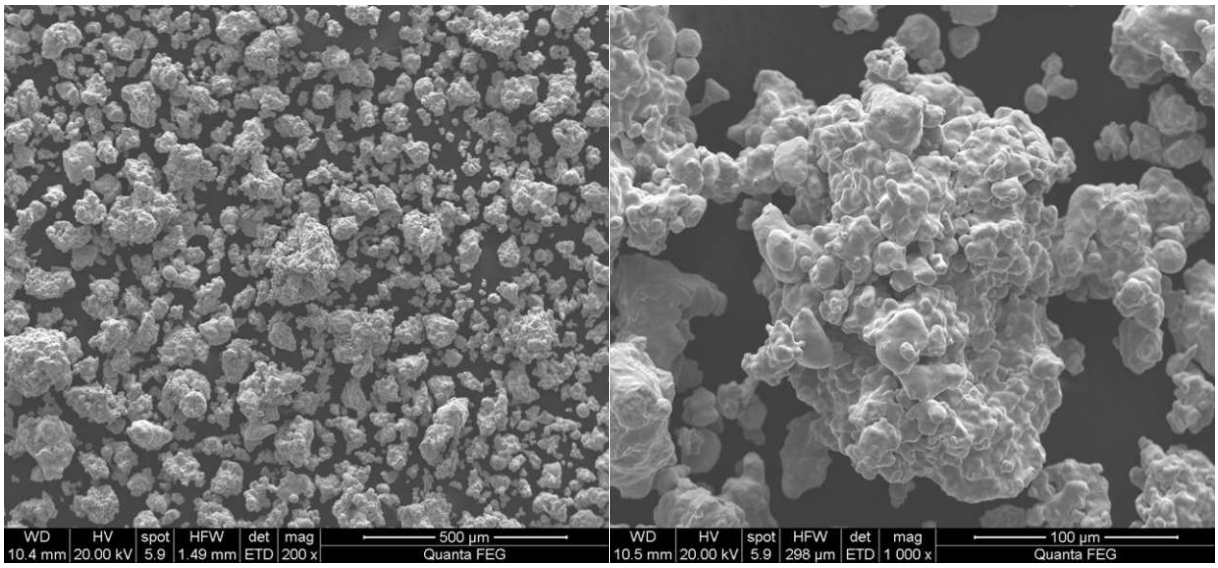

Figure 13: SEM images of used Fe powder, 200x (left), 1000x (right)

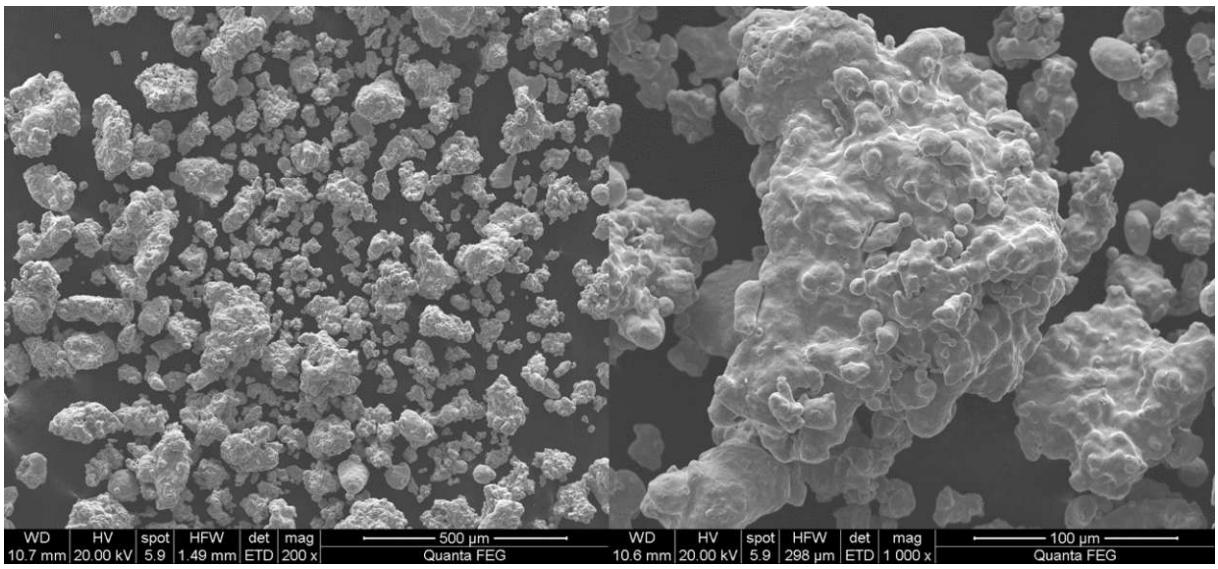

Figure 14: SEM images of used Mo-pre-alloyed basepowder Fe_0.45Mo, 200x (left), 1000x (right)

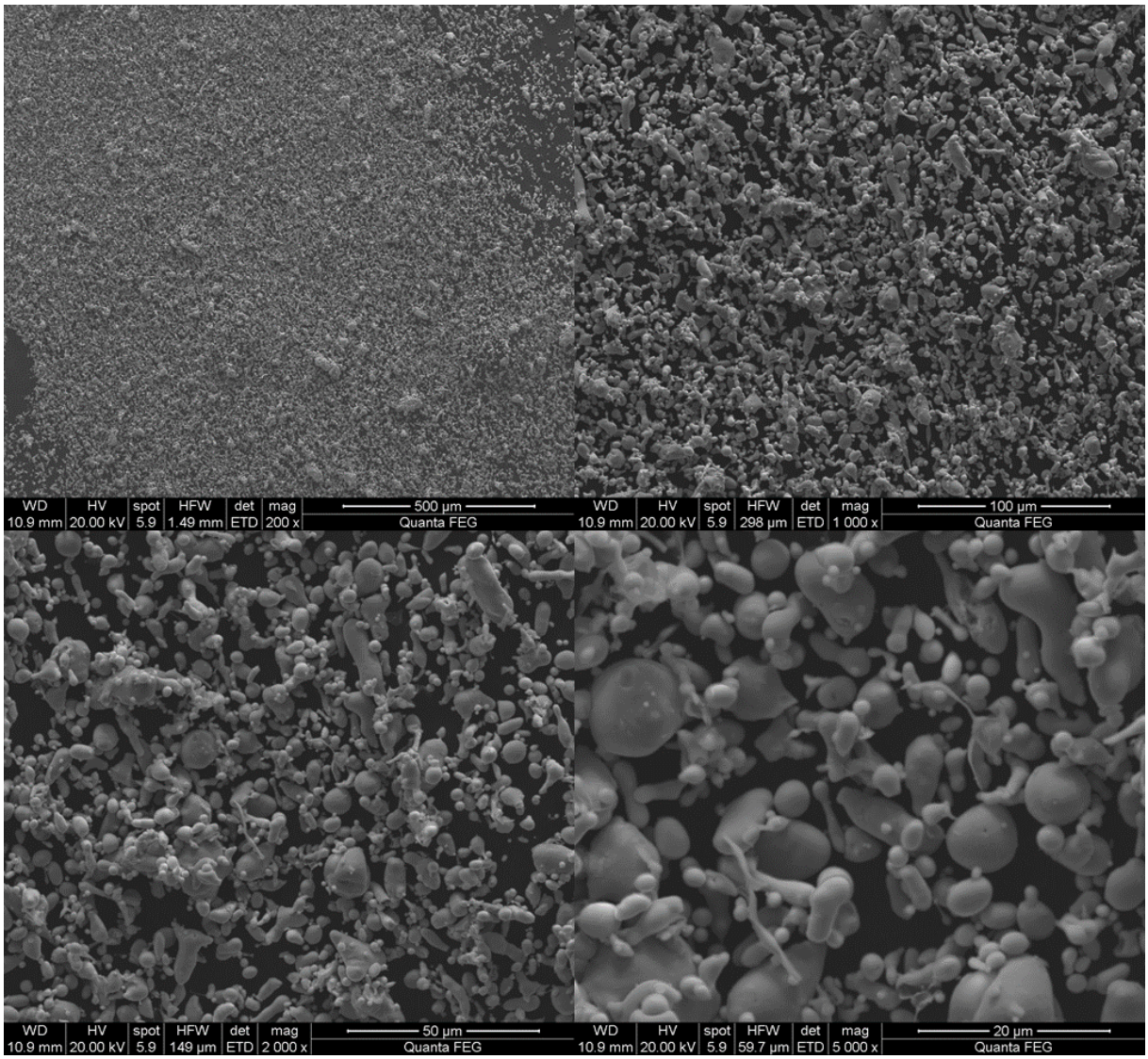

Figure 15: SEM images of used MA1 powder, Fe_33Mn_7,5Si_3,44C, 200x (top left), 1000x (top right), 2000x (bottom left), 5000x (bottom right)

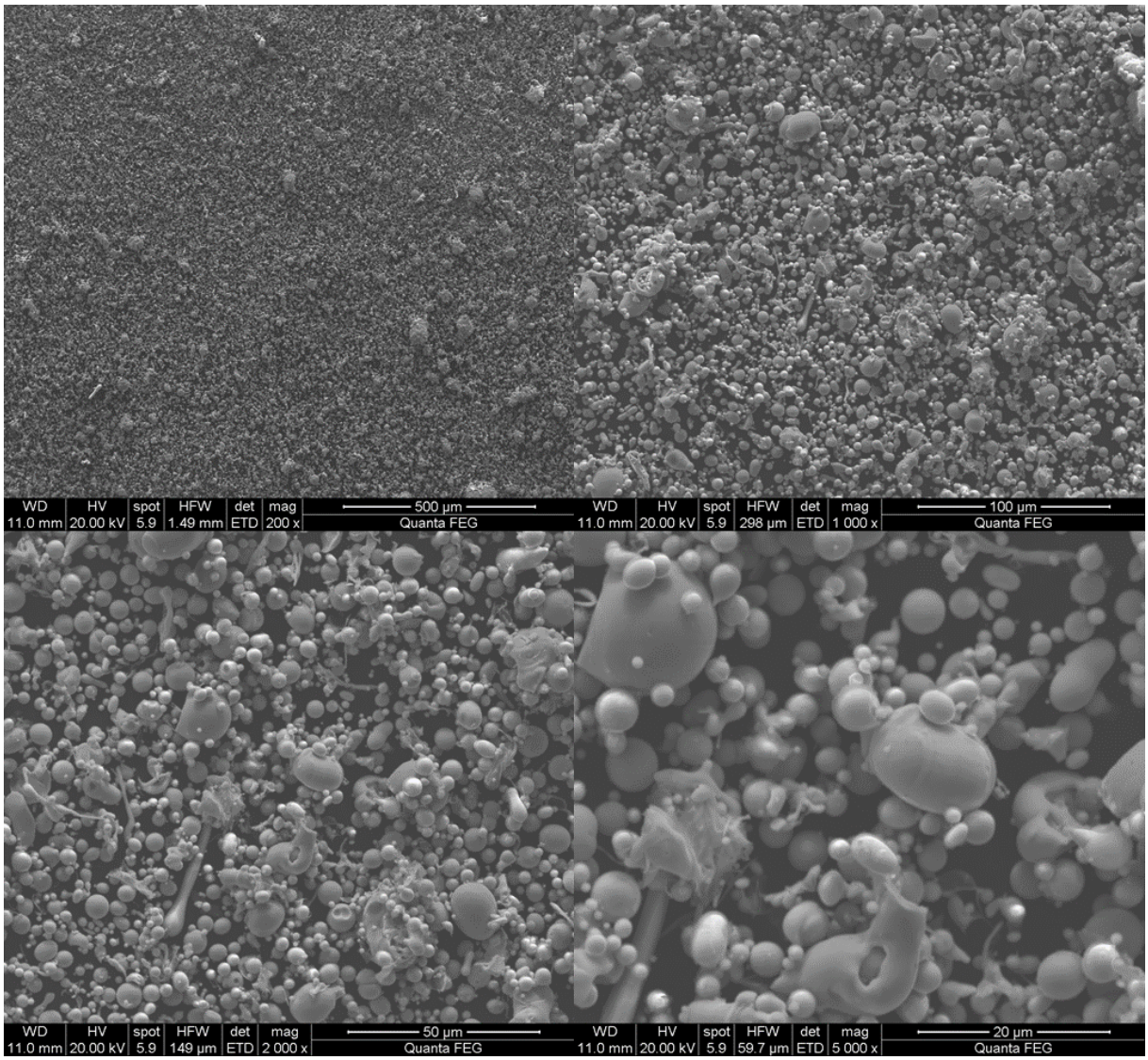

Figure 16: SEM images of used MA2 powder, Fe_40Mn_9Si_1,5C, SEM, 200x (top left), 1000x (top right), 2000x (bottom left), 5000x (bottom right)

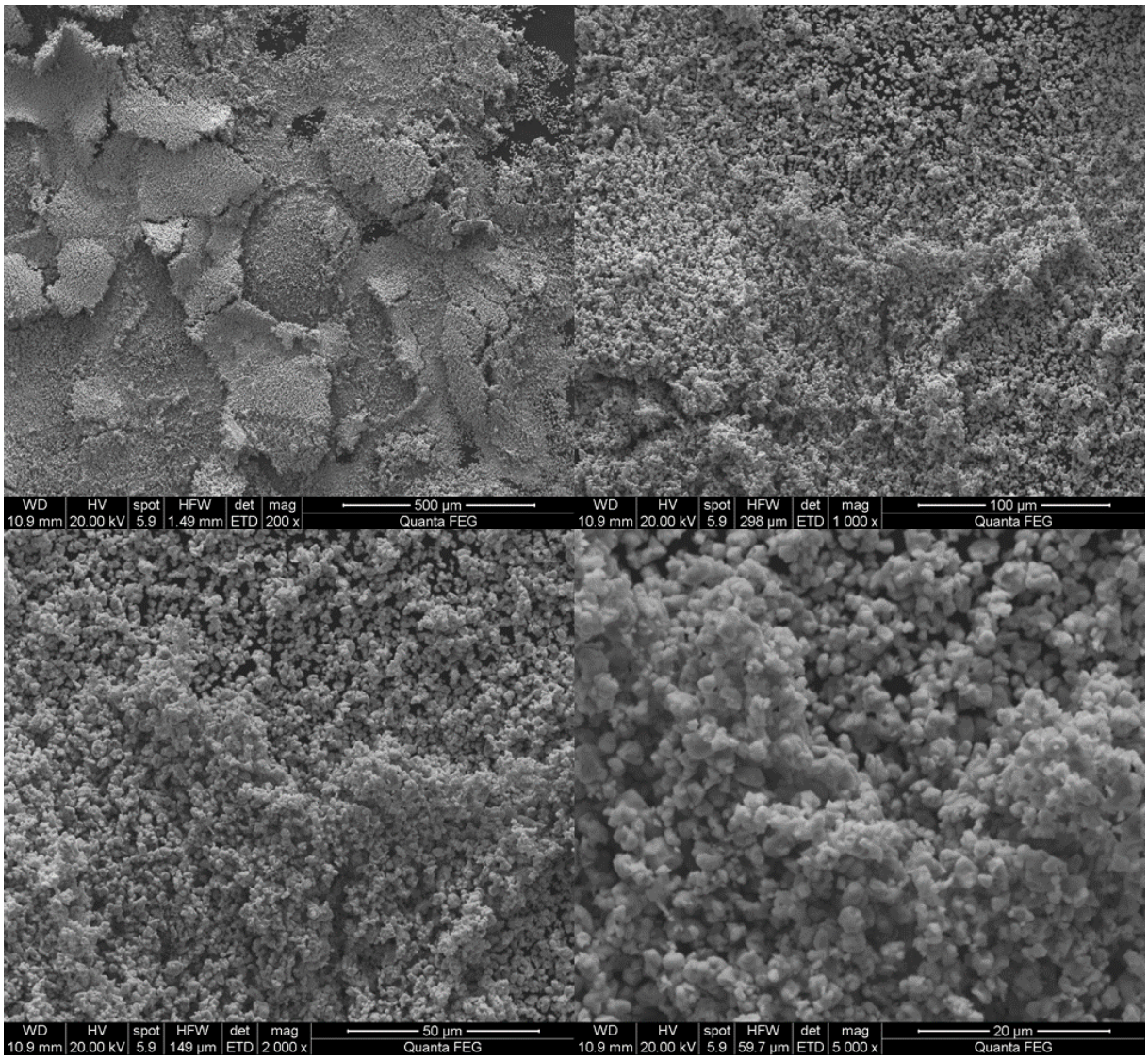

Figure 17: Used Mo_2C powder, SEM, 200x (top left), 1000x (top right), 2000x (bottom left), 5000x (bottom right)

3.2 Pre-pressed samples

48 pre-pressed samples were obtained from Miba AG. There were 4 different compositions (see Table 2), 12 samples per composition.

Table 2: Composition of pre-pressed samples from Miba

Sample number Miba	Composition /wt%
23005	Fe_0.85Cr_0.15Mo + 4 % MA1 + 0,75 % C
23007	Fe_0.85Cr_0.15Mo + 4 % MA2 + 0,75 % C
23010	Fe_0.85Mo + 4 % MA1 + 0,70 % C
23012	Fe_0.85Mo + 4 % MA2 + 0,70 % C

The 2 MA´s and the C were the same as described in Table 1. To all sample compositions 0,6 wt% of EBS was added. The compositions were mixed in a double-cone mixer. First the pre-alloyed base powders and MA´s were mixed for 5 min and then the C and wax was added and mixed for 5 min again.

Both powder mixtures were pressed into Charpy impact bars with dimensions of 10 x 10 x 100 mm. All 36 samples from 23005, 23007 and 23010 were pressed to a density of 7,04 g/cm^3. The 12 samples from 23012 were pressed to a density of 7,05 g/cm^3.

3.3 “In-house” mixing and pressing

36 samples with Mo admixed as Mo_2C were produced. For that 2 compositions were prepared. A plain ferrous base powder was mixed with the same MA´s and C that the pre-pressed samples were prepared with. The sample mixtures were calculated to yield a Mo content of 0,5 wt%. The compositions are listed in Table 3.

Table 3: Samples containing admixed Mo_2C

Powder mixture	Composition /wt%
Fe + Mo_2C + MA1	Fe + 4 % MA1 + 0,5 % Mo_2C + 0,75 % C
Fe + Mo_2C + MA2	Fe + 4 % MA2 + 0,5 % Mo_2C + 0,75 % C

Furthermore 2 compositions with a Mo-pre-alloyed base powder were prepared. Fe-0.45Mo base powder was mixed with the same MA´s and C. The compositions are listed in Table 4.

Table 4: Compositions of samples with Fe_0.45Mo

Powder mixture	Composition /wt%
Fe_0.45Mo + MA1	Fe_0.45Mo + 4 % MA1 + 0,75 % C
Fe_0.45Mo + MA2	Fe_0.45Mo + 4 % MA2 + 0,75 % C

To all sample compositions 0,6 wt% of EBS was added.

3.3.1 Mixing

The powder mixtures were prepared in polyethylene bottles. The bottles were filled to about one third and wire spirals were added. The mixing was carried out in a TURBULA Type T2F tumbling mixer. The mixing process was separated into 3 steps, which are described in Figure 18 .

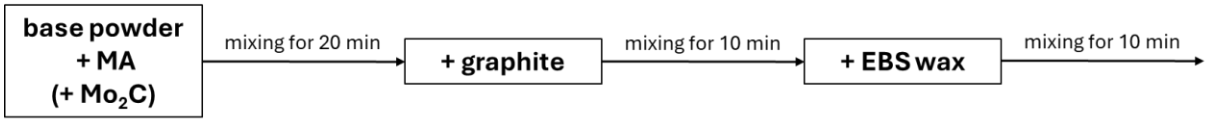

Figure 18: Mixing procedure

The exact weights for all sample compositions are listed in Table 5.

Table 5: Weights of sample compositions

Composition	Fe / g	Fe_0.45Mo / g	MA1 / g	MA2 / g	Mo_2C / g	C / g	EBS / g
Fe + Mo_2C + MA1	473,843	-	20	-	2,656	3,344	2,999
Fe + Mo_2C + MA1*	94,770		4	-	0,531	0,67	0,600
Fe + Mo_2C + MA2	473,844	-	-	20,007	2,654	3,007	2,997
Fe_0.45Mo + MA1	-	476,504	20,004	-	-	3,5	2,999
Fe_0.45Mo + MA2	-	476,5	-	20,003	-	3,502	3,005

*For the composition Mo_2C + MA1 a second, smaller batch was also mixed.

3.3.2 Pressing

All samples were compacted at the same pressure in a Jessernigg & Urban 150-ton hydraulic press. The samples were pressed with a tool for ISO 5754 Charpy impact bars with theoretical dimensions of 55,27 x 10,28 mm [78]. The samples were pressed for ~ 10 s with a pressure of 600 MPa (industry standard). The tool was overfilled with the powder mixtures and the excess powder was carefully wiped off to leave an even powder surface. The sample height varied around ~ 7 mm due to the different powder mixtures. After pressing the samples were deburred, numbered, weighed and the dimensions were measured with a slide gauge.

3.4 Consolidation of materials

3.4.1 Dewaxing

All produced samples and the pre-pressed samples from Miba were dewaxed in a push through tube furnace. The small furnace was designated as a dewaxing furnace. Dewaxing was carried out at 600 °C for 30 min in a N_2 atmosphere. The flow of N_2 was adjusted to ~ 4 L/min with a gas flow meter. Usually 8 samples, sometimes 4 were dewaxed together in a Mo sintering boat filled with sintering corundum granulate (type WFA F22). After dewaxing, the

samples were cooled in the water-jacketed cooling zone of the furnace under2 L/min N_2 for ~ 30 min.

3.4.2 Sintering

All produced samples and the pre-pressed samples from Miba were sintered in a push through tube furnace. The super alloy tube (Kanthal APM) was heated electrically by 6 SiC rods. The furnace was equipped with a water-jacketed cooling exit zone (Figure 22) and a gas quenching unit (Figure 23) at the entering zone. The temperature control unit was a EUROTHERM 2408. In this work 3 different sintering temperatures/profiles were realized: 1140 °C, 1180 °C and 1250 °C. The different sintering profiles are described in Figure 19, Figure 20 and Figure 21. At 1140 and 1180 °C sintering temperature the furnace was preheated to 600 °C. At 1250 °C the samples were pushed in directly at sintering temperature.

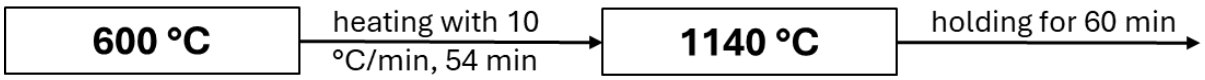

Figure 19: Sintering procedure for 1140 °C sintering temperature

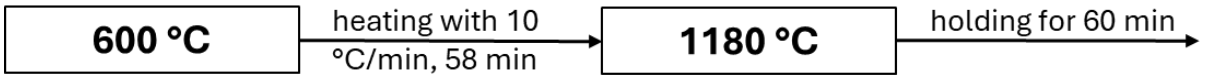

Figure 20: Sintering procedure for 1180 °C sintering temperature

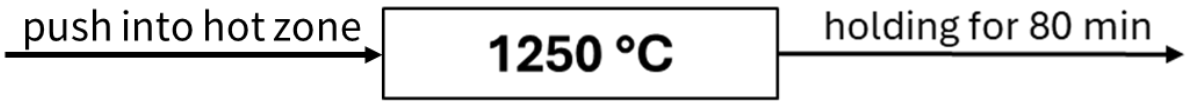

Figure 21: Sintering procedure for 1250 °C sintering temperature

Usually, 6 samples were sintered together in a Mo sintering boat filled with sintering corundum granulate (type WFA F22). It was ensured that for each sinter round the combined weight of the boat, the granulate and the samples was the same (~300 g). As a sintering intensity control 2 ceramic PTCR - LTH rings were added to every sintering round, they were put directly on the samples. The samples were pushed in the middle of the heated furnace with a maximum N_2 counterflow (~20 L/min). The sintering atmosphere was a N_2:H_2 (90:10) mixture. The flows were adjusted to 4,5 L/min N_2 and 0,5 L/min H_2. 5 min before the end of a sintering round the H_2 gas flow was switched off and the N_2 gas flow was increased to ~20 L/min. In this N_2 counterflow the samples were pushed in the exit zone. The water flow in the jacket was switched on and the samples were cooled for 45 min under 2 L/min N_2. After sintering the diameter of the PTCR rings was measured to check the sintering intensity.

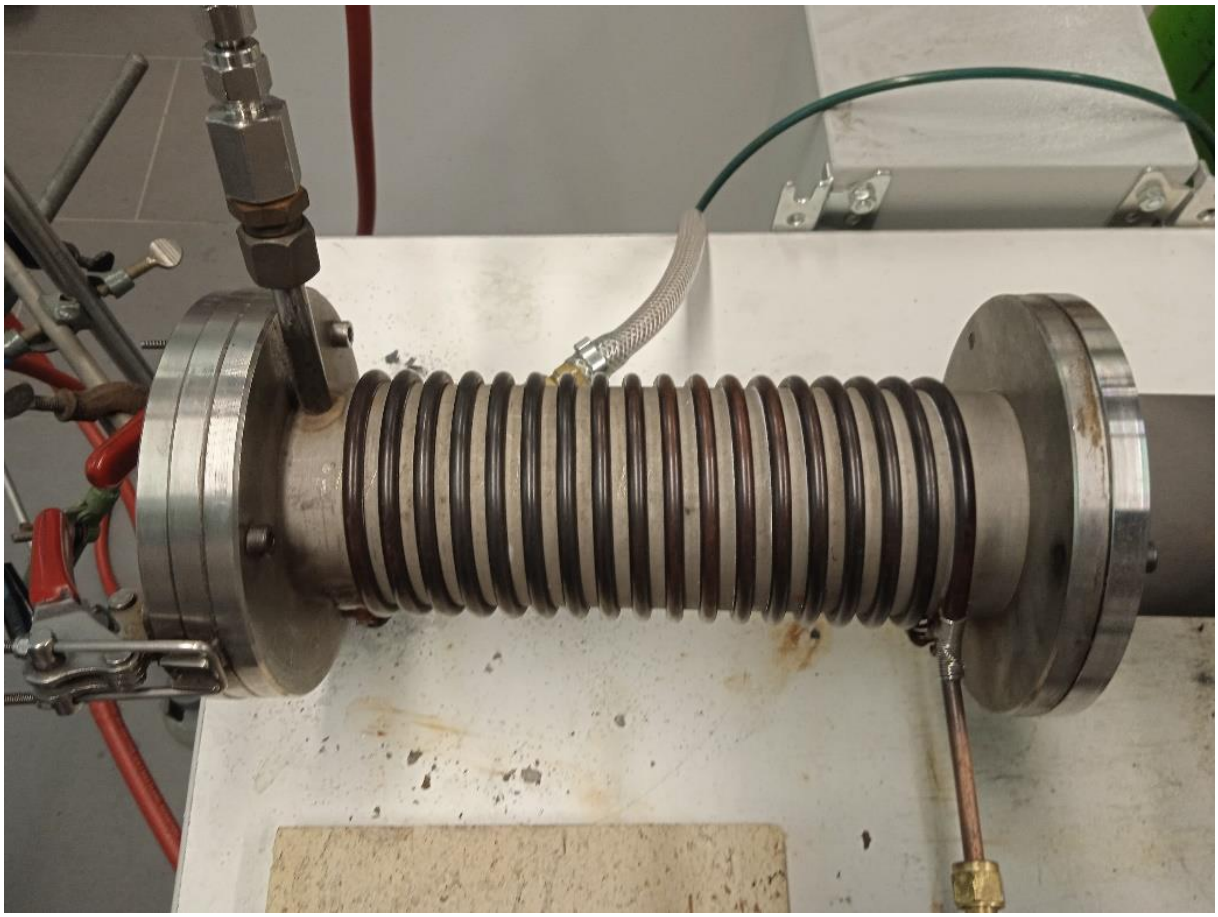

Figure 22: Water-jacketed exit zone of the sintering furnace

3.4.3 Sinter hardening

Some samples were sinter hardened after sintering. For that a special sintering boat with a long metal rod welded to it was used. Usually, 9 samples were hardened together in the special sintering boat filled with sintering corundum granulate (type WFA F22). It was ensured, if possible, that for each sinter round the combined weight of the boat, the granulate and the samples was the same. The samples were austenized at 1100 °C for 30 min under a 5 L/min N_2 flow in the sintering push through tube furnace. After austenizing the boat was pulled into the gas quenching unit in the entering zone with the rod. Simultaneously the gas quenching unit was flooded with a gas flow of 65 L/min N_2 for 8 min. The linearized cooling rate for this gas flow is ~3 K/s. After sinter hardening the samples were taken out of the furnace under a strong N_2 counterflow (~20 L/min).

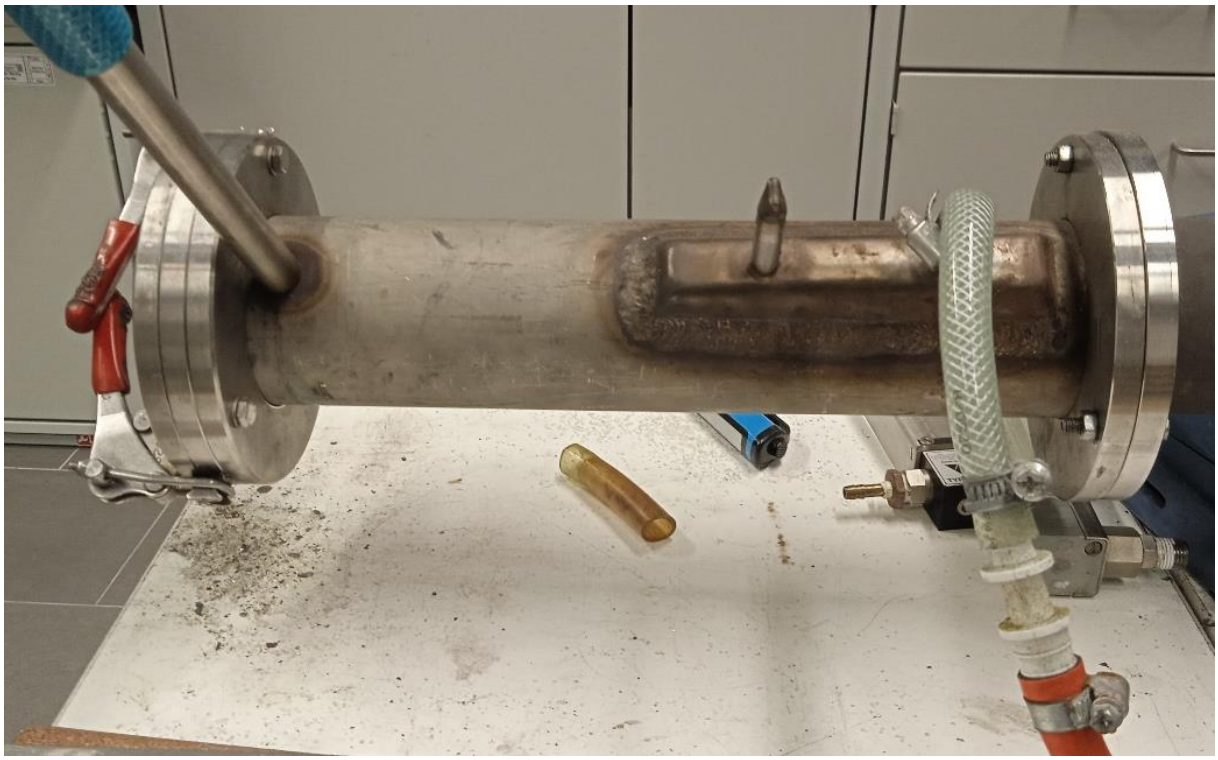

Figure 23: Gas quenching unit at the entering zone of the sintering furnace

3.4.4 Tempering

Sinter hardened steels are usually subjected to a heat treatment referred to as tempering. While tempering the supersaturated martensite releases carbon which forms iron and alloy carbides The toughness of the steel is increased while the strength and hardness is lowered during tempering [33]. Some samples were tempered after sinter hardening. Tempering was carried out in the small push through furnace that was used for dewaxing. 9 samples were put together in a Mo sintering boat filled with sintering corundum granulate (type WFA F22). The samples were tempered at 180 °C for 60 min in a N_2 flow of 2 L/min. After tempering the samples were cooled in the water-jacketed cooling zone of the furnace under 2 L/min N_2 for ~ 15 min.

3.5 Sample overview

Because of the different sample compositions, sintering temperatures and heat treatments an overview of all samples is provided in Table 6. For each sample number 3 individual samples were produced. Then these samples were sintered and treated equally, therefore each sample in was a triplicate. In Table 6 sample numbers with a Mi were the pre-pressed samples from Miba, sample numbers with a Mo were the ones where Mo_2C was admixed and sample numbers with a As were the ones prepared with the Fe_45Mo as base powder. Heat treatment SH means sinter hardened, and heat treatment T means tempered. The exact compositions of the sample mixtures are listed in Table 2, Table 3 and Table 4.

Table 6: Sample overview

Sample number	Base powder	MA	Sintering temperature / °C	Heat treatment
Mi1	Pre-alloyed Fe_0.85Cr_0.15Mo	MA1	1140	SH + T
Mi2			1250	-
Mi3				SH
Mi4				SH + T
Mi5		MA2	1140	SH + T
Mi6			1250	-
Mi7				SH
Mi8				SH + T
Mi9	Pre-alloyed Fe_0.85Mo	MA1	1140	SH + T
Mi10			1250	-
Mi11				SH
Mi12				SH + T
Mi13		MA2	1140	SH + T
Mi14			1250	-
Mi15				SH
Mi16				SH + T
Mo1	Plain Fe admixed with Mo_2C	MA1	1140	-
Mo2				SH + T
Mo3			1180	-
Mo4				SH + T
Mo5			1250	-
Mo6				SH + T
Mo7		MA2	1140	-
Mo8				SH + T
Mo9			1180	-
Mo10				SH + T
Mo11			1250	-
Mo12				SH + T
As1	Pre-alloyed Fe_0.45Mo	MA1	1140	SH + T
As2			1250	
As3		MA2	1140	
As4			1250	

3.6 Samples characterization

3.6.1 Green density

The density of the green samples was determined geometrically for all self-pressed samples. The length l, width b and height h were measured with a slide gauge (Mitutoyo, 505-732). The mass of the green samples m_{green} was determined with a MettlerToledo XS204 DeltaRange automatic scale. The green density ρ_{green} was then calculated according to Equation 1.

Equation 1: Green density

$$\rho_{green} = \frac{m_{green}}{l * b * h}$$

3.6.2 Impact energy

The impact energy IE of the sintered/sintered and heat treated samples was measured according to ISO 5754 [78]. The height h and the width b of the unnotched impact samples were measured before fracturing. The absolute impact energy IE_{abs} was measured with a Charpy impact testing machine, a 50 J pendulum hammer (Wolpert Probat) and then related to the cross section according to Equation 2.

Equation 2: Impact energy

$$IE = \frac{IE_{abs}}{h * b}$$

The Charpy impact test is a simple test. It shows a good "engineering" correlation with fracture toughness, which is a complicated test, for some notched samples [79]. The physical principle of the Charpy impact energy test is the same for notched and unnotched samples. The difference is that unnotched samples take more energy to be fractured than notched samples [80]. Therefore, the impact energy of the unnotched samples is considered as an indicator for the sample toughness in this work.

3.6.3 Sintered density

To obtain the sintered density of the samples their Archimedes density measured. A small piece (~5 x 10 x 10 mm) was cut out of each fractured impact energy sample. The samples were cut in a Struers Labotom-5 with a Struers 54A25 Cut-off Wheel. The cut-out pieces were then deburred, rinsed with water und cleaned in 2-propanol (p.a. ≥99,8% (GC), Sigma-Aldrich) in an ultrasonic bath (Bandelin Sonorex). After cleaning the pieces were dried and impregnated with paraffin. For impregnation the pieces were submerged in a paraffin-cyclohexanol mixture (1:100) for ~ 60 s and then dried overnight. To calculate the sintered density $\rho_{sintered}$ each impregnated piece was weighed to obtain their mass under air m_{air} and then submerged and weighed under water (m_{water}). The temperature of the water was measured and the respective water density ρ_{H2O} was looked up in an online table [81]. The sintered density for each sample piece was then calculated from Equation 3.

Equation 3: Sintered density archimedes

$$\rho_{sintered} = \frac{m_{air}}{m_{air} - m_{water}} * \rho_{H2O}$$

3.6.4 Dimensional change

As the length l was measured geometrically for all self-pressed samples before (l_{green}) and after ($l_{sintered}$) sintering the dimensional change in length in percent was calculated for those samples from Equation 4. A positive value for the dimensional change means an expansion in length and a negative value a contraction.

Equation 4: Dimensional change

$$Dimensional\ change = \left(\frac{l_{sintered} - l_{green}}{l_{green}}\right) * 100$$

3.6.5 Sample embedding

For the hardness measurements and metallography all samples had to be embedded. For that a small piece (~5 x 10 x 10 mm) of each sample was cut out of the fractured pieces from the impact test and cleaned to be embedded. The pieces were cut/embedded that way, so that the cutting surface was perpendicular to the pressing direction of the sample, see Figure 24 [82]

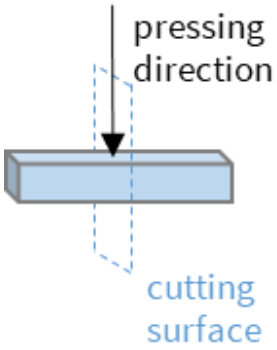

Figure 24: Cutting surface of the embedded samples [82]

Samples that were only sinter hardened were cold embedded in epoxy (Struers EpoFix) and cured overnight. All other samples (sintered, sinter hardened + tempered) were hot embedded in Bakelite (Struers MultiFast Brown) in a Struers CitoPress-1 at 180 °C/250 bar. The embedded samples were then grinded and polished in a Struers Tegramin-30. The grinding/polishing sequence was the same for all samples and is listed in Table 7.

Table 7: Grinding/polishing sequence

Step	Disc	Medium	Grain size / µm	Time / min
Grinding	Struers Piano 220	water	220	5
Polishing 1	Struers Allegro	DiaP. Lar 9, diamond suspension	9	10
Polishing 2	Struers Dac	DiaP. Dac3, diamond suspension	3	14
Polishing 3	Struers Nap	DiaDuo-2, diamond suspension	1	3

After each step the samples were rinsed with water, dried and cleaned with 2-propanol (p.a. ≥99,8% (GC), Sigma-Aldrich) in an ultrasonic bath. After being submerged in 2-propanol in the ultrasonic bath for a few minutes the samples were taken out, rinsed with fresh 2-propanol and thoroughly dried with a hair dryer (Grundig, 1800 W).

3.6.6 Hardness

The hardness measurements were carried out according to ISO 6507 [83]. For the macrohardness a Emco test M4U-025 was used to determine HV 30 (Vicker´s hardness with a force of 30 kg). In PM parts with residual porosity the macrohardness is also called apparent hardness since it is impossible not to include pores in the measurement. To examine individual microstructures the microhardness (HV 0,1, Vicker´s hardness with a force of 0,1 kg) was measured with a Ahotec ecoHARD XM 1270 A. The indentations of the macrohardness were made with the test device in the middle of the sample surfaces and measured with an optical microscope (Olympus GX51 microscope with an Olympus GX-TV0.7XC camera and Olympus BX3M-PSLED light). The microhardness indentations were measured directly on the test device. For macrohardness 5 indentations per sample were measured. The individual HV values were calculated according to Equation 5, where F is the force in kg (30 for HV 30 and 0,1 for HV 0,1) and a & b are the diagonals of the indentation in mm.

Equation 5: Vicker´s hardness

$$HV = 0{,}1891 * \frac{F * 9{,}81}{(\frac{a * b}{2})^2}$$

3.6.7 Metallography/microstructure

After the hardness measurements the microstructures of the polished, embedded samples were characterized. First pictures at different magnifications of the unetched samples were taken on the optical microscope to get an overview of the porosity of all samples. After that all samples were etched to visualize the microstructures. As an etching agent 1 %/ 3 % Nital (1 mL/ 3 mL HNO_3 in 100 mL methanol) was used. Etching was most effective when the etching agent was applied for a short time (~10 s), rinsed off with water and the sample was dried and the whole process repeated. Usually after 2-3 repetitions the desired etching intensity was achieved. From the etched samples pictures at different magnifications were taken on the optical microscope.

3.6.8 Scanning electron microscopy (SEM)

Selected embedded samples were inspected via SEM and energy-dispersive X-ray detection (EDX). In this representative samples the alloying element distribution was investigated. The samples were freshly polished (1 µm) to remove the etched surface. The used SEM was a FEI ESEM Quanta 200 with a W cathode. Measurements were carried out with an acceleration voltage of 20 keV. To obtain information of alloying element distribution the SEM was operated in backscatter electron (BSE) mode combined with EDX point analysis and mapping. The fracture surfaces of selected samples were scanned in secondary electron (SE) mode to obtain information about the fracturing mechanism. SEM pictures of the used powders were taken in SE mode. SE mode is generally better for topological information and BSE for element contrast [84].

4 Results and discussion

4.1 Pre-pressed samples

4.1.1 Microstructure

The microstructures of all pre-pressed samples were visualized by etching with 3 % Nital and representative microscopic pictures are shown and discussed in the following figures. The microstructures of the samples are complex mixtures of different phases. Ferrite, perlite, bainite, and martensite as well as undissolved MA particles occurred as phases in the microstructures.

The general order of processes during sintering in the investigated PM steel system is as follows: C is rapidly dissolved right after the α-γ transition [42], so for the investigated steel samples above 700 °C. This dissolved C can then form carbides with Cr and Mo, if these alloying elements are present. If these carbides are formed, they need to be dissolved so that the alloying elements can give the desired effects in the steel [55]. At roughly the same temperature (~ 700 °C) the homogenization of Mn due to Mn vapour formation starts [85]. Due to its high vapour pressure Mn is the only common metal alloying element PM steels where gas phase transport is an important transport mechanism [55]. At higher temperatures the MA´s are melting and forming a transient liquid phase [4], [6], [86]. This liquid phase is extremely important for the homogenization of alloying elements that are present as carbides at these temperatures (Mo, Cr). Therefore, the formation and distribution of this liquid phase is crucial to the distribution of alloying elements, but there needs to be differentiated between pre-alloyed and plain ferrous base powders. While the alloying elements in pre-alloyed base powders are already distributed in the ferrous base powder, alloying elements admixed (as elemental powders or carbides) are not. Admixed powders need to be dissolved to be distributed into the plain ferrous base powder. Therefore, the formation of a transient liquid phase during sintering is necessary to distribute admixed alloying elements, especially if they are present as carbides with a high melting point.

In Figure 25 the obtained microstructures of the prepressed samples with Fe_0.85Cr_0.15Mo after Nital etching are shown at 200x magnification. The as sintered samples sintered at 1250 °C showed a mixture of martensite, bainite, perlite and ferrite. The lighter white-grey regions are a mixture of ferrite and very fine laminar pearlite. These regions most likely resemble the cores of the base powder particles. Thie lighter brownish regions are martensite, and the dark regions are bainite, but the two are hard to differentiate for some samples, especially when the samples are slightly over etched. These phases can only form in regions where the alloying content was high enough at the given cooling rates, hence around the dissolved MA particles. After sinter hardening the microstructure is mainly martensitic (light brown regions) with dark bainite inclusions or “islands”. After tempering the samples sintered at 1250 °C the martensitic microstructure appears more refined and homogeneous. There seems to be less ferrite and pearlite after tempering. Also, ferrite forms inside of the bainite islands. The feathery appearance of the ferrite laths suggest that the inclusions are upper bainite. The sinter hardened and tempered samples that were sintered at 1140 °C show a similar combination of

phases as the sinter hardened and tempered samples sintered at 1250 °C. The amount of bainite island seems to be significantly higher in the samples sintered at 1140 °C and the microstructure appears less homogeneous in general compared to the samples sintered at 1250 °C. This is expectable as the transport mechanisms like diffusion and therefore the distribution of alloying elements are enhanced at higher temperatures. Also, there are undissolved particles (white) visible in the microstructure. Due to the size (roughly around 10 µm) of those undissolved particles, they were identified as MA particles. It can be assumed that those undissolved particles are remains of very big MA particles or agglomerates of many small MA particles that sintered together. Therefore, a sintering temperature of 1140 °C seems to be too low to sufficiently dissolve all components and homogenize the alloying elements in the microstructure. Both MA´s form comparable microstructures in the different treatments and sintering temperature.

Figure 26 shows the microstructures of the prepressed samples with Fe_0.85Mo after Nital etching at 200x magnification. The microstructures are similar to the ones observed in the samples with Fe_0.85Cr_0.15Mo: A mixture of martensite, bainite, perlite and ferrite in the as sintered samples. Martensite with bainite islands are formed after sinter hardening, which transform into upper bainite with ferrite after tempering. It is also evident, that with a sintering temperature of 1140 °C after sinter hardening and tempering not all components are sufficiently dissolved as there are undissolved MA particles in the microstructure. Also, the higher sintering temperature of 1250 °C leads to a more refined, homogeneous martensitic structure compared to the sinter hardened sample or the one sintered at lower temperature. As discussed in 2.2.2, Cr and Mo as alloying elements in steel have a few similarities. Both are α-Fe stabilizers, that increase hardenability in steel. Therefore, it makes sense that the same phases are formed in the microstructure. The main difference to the samples with Fe_0.85Cr_0.15Mo is, that in the samples that were sintered at 1140 °C significantly less undissolved MA particles could be found. This can probably be contributed to the “internal getter effect” of the Mn and Si in the MA´s. Theoretically the higher O content of the Fe_0.85Cr_0.15Mo combined with the “internal getter effect” in the MA´s could have led to the formation of stabilizing oxide layers around the MA particles and therefore less of them were dissolved.

The same microstructures are shown at 50x magnification in Figure 27 and Figure 28. Here it is evident, that a higher sintering temperature leads to a more refined martensitic microstructure with less bainite/ferrite inclusions and no more undissolved MA particles in the sinter hardened and tempered samples. Therefore, it can be said that a sintering temperature leads to significantly more homogeneous microstructures compared to 1140 °C.

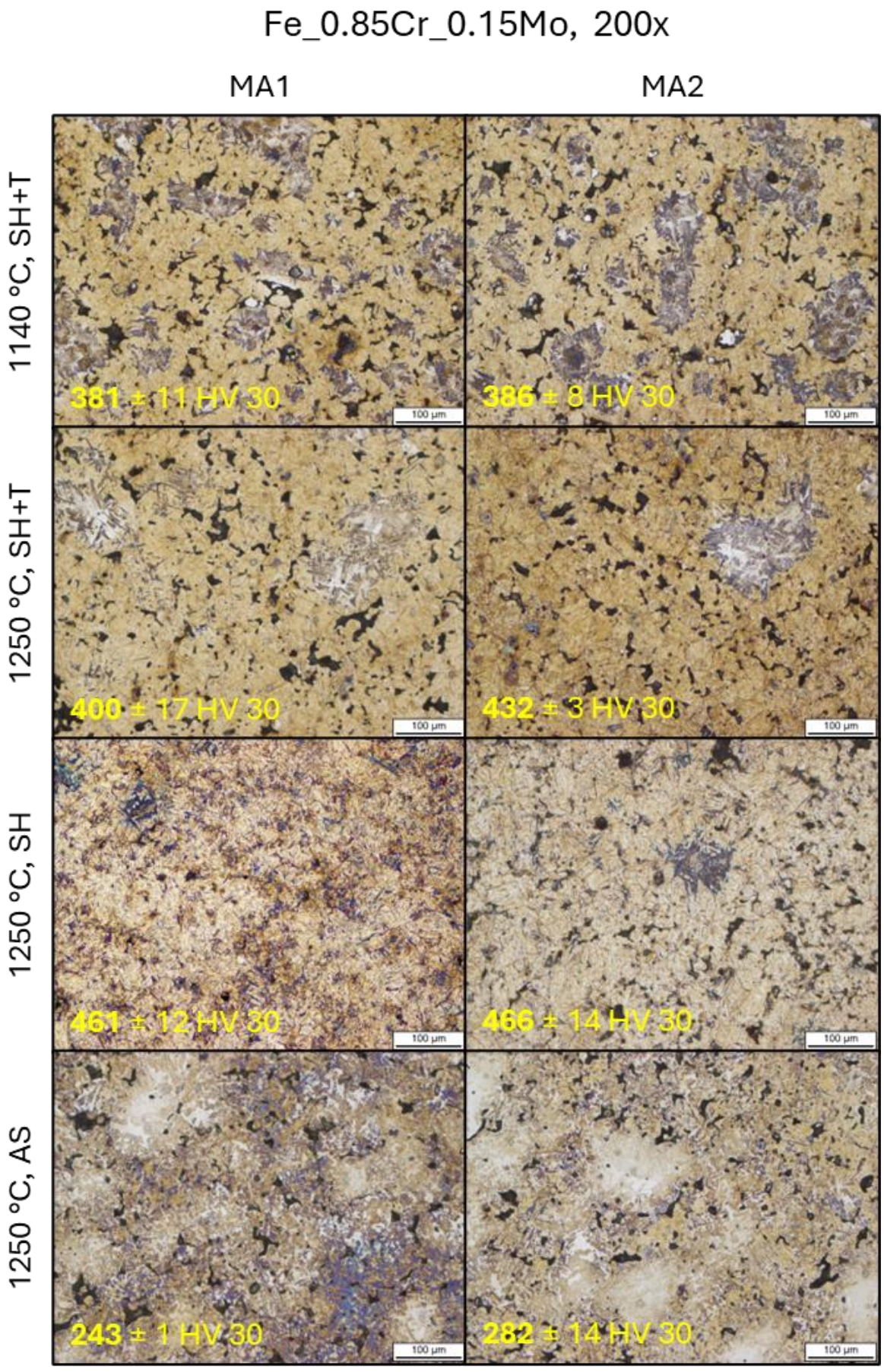

Figure 25: Nital-etched microstructures of the samples with Fe_0.85Cr_0.15Mo at 200x magnification

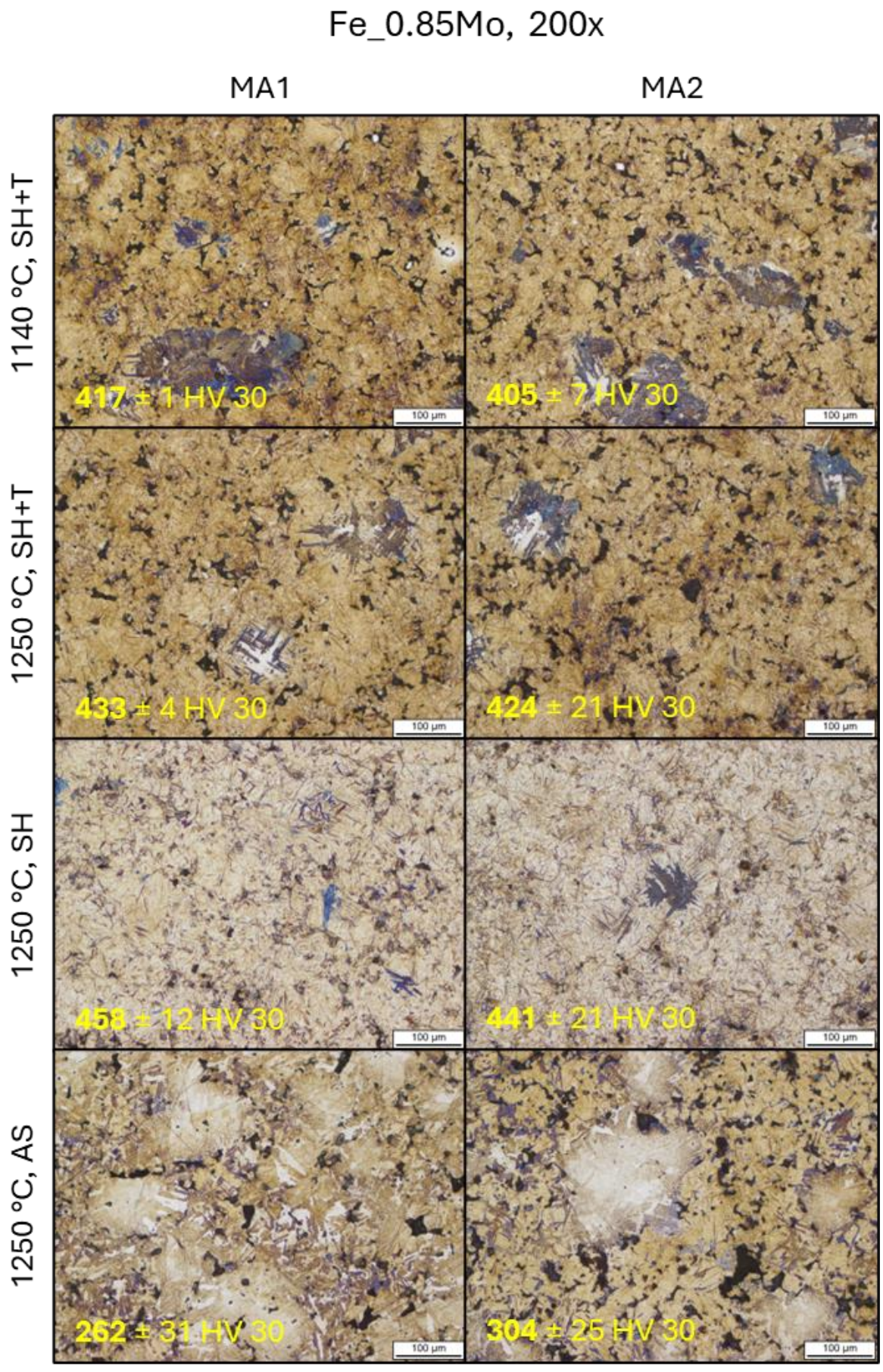

Figure 26: Nital-etched microstructures of the samples with Fe_0.85Mo at 200x magnification

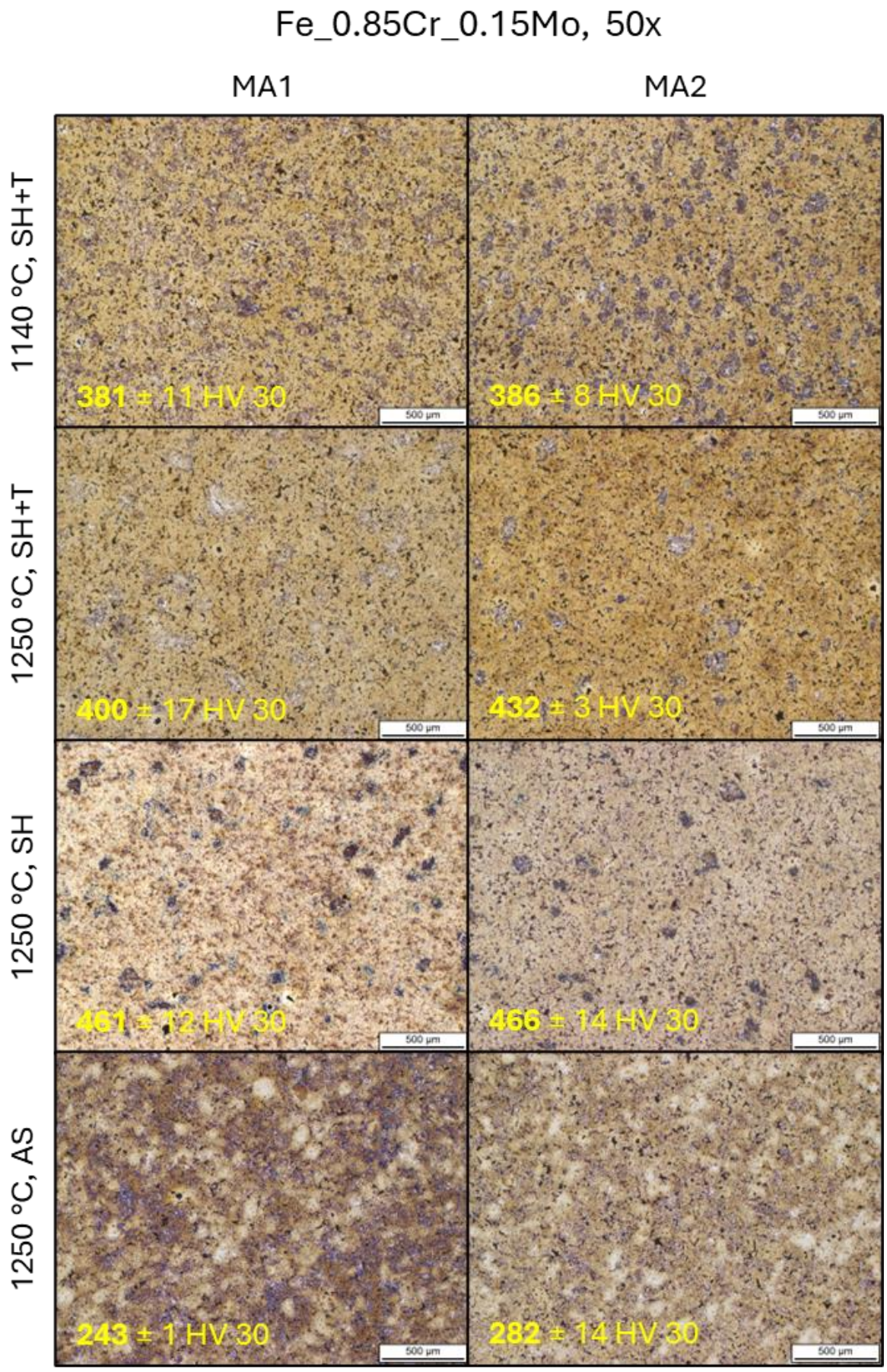

Figure 27: Nital-etched microstructures of the samples with Fe_0.85Cr_0.15Mo at 50x magnification

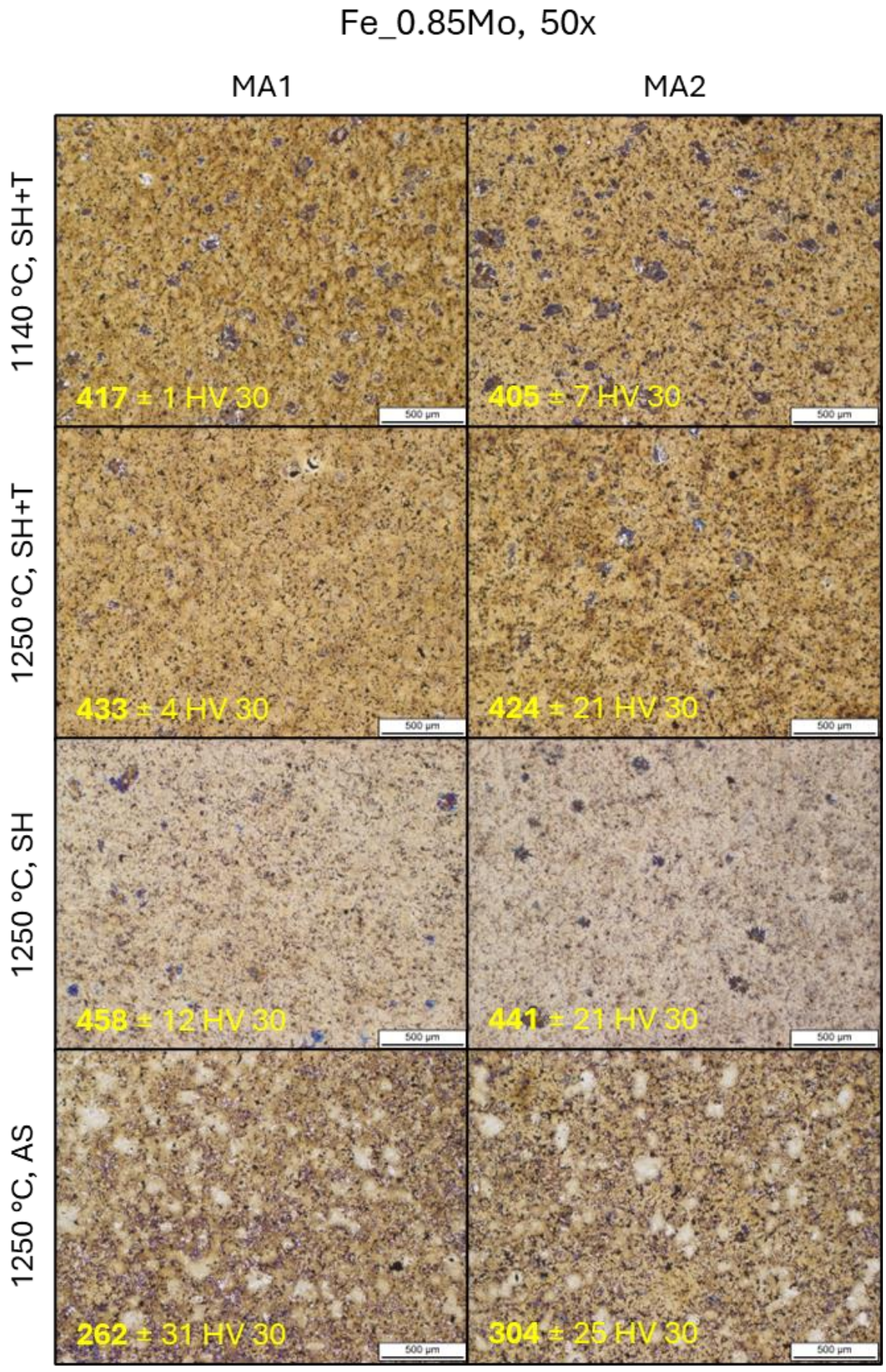

Figure 28: Nital-etched microstructures of the samples with Fe_0.85Mo at 50x magnification

4.1.2 Mechanical properties

For the pre-pressed samples, the green density was not measured. Samples Mi1-Mi12 were pressed to a green density of 7,04 g/cm^3, Mi13-Mi16 to a green density of 7,05 g/cm^3. Since the green samples were not measured also no dimensional change could be calculated. Also, the sintered density was determined geometrically, not via the Archimedes method. From each sample number all 3 individual samples were measured. For each sample 5 indentations were measured for the HV30 value. The values of the sintered density, impact energy and HV30 for the pre-pressed samples are listed in Table 8 (Fe_0.85Cr_0.15Mo) and Table 9 (Fe_0.85Mo).

Table 8: Mechanical properties of the pre-pressed samples with Fe_0.85Cr_0.15Mo as base powder

Sample number	Sample description	Density / g/cm^3		Impact energy / J/cm^2		HV 30	
		green	sintered	value	average	value	average
Mi1	Fe_0.85Cr_0.15Mo, MA1, 1140 °C, SH+T	7,04	**7,01** ± 0,03	13,3 10,3 7,4	**10** ± 3	369 390 383	**381** ± 11
Mi2	Fe_0.85Cr_0.15Mo, MA1, 1250 °C, AS	7,04	**7,02** ± 0,02	12,5 14,3 23,7	**17** ± 6	242 243 243	**243** ± 1
Mi3	Fe_0.85Cr_0.15Mo, MA1, 1250 °C, SH	7,04	**7,02** ± 0,03	10,5 8,6 16,3	**12** ± 4	464 448 471	**461** ± 12
Mi4	Fe_0.85Cr_0.15Mo, MA1, 1250 °C, SH+T	7,04	**7,01** ± 0,04	12,9 9,8 17,3	**13** ± 4	408 412 380	**400** ± 17
Mi5	Fe_0.85Cr_0.15Mo, MA2, 1140 °C, SH+T	7,04	**7,02** ± 0,02	8,7 7,8 9,7	**9** ± 1	388 377 393	**386** ± 8
Mi6	Fe_0.85Cr_0.15Mo, MA2, 1250 °C, AS	7,04	**7,03** ± 0,01	10,2 11,3 18,5	**13** ± 5	276 298 272	**282** ± 14
Mi7	Fe_0.85Cr_0.15Mo, MA2, 1250 °C, SH	7,04	**7,00** ± 0,03	8,7 7,8 8,4	**8** ± 1	457 483 459	**466** ± 14
Mi8	Fe_0.85Cr_0.15Mo, MA2, 1250 °C, SH+T	7,04	**7,03** ± 0,06	16,1 11,8 13,4	**14** ± 2	431 430 435	**432** ± 3

Table 9: Mechanical properties of the pre-pressed samples with Fe_0.85Mo as base powder

Sample number	Sample description	Density / g/cm³		Impact energy / J/cm²		HV 30	
		green	**sintered**	value	average	value	average
Mi9	Fe_0.85Mo, MA1, 1140 °C, SH+T	7,04	**7,05** ± 0,00	14,1 16,9 21,2	**17** ± 4	430 405 417	**417** ± 12
Mi10	Fe_0.85Mo, MA1, 1250 °C, AS	7,04	**7,04** ± 0,02	22,2 23,9 22,1	**23** ± 1	290 268 229	**262** ± 31
Mi11	Fe_0.85Mo, MA1, 1250 °C, SH	7,04	**7,01** ± 0,01	15,5 24,0 27,6	**22** ± 6	469 445 458	**458** ± 12
Mi12	Fe_0.85Mo, MA1, 1250 °C, SH+T	7,04	**7,02** ± 0,05	21,8 27,8 22,8	**24** ± 3	433 437 428	**433** ± 4
Mi13	Fe_0.85Mo, MA2, 1140 °C, SH+T	7,05	**7,00** ± 0,02	20,7 10,8 14,1	**15** ± 5	412 404 398	**405** ± 7
Mi14	Fe_0.85Mo, MA2, 1250 °C, AS	7,05	**7,01** ± 0,02	24,4 23,4 24,1	**24** ± 1	309 327 277	**304** ± 25
Mi15	Fe_0.85Mo, MA2, 1250 °C, SH	7,05	**7,01** ± 0,01	25,4 19,3 23,1	**23** ± 3	465 424 434	**441** ± 21
Mi16	Fe_0.85Mo, MA2, 1250 °C, SH+T	7,05	**7,02** ± 0,02	23,4 21,8 32,7	**26** ± 6	437 434 400	**424** ± 21

The sintered densities correspond to a relative density of 89-89,5 % compared to pure Fe. This would correlate to a porosity of ~10,5-11 %.

In Figure 29 the densities for the prepressed samples are compared. The green densities were not measured but obtained from Miba. The sintered densities range from 7 to 7,05 g/cm^3. There are no clear differences between the two MA´s. Also, no significant differences between the different heat treatments could be found. The differences in sintered densities are below 0,05 g/cm^3.

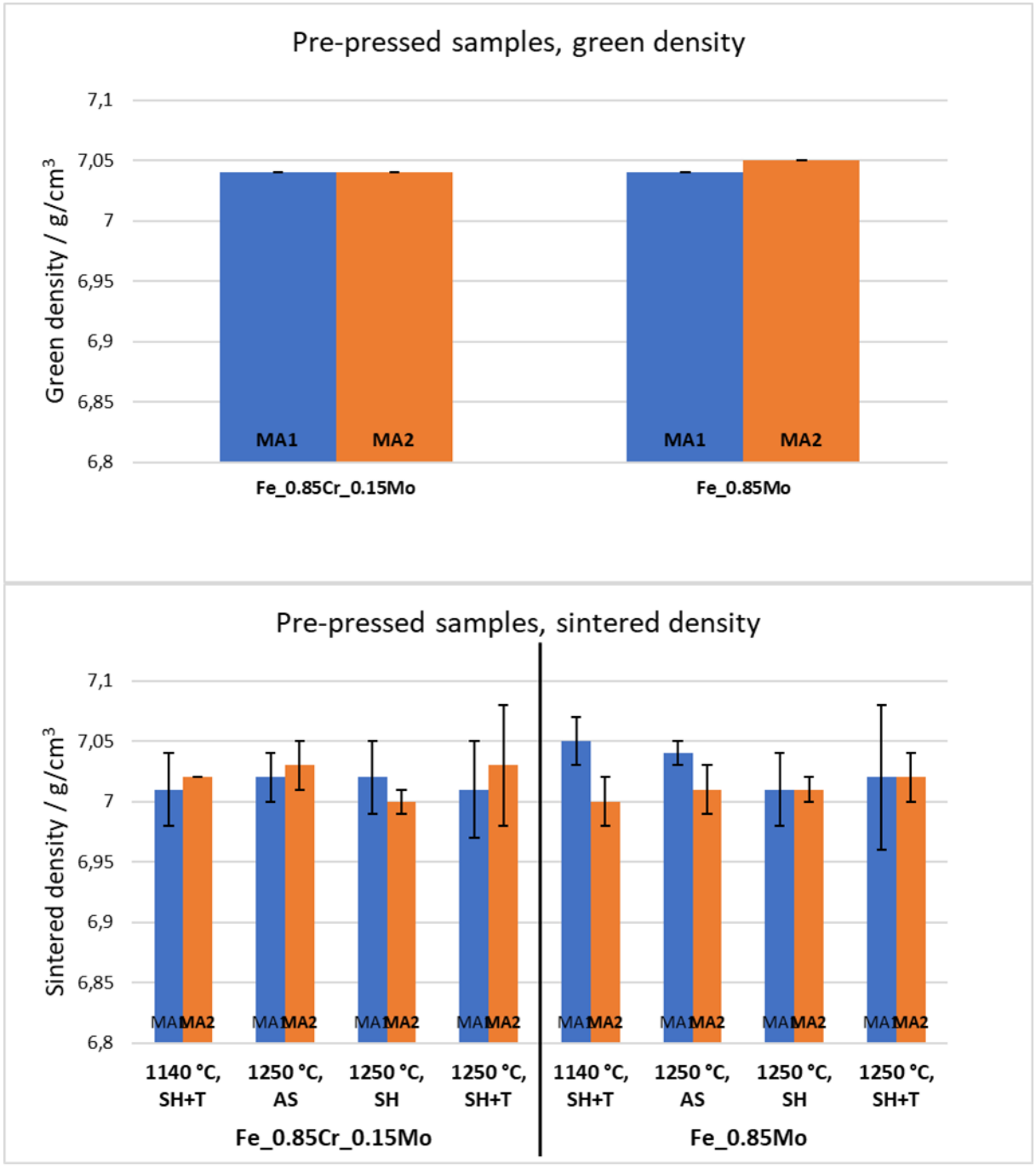

Figure 29: Green and sintered densities of the prepressed samples

The obtained HV30 and impact energy values for the sinter hardened and tempered samples are shown in Figure 30. Fe_0.85Mo as base powder leads to significantly higher impact energies and slightly higher hardness. The difference between the two base powders is that in Fe_0.85Cr_0.15Mo the O content is significantly higher than in the Fe_0.85Mo, see Table 1. The "internal getter effect" of the Cr in the base powder and Mn/Si in the MA´s combined with the presence of O in the powder could lead to the formation of oxides. These oxides impair the sintering contacts and would therefore lead to a lower impact energy while the hardness is not affected. This explanation also backed up by the microstructures as in undissolved MA particles were found. The higher O content of the Fe_0.85Cr_0.15Mo base powder is therefore the most likely explanation for the inferior impact energy values compared to the Fe_0.85Mo base powder. Geroldinger showed that the O content of the base powder is crucial for the effect of MA´s containing O sensitive elements [87]. There is no clear difference between the two MA´s in hardness or impact energy. MA2 seems to lead to higher hardness for the samples with Fe_0.85Cr_0.15Mo as base powder but this tendency is inversed for the samples with Fe_0.85Mo as base powder. The only difference between the two MA´s that more undissolved MA particles were found in the samples with MA2. This is most likely explained by the higher O content of the MA2 compared to MA 1 (see Table 1). The "internal getter effect" of Mn and Si on the MA´s probably led to the formation of an oxide layer around the MA particles that prevented full dissolution at lower sintering temperatures. The samples sintered at 1250 °C show significantly higher impact energies and comparable hardness values compared to the ones sintered at 1140 °C. The significant difference in impact energy can be attributed to the better distribution of alloying elements due to enhanced diffusion and the formation of more spherical porosity at higher temperatures. The enhancing effect of the sintering temperature is more significant in the samples with Fe_0.85Mo. The Fe_0.85Cr_0.15Mo has a higher O content and a higher content of O sensitive elements (Cr). This suggests that the sintering conditions are not enough for a satisfactory reduction of Cr oxides at 1250 °C.

In Figure 31 the mechanical properties of the prepressed samples sintered at 1250 °C are compared. Here the impact of the different heat treatments becomes evident. The as sintered samples have a low hardness and good impact energies. After sinter hardening the hardness in drastically improved from ~250 HV 30 to~450 HV30 and the impact energy is slightly lowered. Tempering then raises the impact energy to the level it was as sintered or slightly higher while the hardness slightly decreases again. Therefore, the combination of sinter hardening with tempering at a higher sintering temperature leads to the best combination of mechanical properties for the pre-pressed samples. Those effects of the treatments are similar with both MA´s. There is no trend to higher hardness with a particular MA. The effects are also similar for both base powders. The impact energy values are not dramatically affected by sinter hardening and tempering. But the values for the impact energy must be viewed with caution as there is a considerable distribution between the individual values for some samples. This results in a large standard derivation (up to ~6 J/cm^2) for those samples. There are no significant differences between the two MA´s in impact energy. The impact energy remarkably increases with Fe_0.85Mo as base powder, most likely due to the lower O content of the powder.

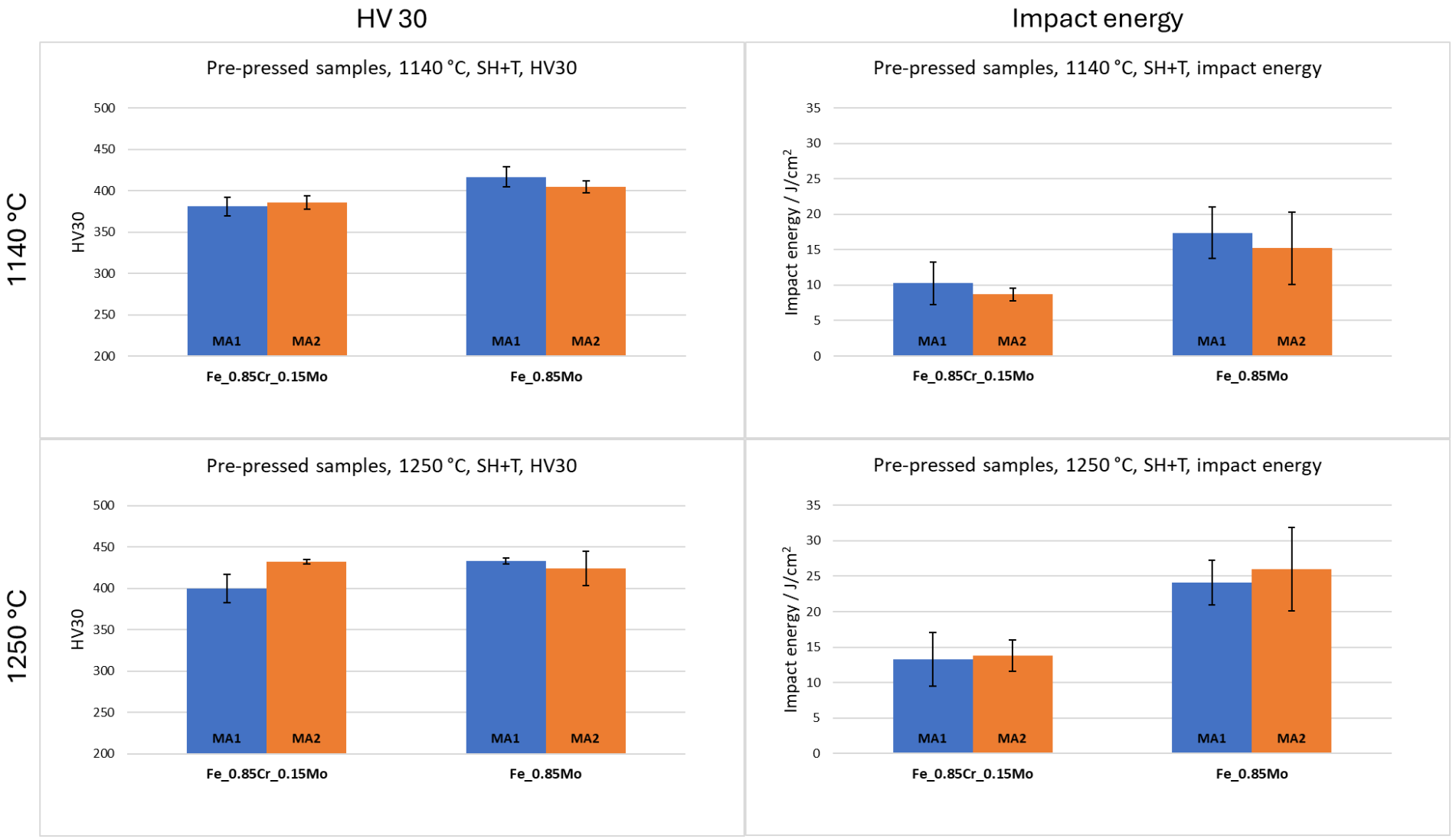

Figure 30: Mechanical properties of the prepressed samples

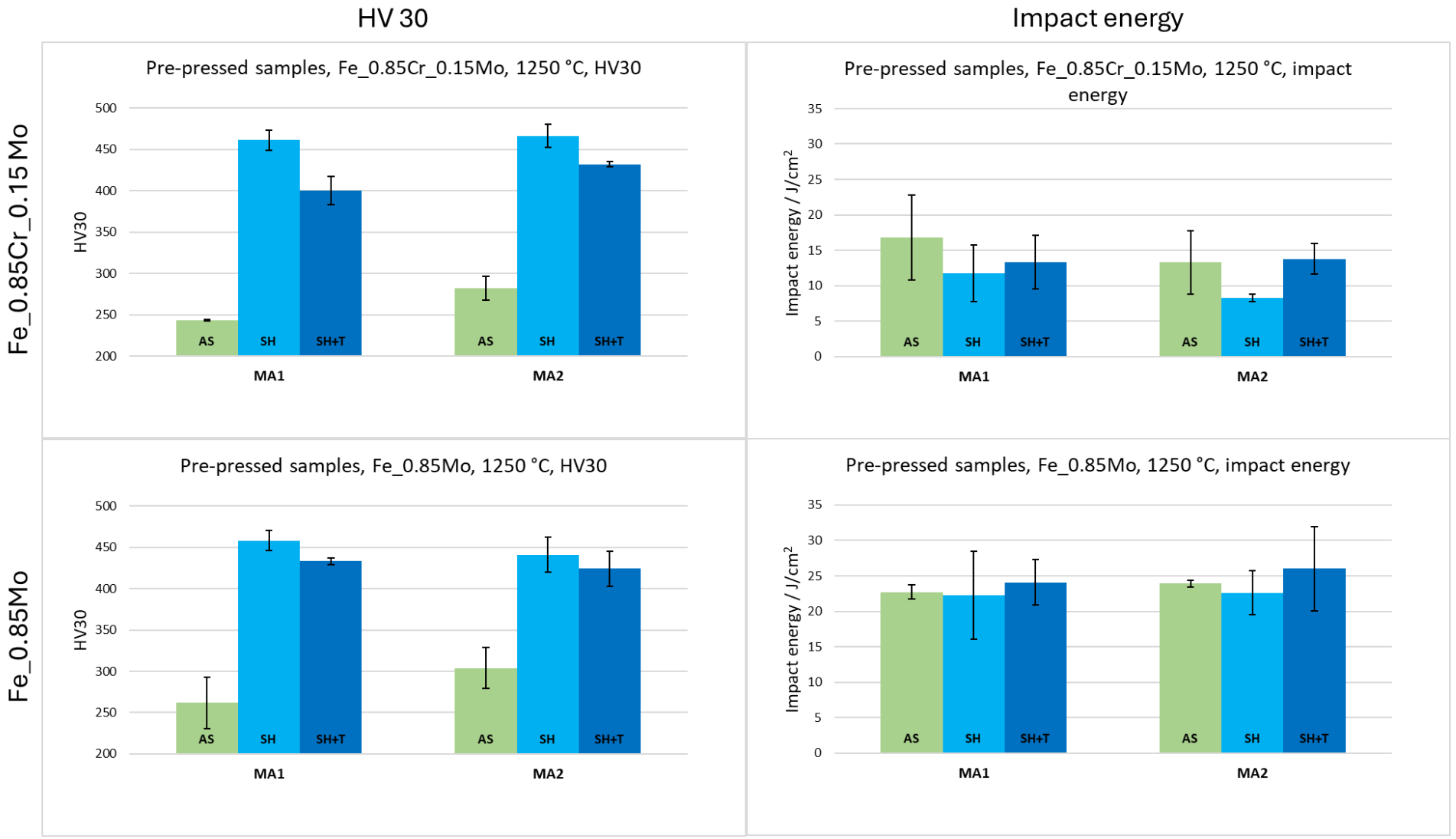

Figure 31: Comparison of the mechanical properties of the prepressed samples sintered at 1250 °C

The following figures compare the different sample compositions with the same sintering temperatures and heat treatments. Figure 32 shows the mechanical properties of the as sintered samples sintered at 1250 °C, Figure 33 the sinter hardened at 1250 °C, Figure 34 the sinter hardened and tempered at 1250 °C and Figure 35 the sinter hardened samples sintered at 1140 °C. It is apparent for all sintering temperatures and treatments, the samples with Fe_0.85Mo as base powder show similar hardness but considerably higher impact energies compared to the samples with Fe_0.85Cr_0.15Mo as base powder. All samples with Fe_0.85Mo show significantly higher impact energy and comparable or even higher hardness than the equivalently sintered and treated samples with Fe_0.85Cr_0.15Mo. The O content of the base powder is most likely the explanation for the difference in impact energy as already discussed. The slightly higher hardness in the samples with Fe_0.85Mo could be the higher Mo content.

The sinter hardened and tempered samples sintered at 1140 °C show lower impact energies but comparable hardness to the equivalent samples sintered at 1250 °C. This suggests a good distribution and therefore an efficient use of alloying elements, stronger sintering contacts and the presence of more rounded porosity. However, the non-complete reduction of oxides leads to lower impact energies. This is also supported by the presence of undissolved MA particles in the microstructures of those samples, see 4.1.1.

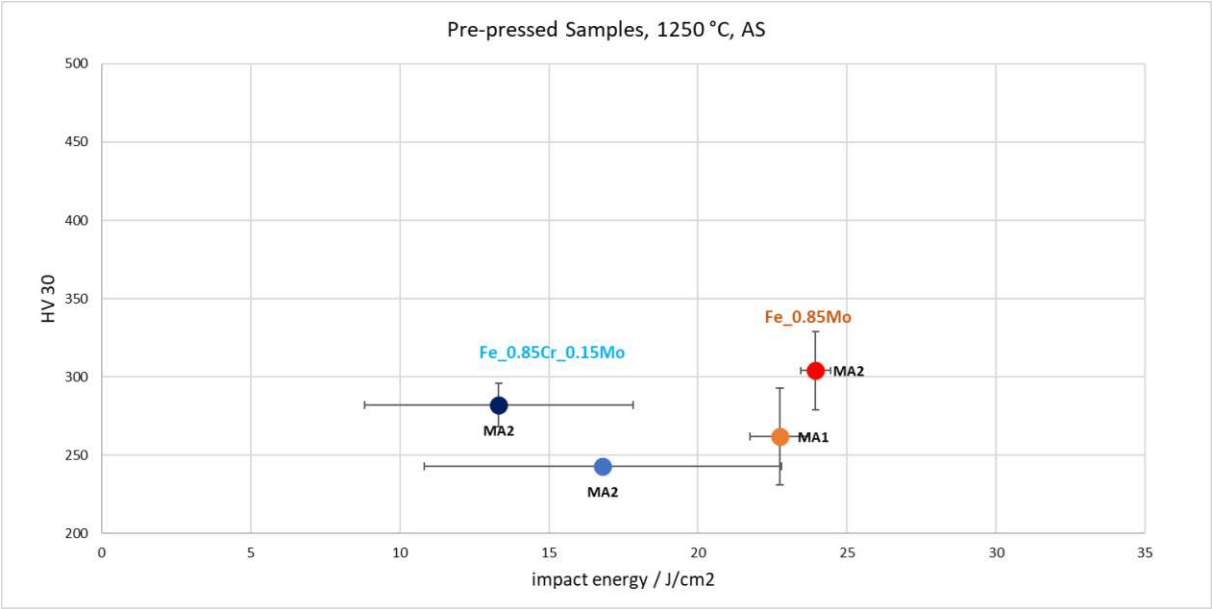

Figure 32: Comparison of mechanical properties of pre-pressed samples sintered at 1250 °C, as sintered

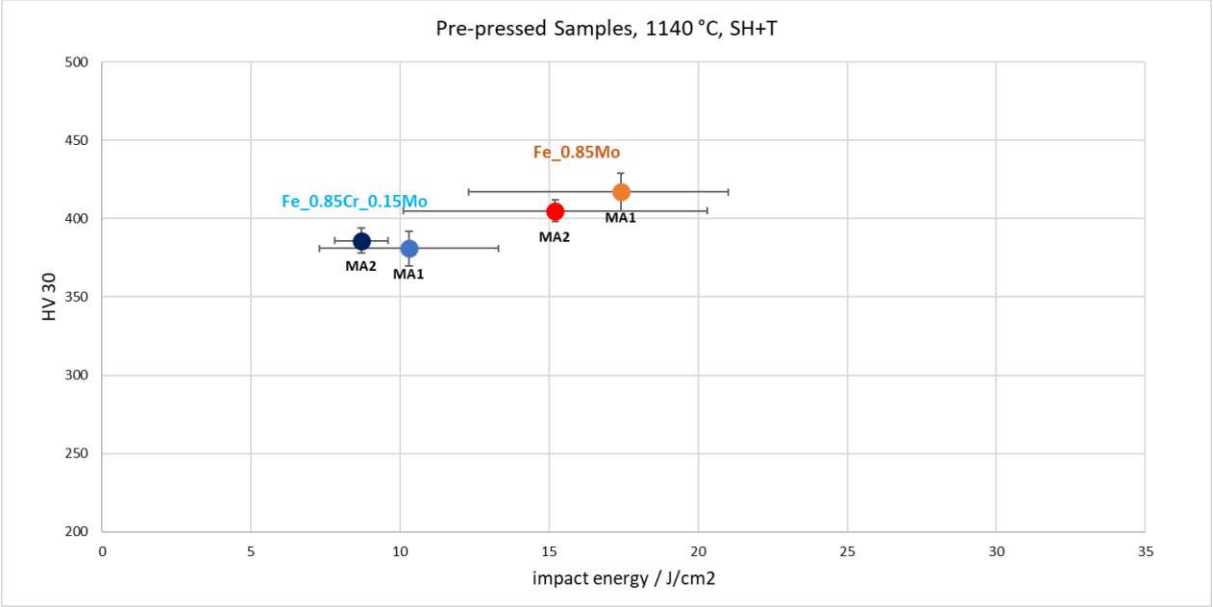

Figure 33: Comparison of mechanical properties of pre-pressed samples sintered at 1250 °C, sinter hardened

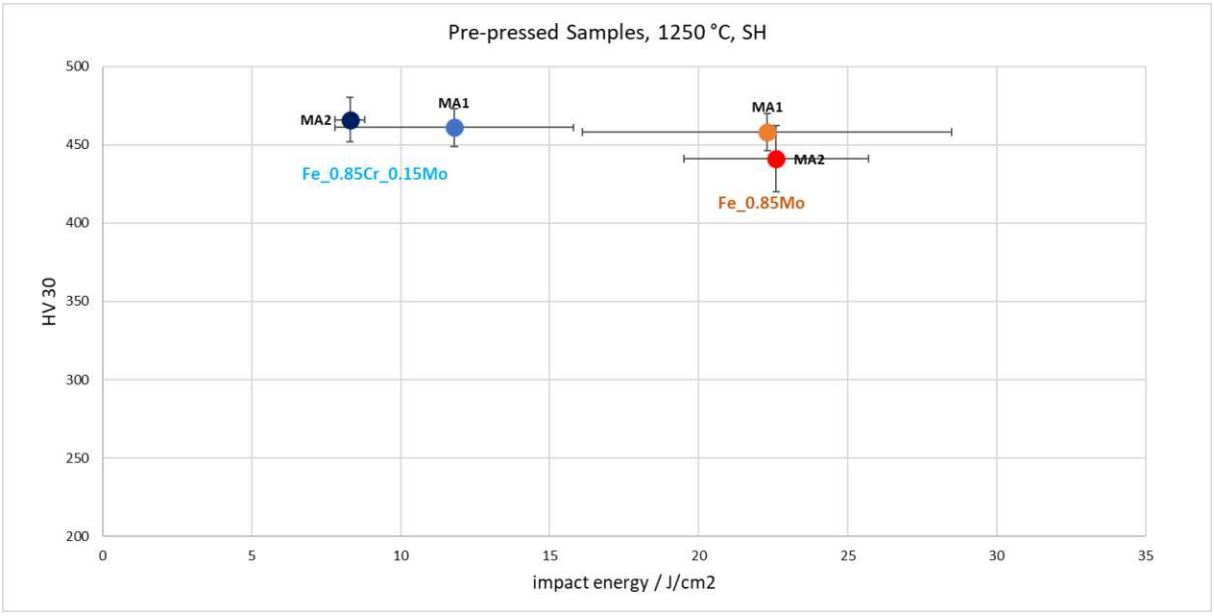

Figure 34: Comparison of mechanical properties of pre-pressed samples sintered at 1250 °C, sinter hardened and tempered

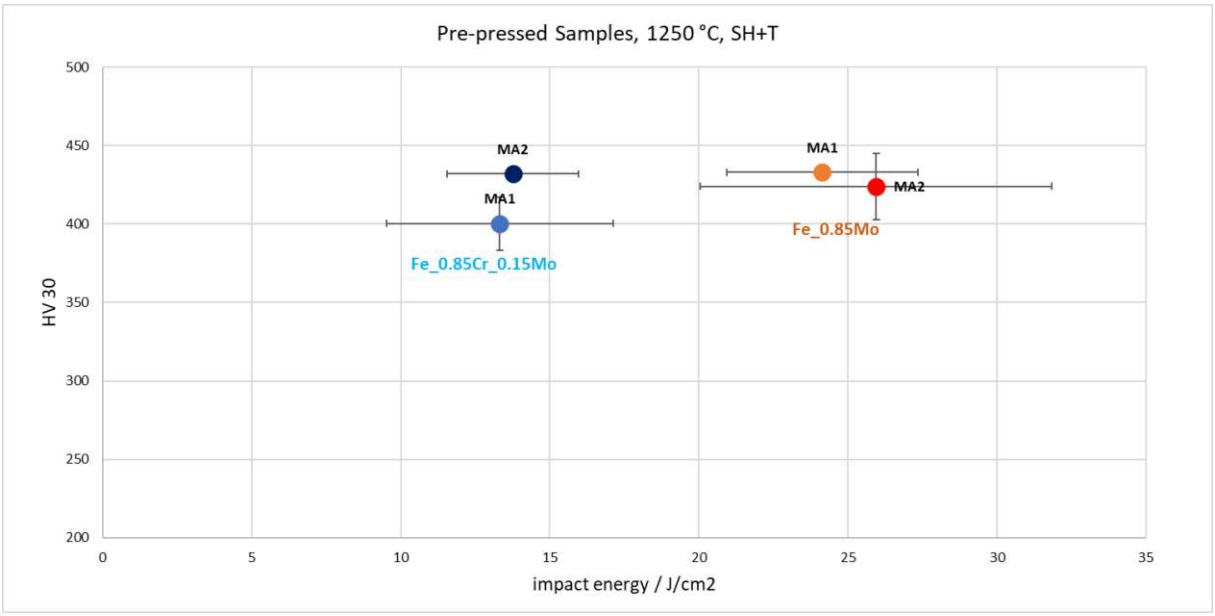

Figure 35: Comparison of mechanical properties of pre-pressed samples sintered at 1140 °C, sinter hardened and tempered

4.2 Mo-admixed samples

4.2.1 Microstructure

The microstructures of all Mo-admixed samples were visualized by etching with 3 % Nital and representative microscopic pictures are shown and discussed in the following figures. The microstructures of the samples are complex mixtures of different phases. Ferrite, pearlite, bainite, and martensite were found in the microstructures. Also undissolved MA particles were found, but only with MA2.

The general order of processes during sintering in the investigated PM steel system is as follows: C is rapidly dissolved right after the α-γ transition [42], so for the investigated steel samples above 700 °C. This dissolved C can then form carbides with Cr and Mo, if these alloying elements are present. If these carbides are formed, they need to be dissolved so that the alloying elements can give the desired effects in the steel [55]. At roughly the same temperature (~ 700 °C) the homogenization of Mn due to Mn vapour formation starts [85]. Due to its high vapour pressure Mn is the only common metal alloying element PM steels where gas phase transport is an important transport mechanism [55]. At higher temperatures the MA´s are melting and forming a transient liquid phase [4], [6], [86]. This liquid phase is extremely important for the homogenization of alloying elements that are present as carbides at these temperatures (Mo, Cr). Therefore, the formation and distribution of this liquid phase is crucial to the distribution of alloying elements, but there needs to be differentiated between pre-alloyed and plain ferrous base powders. While the alloying elements in pre-alloyed base powders are already distributed in the ferrous base powder, alloying elements admixed (as elemental powders or carbides) are not. Admixed powders need to be dissolved to be distributed into the plain ferrous base powder. Therefore, the formation of a transient liquid phase during sintering is necessary to distribute admixed alloying elements, especially if they are present as carbides with a high melting point, as it is the case with the admixed Mo_2C.

A calculation mistake regarding the C content of both sample mixtures became evident. Both mixtures, Fe + Mo_2C + MA1 and Fe + Mo_2C + MA2, should have been mixed to yield the same C content, but due to this mistake the mixture with **MA1 had a nominal C content of 0,84 wt%** and **mixture with MA2 had a nominal C content of 0,7 wt%**. Also, since MA2 has a higher O content (see Table 1) during sintering the C burnup was probably higher in the samples with MA2 than in MA1 and this would even further increase the C content of MA1 compared to MA2. The nominal C contents of the mixtures are noted in the following Figures of the microstructures.

In Figure 36 the obtained microstructures of the as sintered Mo admixed samples with MA1 after Nital etching are shown. The microstructures of the as sintered samples mainly consisted of two regions: light, very fine lamellar regions and dark-brown regions. To identify those regions the microhardness (HV 0,1) was measured in a representative sample sintered at 1250 °C. The lighter regions showed HV 0,1 values of ~200-300 and the darker regions showed HV 0,1 values of ~300-400. Fine lamellar pearlite shows HV values of 250 and upper bainite of 350-450 [88]. Due to the laminar structure and the hardness, the lighter phases were identified as pearlite. The darker regions could be identified as upper bainite due to their hardness, spot like appearance which look similar to the structures found in the pre-pressed

samples. The higher the sintering temperature was, the more homogeneous were the resulting microstructures, but the differences in the as sintered samples are only marginal.

The as sintered Mo-admixed samples with MA2 yielded similar phases as the as sintered Mo-admixed samples with MA1: bainite and pearlite, see Figure 37. The only difference to the Mo-admixed samples with MA1 was, that the microstructures of the as sintered samples with MA2 sintered at 1140 and 1180 °C contained undissolved MA particles. The samples sintered at 1140 °C contained more undissolved MA particles than the ones sintered at 1180 °C. At a sintering temperature of 1250 °C no MA particles were found. In the pre-pressed samples undissolved MA particles of both MA´s were found in the samples sintered at 1140 °C. The Mo-admixed system with a Fe base powder led to the dissolution of the MA1 particles even at low sintering temperatures. There are two different factors that need to be considered for this phenomenon: the difference in C content of the mixtures and the difference in O content of the MA´s. Geroldinger showed that the melting behaviour of MA´s in PM steels is affected strongly by the C content if O sensitive elements like Cr are present. The C content has an influence on wettability, alloying and infiltration in the same way as the temperature does [87]. As Mn and Si are also very O sensitive elements are present in the MA´s it seems logical that the C content has a big influence on the behaviour of the MA´s. The higher O content of MA2 combined with a higher alloying content compared to MA1 is another factor as to why the particles were not completely dissolved in the Mo-admixed samples. There could have been oxide layer formation around the MA particles due to the higher amount of Si and Mn, both alloying elements with a high affinity for O. Those oxide layers could have prevented the dissolving of those particles at lower sintering temperatures.

After sinter hardening and tempering the microstructures of the Mo-admixed samples with MA1 are mainly martensitic (light brown regions) with inclusions or “islands”, see Figure 38. These “islands” consist of light ferrite and dark upper bainite. The higher the sintering temperature was the more homogeneous were the resulting microstructures. Higher sintering temperatures led to microstructures with a higher amount of martensite and less upper bainite/ferrite inclusions. The martensitic microstructures were more refined in the samples sintered at 1250 °C. After tempering and annealing also all MA particles were dissolved.

Figure 39 shows that with MA2 after sinter hardening and tempering the same microstructures were obtained in the Mo-admixed samples. There are no significant differences between the microstructures compared to the Mo-admixed samples with MA1. Again, higher sintering temperatures led to more refined martensitic structures with less bainite/ferrite inclusions and no undissolved MA particles could be found.

In the Mo-admixed system with a Fe base powder the MA particles seem to have been more sufficiently dissolved than in the prepressed samples with pre-alloyed base powders. No undissolved MA1 particles were found and after sinter hardening and tempering all undissolved MA2 particles were dissolved. This could be due to the fact that the C content in the Mo-admixed samples were different. Higher sintering temperatures led to more homogeneous martensitic microstructures after sinter hardening and tempering.

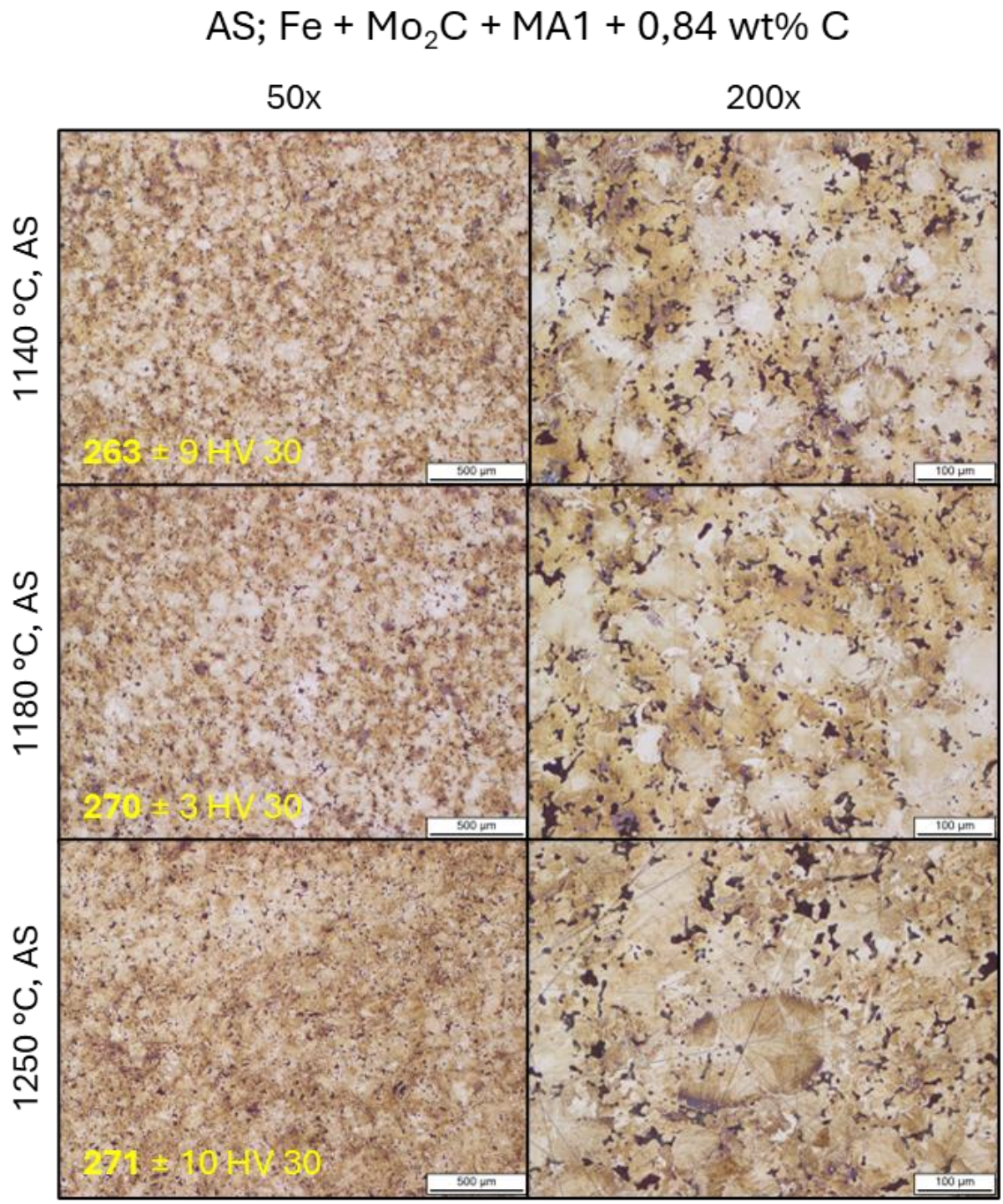

Figure 36: Nital-etched microstructures of the as sintered Mo-admixed samples with MA1

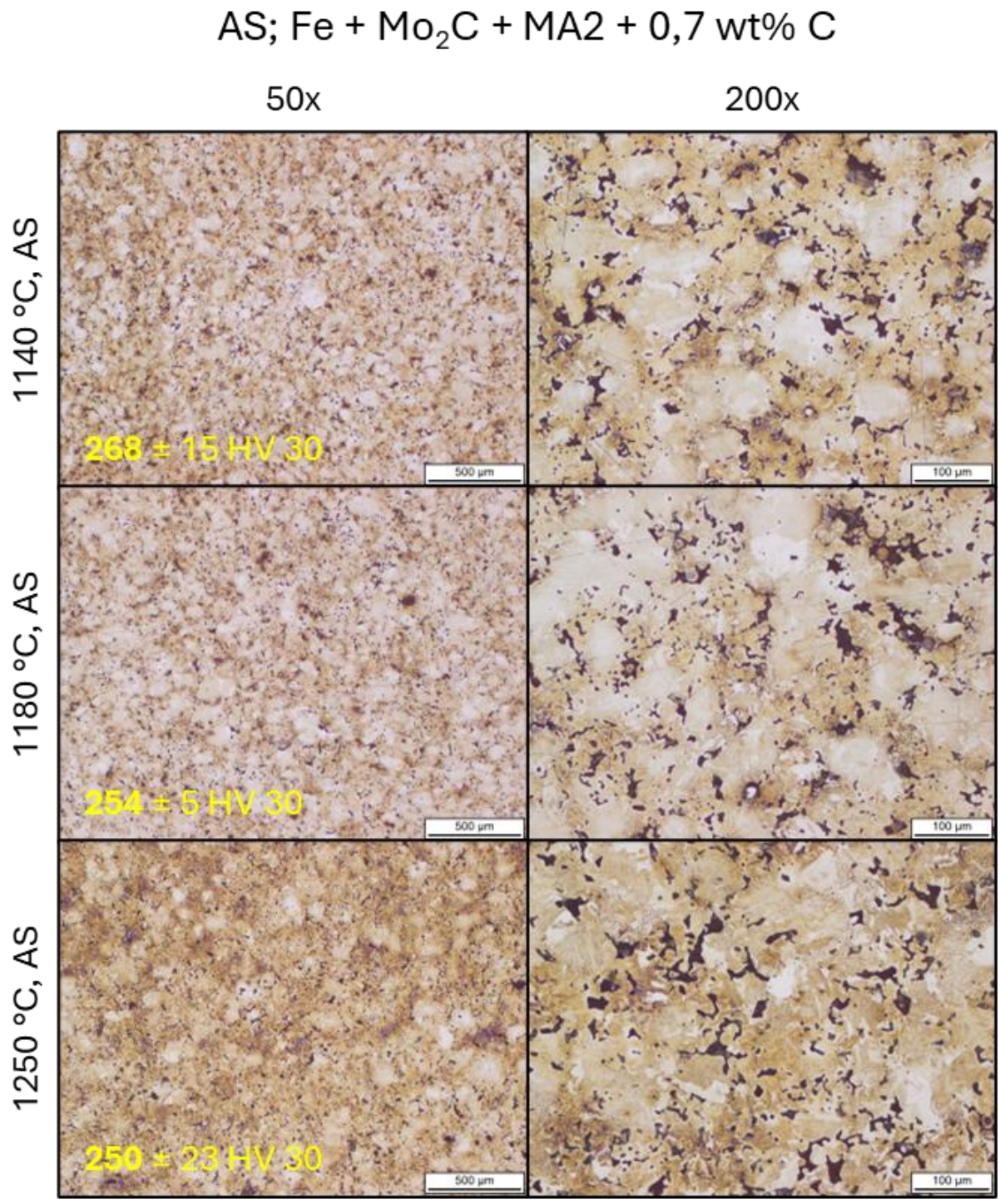

Figure 37: Nital-etched microstructures of the as sintered Mo-admixed samples with MA2

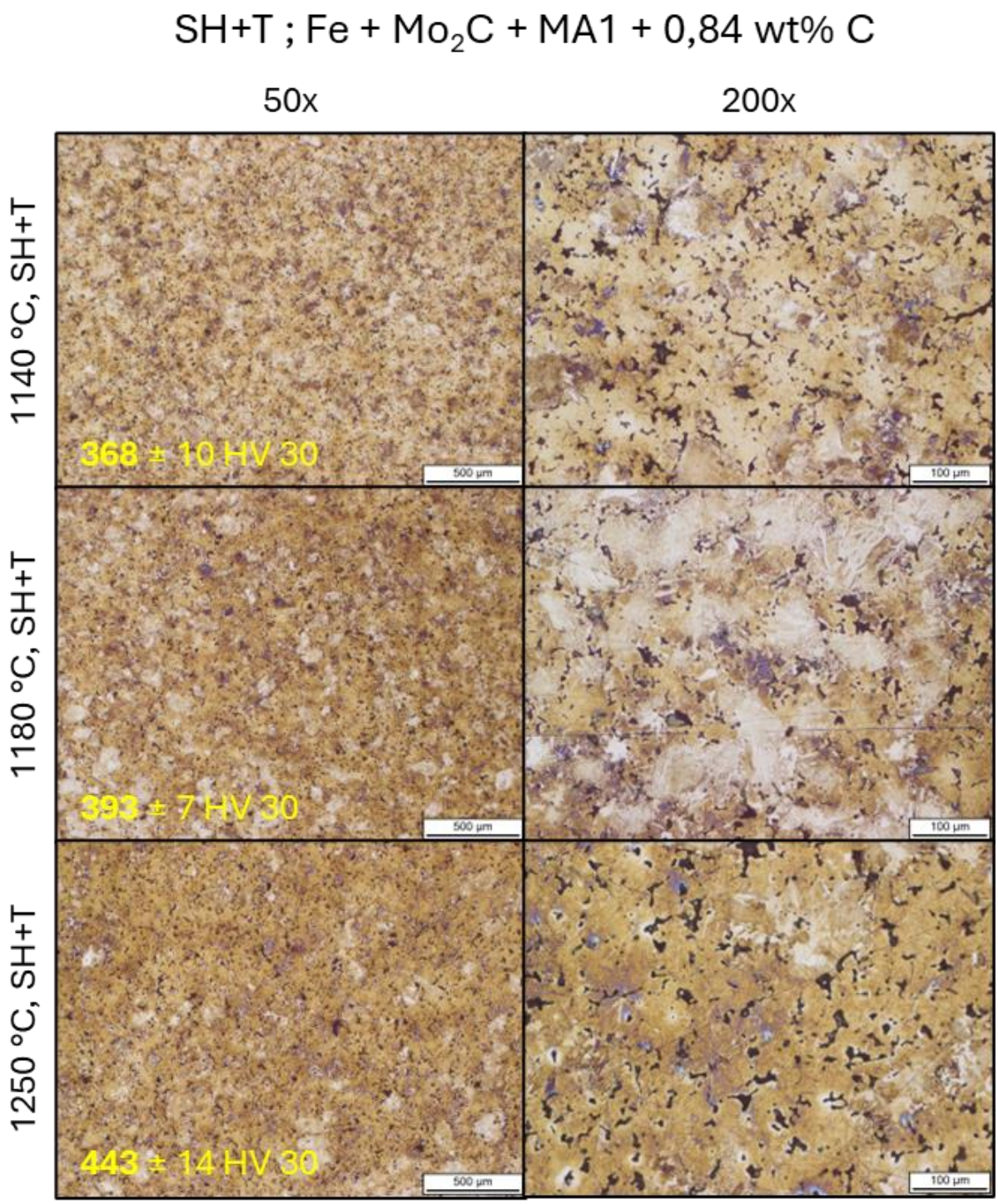

Figure 38: Nital-etched microstructures of the sinter hardened Mo-admixed samples with MA1

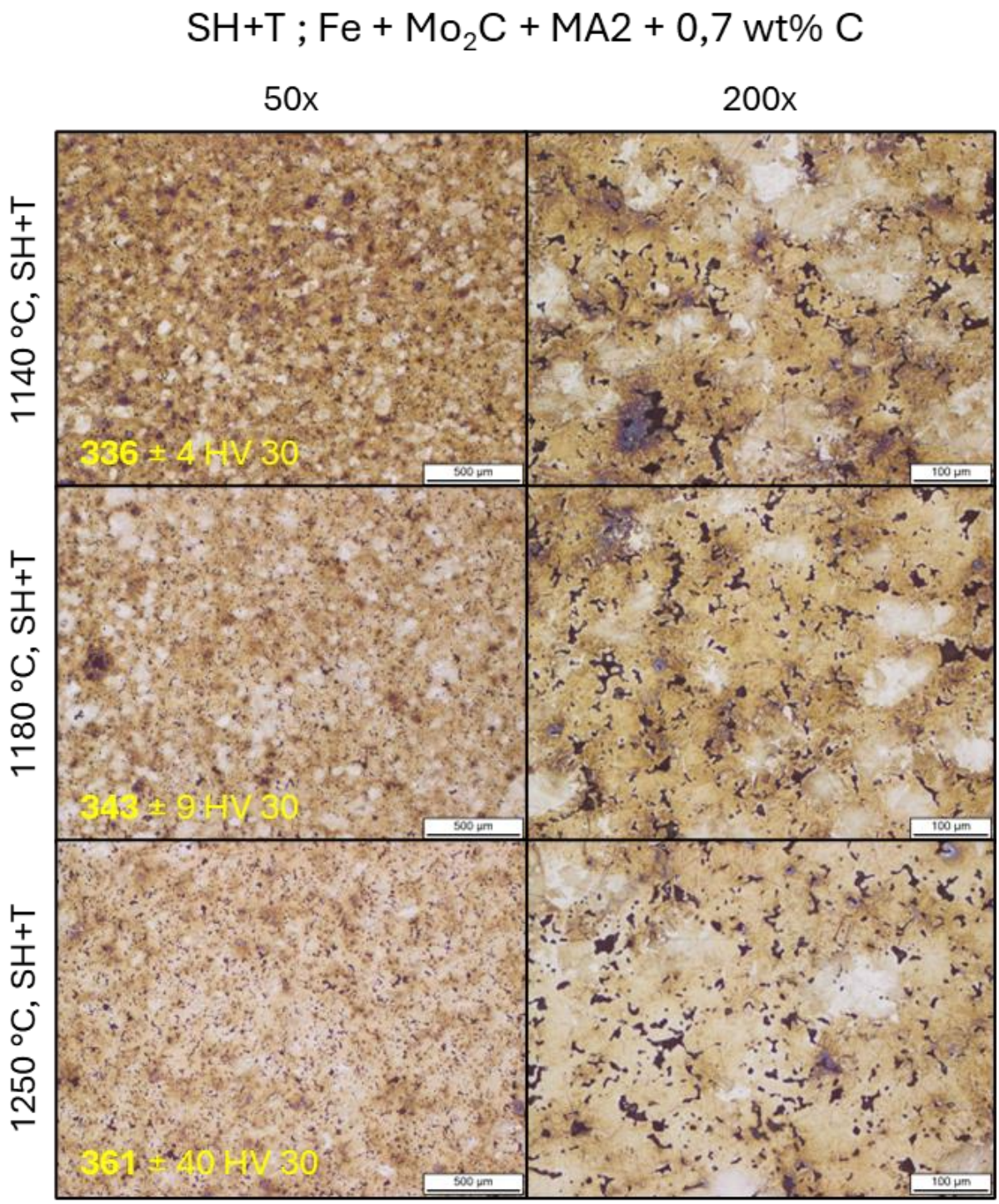

Figure 39: Nital-etched microstructures of the sinter hardened Mo-admixed samples with MA2

4.2.2 Mechanical properties

The green density for the Mo-admixed samples was measured geometrically, the sintered density was determined via the Archimedes method. From each sample number all 3 individual samples were measured. For each sample 5 indentations were measured in the middle of the embedded surface for the HV30 value. The values of the green and sintered density, dimensional change, impact energy and HV30 for the Mo-admixed samples are listed in Table 10.

Table 10: Mechanical properties of the samples with Fe as base powder with Mo_2C admixed

Sample number	Sample description	Density / g/cm³		Dimensional change / %	Impact energy / J/cm²	HV 30
		green	sintered			
Mo1	Fe + Mo_2C, MA1, 1140 °C, AS	**6,92** ± 0,02	**7,01** ± 0,02	**0,05** ± 0,01	**11** ± 3	**263** ± 9
Mo2	Fe + Mo_2C, MA1, 1140 °C, SH + T	**6,93** ± 0,01	**7,01** ± 0,03	**-0,04** ± 0,01	**12** ± 4	**368** ± 10
Mo3	Fe + Mo_2C, MA1, 1180 °C, AS	**6,93** ± 0,01	**6,94** ± 0,04	**0,04** ± 0,15	**18** ± 2	**270** ± 3
Mo4	Fe + Mo_2C, MA1, 1180 °C, SH + T	**6,93** ± 0,00	**7,01** ± 0,02	**-0,09** ± 0,03	**17** ± 3	**393** ± 7
Mo5	Fe + Mo_2C, MA1, 1250 °C, AS	**6,93** ± 0,01	**6,99** ± 0,01	**-0,08** ± 0,07	**18** ± 3	**271** ± 10
Mo6	Fe + Mo_2C, MA1, 1250 °C, SH + T	**6,93** ± 0,01	**6,99** ± 0,05	**-0,07** ± 0,07	**12** ± 1	**443** ± 14
Mo7	Fe + Mo_2C, MA2, 1140 °C, AS	**6,90** ± 0,01	**6,96** ± 0,06	**0,06** ± 0,09	**15** ± 2	**268** ± 15
Mo8	Fe + Mo_2C, MA2, 1140 °C, SH + T	**6,90** ± 0,00	**7,00** ± 0,02	**0,02** ± 0,05	**18** ± 5	**336** ± 4
Mo9	Fe + Mo_2C, MA2, 1180 °C, AS	**6,90** ± 0,01	**6,97** ± 0,03	**0,01** ± 0,06	**18** ± 2	**254** ± 5
Mo10	Fe + Mo_2C, MA2, 1180 °C, SH + T	**6,91** ± 0,00	**7,02** ± 0,02	**-0,04** ± 0,02	**16** ± 2	**343** ± 9
Mo11	Fe + Mo_2C, MA2, 1250 °C, AS	**6,90** ± 0,00	**7,00** ± 0,03	**-0,13** ± 0,05	**17** ± 2	**250** ± 25
Mo12	Fe + Mo_2C, MA2, 1250 °C, SH + T	**6,90** ± 0,01	**6,93** ± 0,01	**-0,08** ± 0,01	**20** ± 6	**361** ± 40

The sintered densities correspond to a relative density of 88,1-89,1 % compared to pure Fe. This would correlate to a porosity of ~10,9-11,9%.

Between the measurement of the prepressed samples and the Mo-admixed samples the Charpy impact testing machine and the hardness testing machine were moved and not calibrated. Therefore, the values for impact energy and hardness were not directly compared to each other. Generally, the values for impact energy must be viewed with caution.

In Figure 40 the densities for the Mo-admixed samples are compared. The green densities were measured geometrically and the sintered densities via Archimedes method. After sintering all samples experienced densification compared to the green density. There are no clear differences between the two MA´s in their densities. Also, no significant differences between the different sintering temperatures were found. The differences in sintered densities are below 0,1 g/cm^3. The comparison of the dimensional change shows that in the as sintered condition, in the samples sintered at 1140 and 1180 °C swelling occurred while the samples sintered at 1250 °C showed shrinkage (~0,1 %). After sinter hardening and tempering almost all samples experienced shrinkage. These results combined with the presence of undissolved MA particles in the microstructures suggest that there is a sintering temperature 1250 °C leads to slight densification and better homogenization compared to the lower sintering temperatures.

Figure 41 compares the hardness and impact energy values of the Mo-admixed samples. In the as sintered samples, the hardness of all samples is quite similar around ~250 HV30. The hardness of the samples with MA1 is slightly higher than the hardness of the samples with MA2. This seems counter intuitive as MA2 has a higher alloying content and therefore should lead to higher hardness. But as discussed in 4.2.2 the C content of both sample mixtures was not identical and the higher nominal C content in the samples with MA1 most likely explains the higher hardness. This difference is even more evident after sinter hardening and tempering. The samples with MA1 show significantly higher hardness values than the samples with MA2. Here also the influence of the sintering temperature is clear: a higher sintering temperature leads to higher hardness in the sinter hardened and tempered samples. Therefore, at this cooling rate it is possible to develop martensitic microstructures in the more highly alloyed areas. This is supported by the presence of a more refined and homogeneous martensitic microstructure.

In the as sintered condition, the impact energy values of the samples sintered at 1140 °C are significantly lower than the samples sintered at 1180 and 1250 °C. In the as sintered condition, the impact energy is mainly affected by the sintering temperature. There is only a very slight difference between the two MA´s: samples with MA2 have a slightly higher impact energy. This seems logical as they also have slightly lower hardness values compared to the samples with MA1. After sinter hardening and tempering there is no clear trend with the impact energies. Impact energy after sinter hardening and tempering is influenced by the C content and the microstructure. While for the samples with MA1 the values are similar (1140 and 1180 °C) or lower (1250 °C) for the samples with MA2 the impact energy increases at all sintering temperatures. This is very surprising as sinter hardening enhances the formation of martensite (see the microstructure and hardness values) which is a very brittle phase. Also, MA2 has a higher O content than MA1 (see Table 1) and there is generally an inverted trend between

impact energy and O content. The most likely explanation for the inconsistency of the impact energy values is that due to the moving of the Charpy impact testing machine without calibration, measuring errors occurred. As the Charpy bars can only be tested once no remeasurements could be conducted. The results of the prepressed samples suggested that there are no major differences in the impact energy between MA1 and MA2.

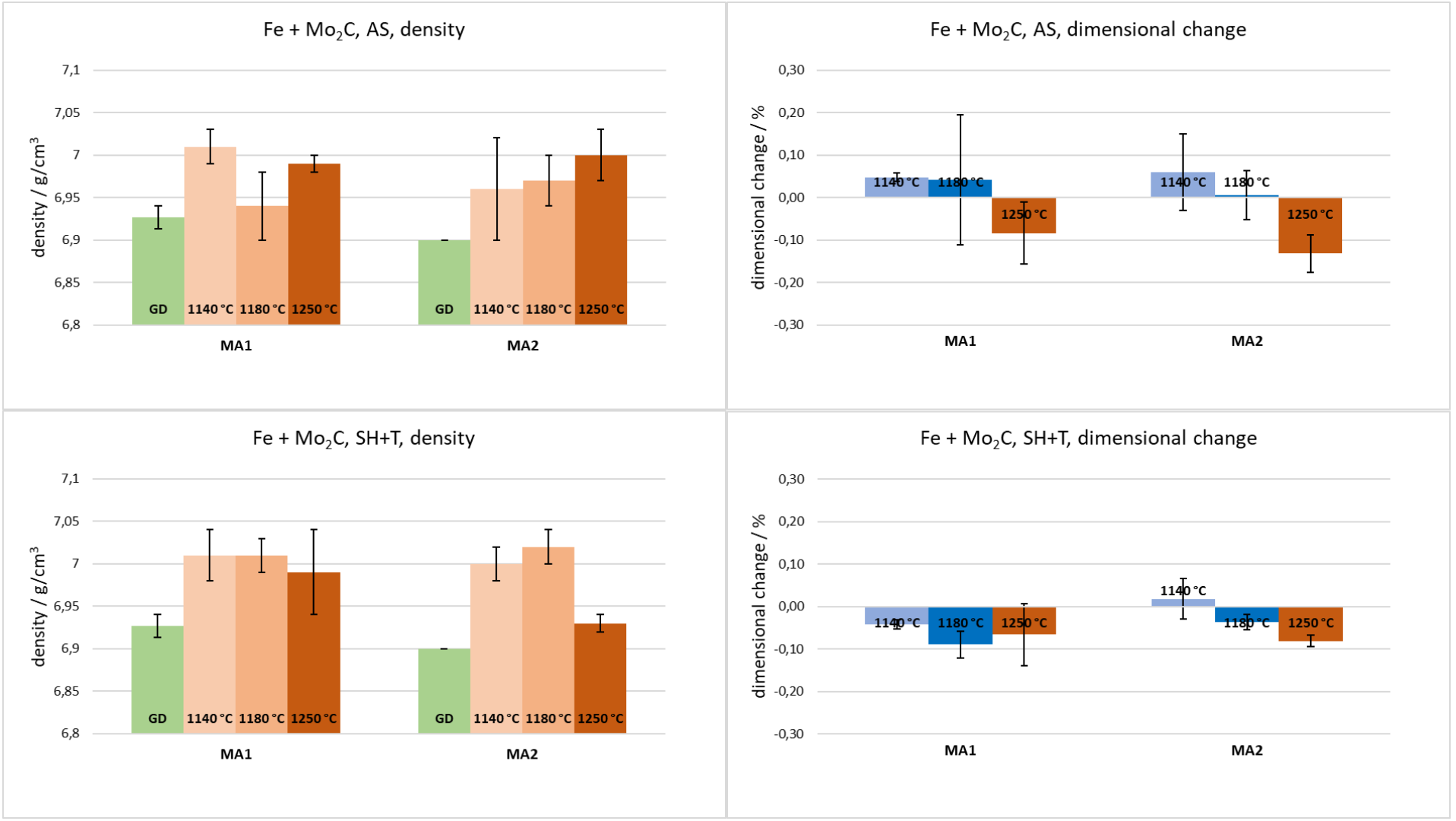

Figure 40: Densities and dimensional changes of the Mo-admixed samples

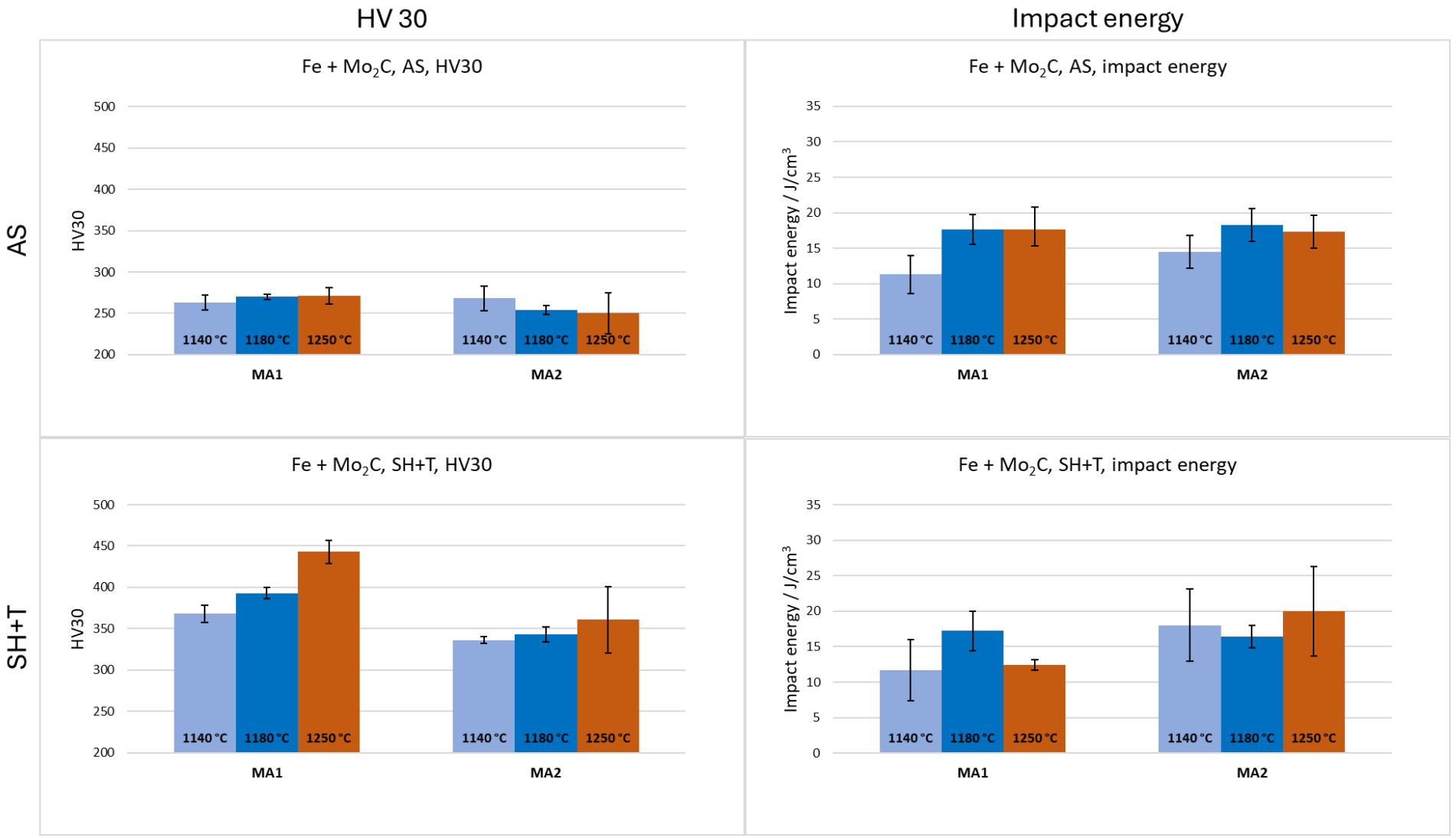

Figure 41: Mechanical properties of the Mo-admixed samples

One factor that also needs to be discussed are the sintering temperatures. Since the samples were pushed into the furnace inside of a sintering boat and it was complicated to position the boats always exactly on the same position in the furnace. Therefore, to control the sintering intensity two ceramic process temperature control rings (type PTCR – LTH, temperature range 970-1250 °C, Schupp) were put in each sintering boat before the sintering. The rings were first dewaxed according to the manufacturers specifics and the diameter was measured before and after sintering with a micrometer (PTCR micrometer-D, Mitutoyo) to obtain the sintering intensity. The effective sintering temperatures and the difference to the adjusted sintering temperatures are shown in Table 11. This value is just an indicator as the rings are not used to determine the exact sintering temperature, but rather the sintering intensity of the different sintering temperatures. The temperature values of the PTCR-rings show that the first ring always had a higher sintering intensity than the second one. The rings were always put into the sintering boat in the same order, therefore it is evident, that there was a clear temperature gradient inside the furnace. This could have led to a heterogeneity along the length of the samples.

Table 11: Effective sintering temperatures of the Mo-admixed samples

Sintering round	Adjusted temperature / °C	PTCR-ring temperature /°C		Difference / °C
		value	average	
1	1140	**1125**	1122 ± 5	19
		1118		
2	1140	**1132**	1126 ± 9	14
		1120		
3	1180	**1166**	1162 ± 6	19
		1157		
4	1180	**1161**	1156 ± 7	24
		1151		
5	1250	**1231**	1231	19
		ring broke		
6	1250	**1241**	1235 ± 9	15
		1229		

4.2.3 SEM

To confirm that the undissolved particles found in the etched samples were really MA2 particles and to get an overview of elemental distribution, 4 representative samples with MA2 were examined by SEM. To see the inhomogeneities as good as possible back-scattered electron (BSE) scans were made of the 4 samples. An elemental mapping by EDX was conducted for one sample.

Figure 42 shows the BSE picture of a as sintered Mo-admixed sample with MA2, sintered at 1140 °C. Optically different areas could be differentiated. Via EDX elemental mapping (see Figure 43) and EDX point analysis the following regions could be identified, see Table 12. It needs to be considered that the mapping/point analysis by EDX is not a quantitative method. Especially for light elements like C it is more of a qualitative method. Therefore the obtained "compositions" should only be taken to qualify certain regions, not quantify.

Table 12: Identified phases via SEM/EDX in Mo-admixed sample with MA2, sintered at 1140°C, as sintered

Number	Optical appearance	Region	Qualitative EDX composition / wt%
1	black spots	pores	-
2	light grey areas	Mn-enriched ferrous	Fe_2Mn_0.7Mo_0.2Si
3	dark grey areas	Mn-poor ferrous	Fe_0.2Mn_0.2Mo_0.1Si
4	grey particles in black spots	MA2 particles	Fe_2.1Mn_4.5Si_16C
5	small white spots	Mo_2C particles	Mo_42Fe_5.9C_1.5Si_0.9Mn

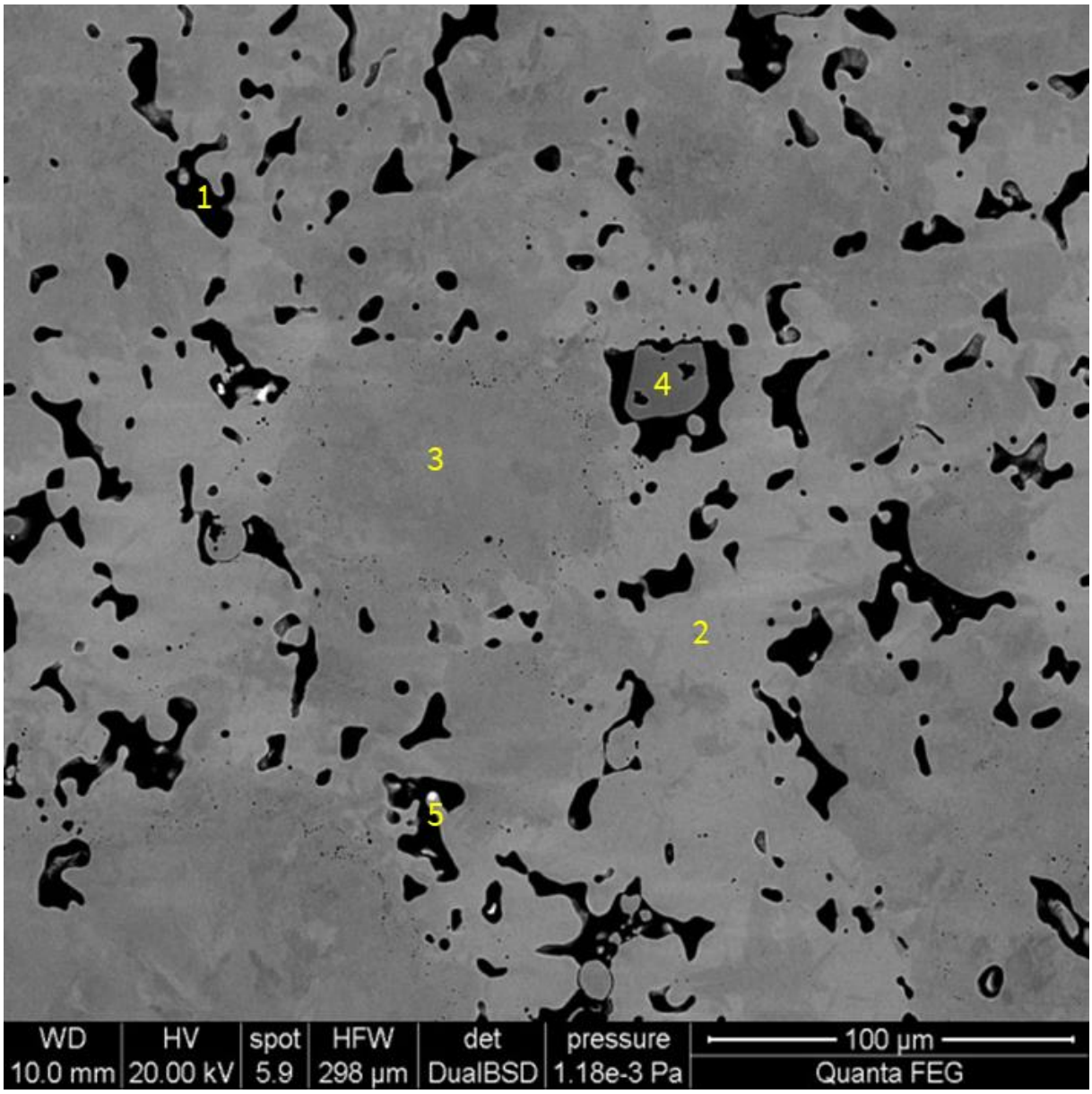

Figure 42: SEM picture in BSE-mode of a polished Mo-admixed sample with MA2 sintered at 1140 °C, as sintered

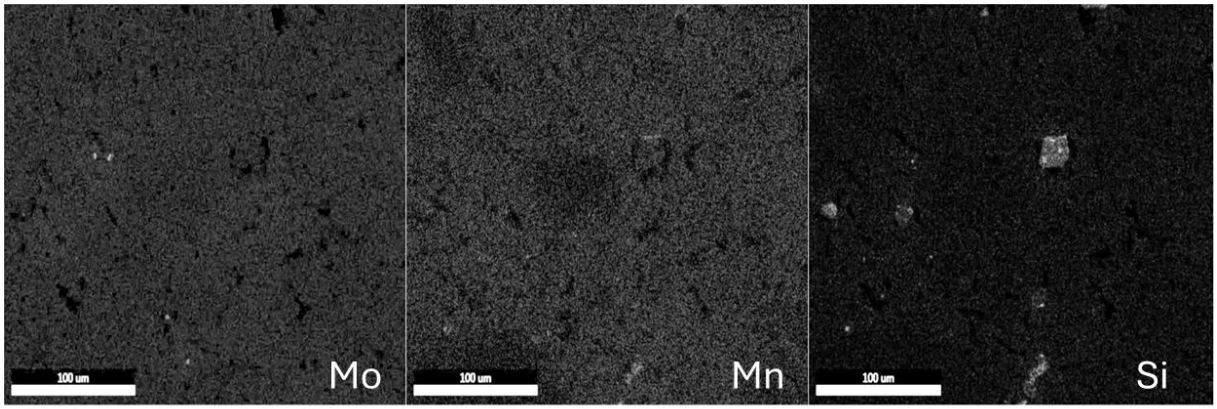

Figure 43: Elemental distribution of Mo, Mn and Si of the polished Mo-admixed sample of with MA2 sintered at 1140 °C shown in Figure 42

In the BSE picture of the sample the ferrous region is clearly distinguishable into a lighter and a darker region. EDX elemental analysis showed that there is a difference in alloying element content between these 2 regions, especially Mn. The dark region has a low Mn (~0,15 wt%) content while the light region contains over 2 wt% Mn. This trend is not as clear with Si or Mo. The Si distribution in Figure 43 clearly shows the undissolved MA2 particles, which are also visible in the BSE picture. The Mo distribution in Figure 43 clearly shows small white spots of a region with a Mo content of ~ 50 wt%. The comparison to the particle size of the Mo_2C powder (see Figure 17) clearly shows that those white spots are undissolved Mo_2C particles. Those were not visible in the microscopical pictures of the etched samples, due to their size. Therefore, a sintering temperature of 1140 °C was not sufficient to fully dissolve and distribute the MA2 or the Mo_2C particles.

Figure 44 shows the BSE picture of a as sintered Mo-admixed sample with MA2, sintered at 1140 °C after sinter hardening and tempering. Optically the same regions as in the as sintered sample were visible, which was confirmed by EDX point analysis. The ratio of the regions was different in the as sintered and the heat-treated sample. The direct comparison in Figure 45 of the as sintered and heat-treated sample show that after sinter hardening and tempering significantly less dark (Mn-poor) and lighter (Mn-rich) ferrous regions occurred. Also, in the heat-treated sample less undissolved Mo_2C particles were found. This suggests that the heat treatment further dissolves the particles and homogenizes the samples. These results must be viewed with caution, as it might be an oversimplification to assume that the lighter and darker regions are only caused by the alloying content. It cannot be excluded that the different optical regions in all investigated samples are also caused by effects of the microstructures themselves.

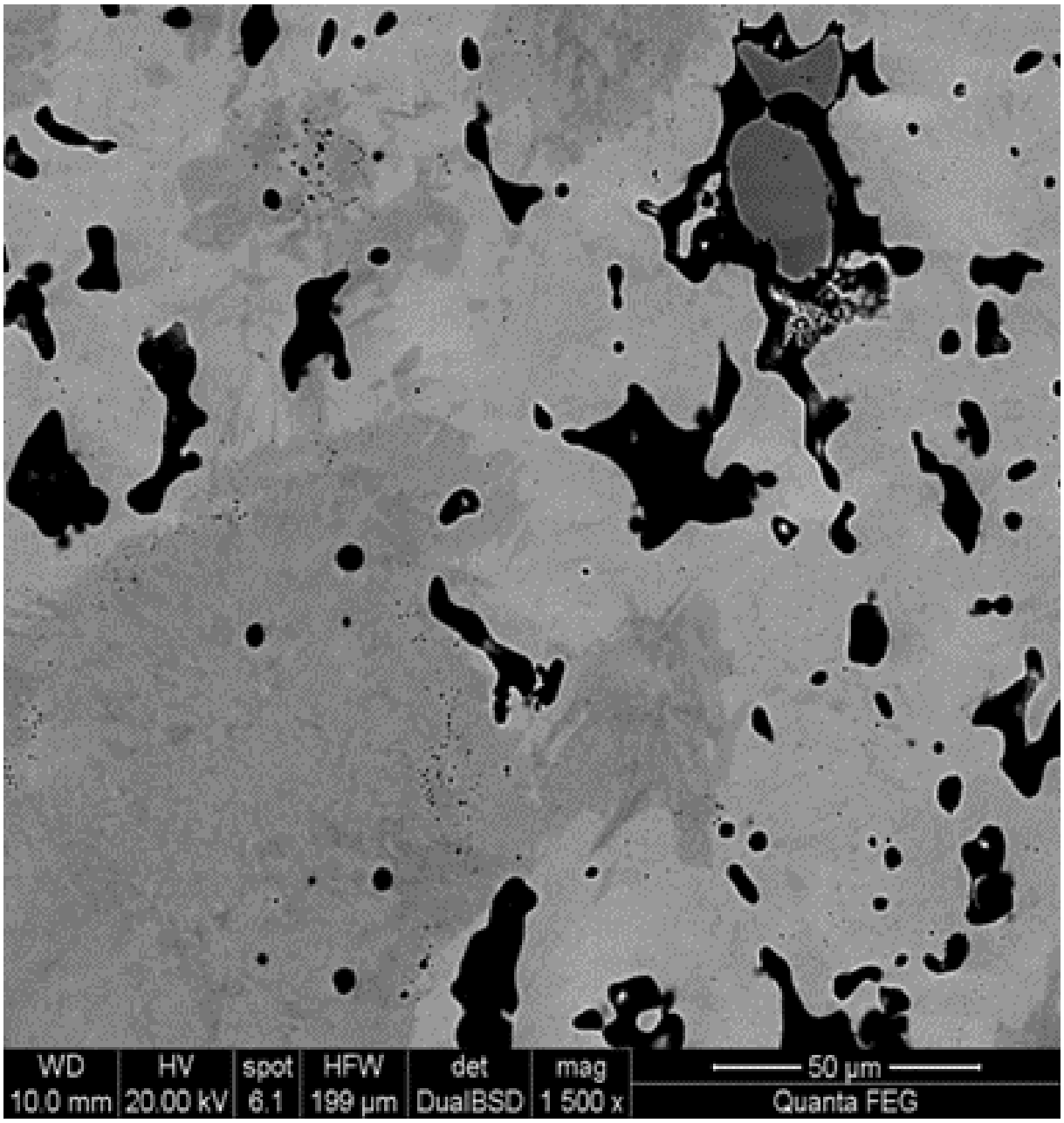

Figure 44: SEM picture in BSE-mode of a polished Mo-admixed sample with MA2 sintered at 1140 °C, sinter hardened and tempered

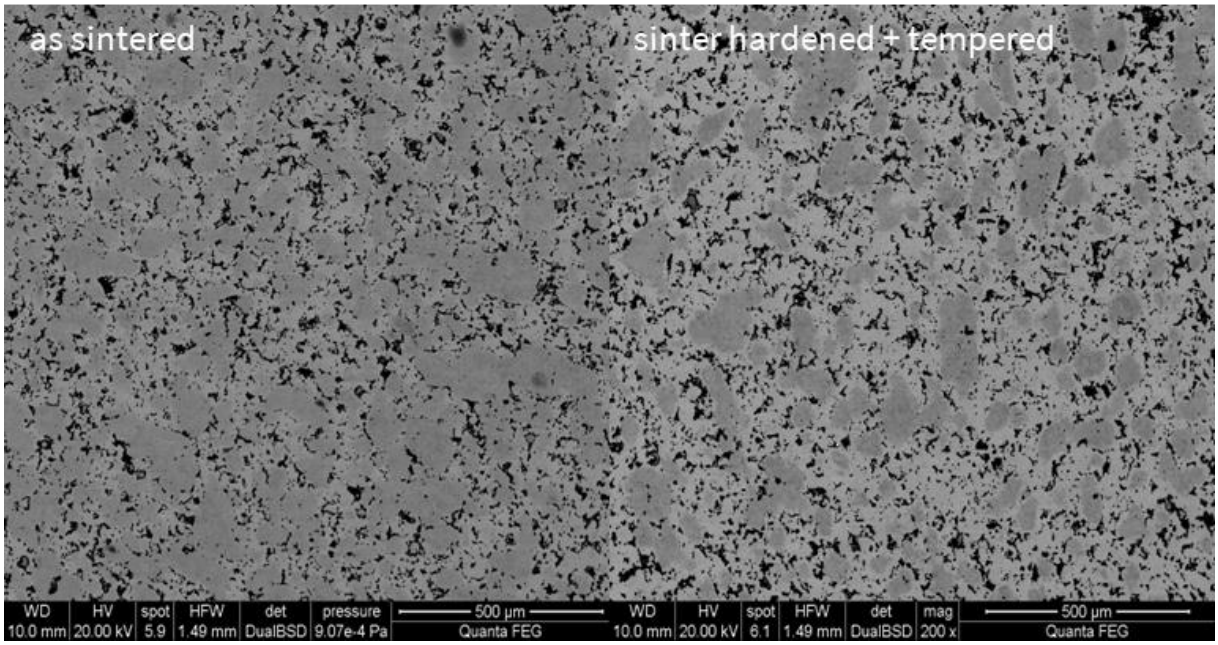

Figure 45: SEM picture in BSE-mode of polished Mo-admixed samples of with MA2 sintered at 1140 °C

Figure 46 shows the SEM analysis of two samples with MA2 sintered at 1250 °C. In the samples sintered at the higher temperature again two different ferrous phases, Mn poor and Mn rich, occurred. The heat treatment again facilitated the formation of more light, Mn rich ferrous phase. No undissolved MA2 or Mo_2C particles could be found at a sintering temperature of 1250 °C. Therefore, sintering at 1250 °C sufficiently dissolves all particles in the system and encourages homogenization in the samples, especially after sinter hardening and tempering. This corresponds to the superior mechanical properties compared to the samples sintered at lower temperatures. It must be pointed out that sinter hardening was carried out different in this work than it is usually in the industry where the samples are quenched immediately after sintering. The step of cooling them moderately and reheating them again (at 1100 °C for 30 minutes) could have contributed significantly to the distribution of alloying elements.

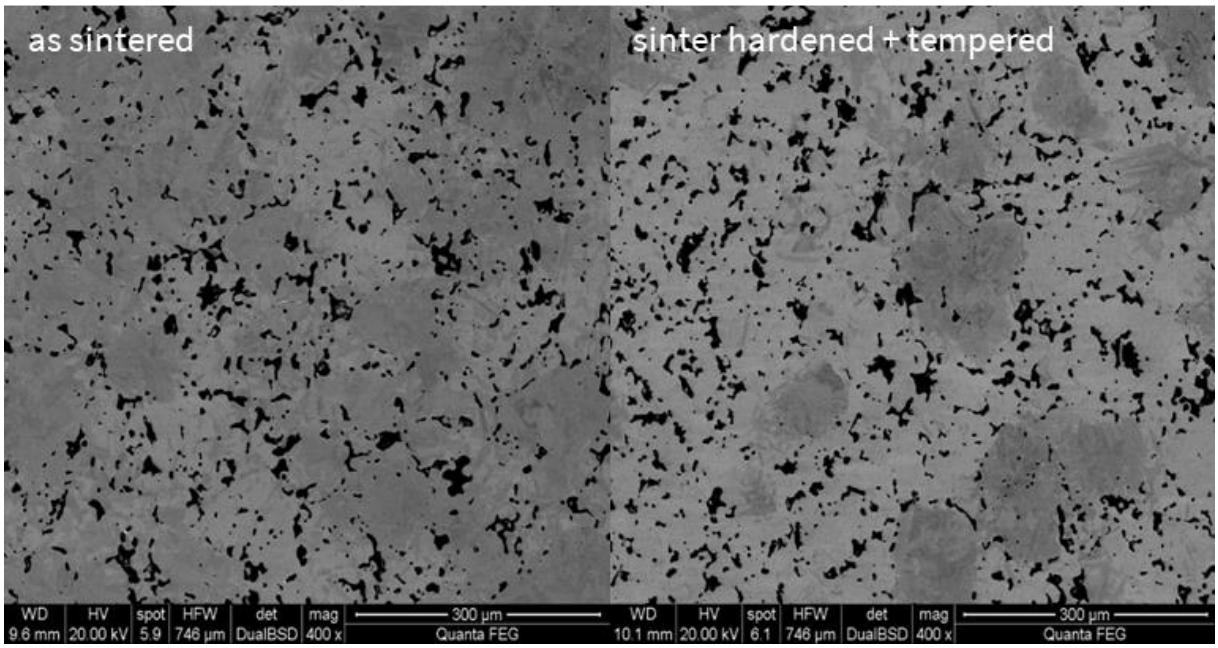

Figure 46: SEM picture in BSE-mode of polished Mo-admixed samples of with MA2 sintered at 1250 °C

4.3 Mo-pre-alloyed samples

4.3.1 Microstructure

The microstructures of all Mo-pre-alloyed samples were visualized by etching with 1 % Nital and representative microscopic pictures are shown and discussed in the following figures. The microstructures of the samples are complex mixtures of different phases. Ferrite, pearlite, bainite, and martensite as well as undissolved MA2 particles occurred as phases in the microstructures.

A calculation mistake regarding the C content of both sample mixtures became evident. Both mixtures, Fe_0.45Mo + MA1 and Fe_0.45Mo + MA2, should have been mixed to yield the same C content, but due to this mistake the mixture with **MA1 had a nominal C content of 0,84 wt%** and **mixture with MA2 had a nominal C content of 0,77 wt%**. Also, since MA2 has a higher O content (see Table 1) during sintering the C burnup was probably higher in the samples with MA2 than in MA1 and this would even further increase the C content of MA1 compared to MA2. The nominal C contents of the mixtures are noted in the following Figures of the microstructures.

The microstructures of the Mo-pre-alloyed samples are shown in Figure 47 and Figure 48. All samples were sinter hardened and tempered. They showed similar microstructures as the pre-pressed and Mo-admixed samples that were sinter hardened and tempered: mainly martensite with “islands” of upper bainite/pearlite. To verify those phases in the sample with MA1 sintered at 1250 °C (Figure 47) microhardness was measured. The darker spots showed HV 0,1 values of ~300-400 and the light brown main phase HV 0,1 values of ~830. Upper bainite shows HV values 350-450 and martensite > 550 [88]. Therefore, the microstructures are classified as martensitic with inclusions of upper bainite. The microstructures looked basically similar for all different Mo-pre-alloyed samples. The only main difference was that in the samples with MA2 sintered at 1140 °C again undissolved MA particles were found. This could again either be explained by the different C content or the higher O content of MA2. This confirmed the tendency of MA2 to not completely dissolve at sintering temperatures of 1140 °C which was obtained in the pre-pressed and Mo-admixed samples.

In direct comparison the samples sintered at 1250 °C showed a higher amount of martensite and less upper bainite/ferrite inclusions. The martensitic microstructures were more refined and homogeneous in the samples sintered at 1250 °C.

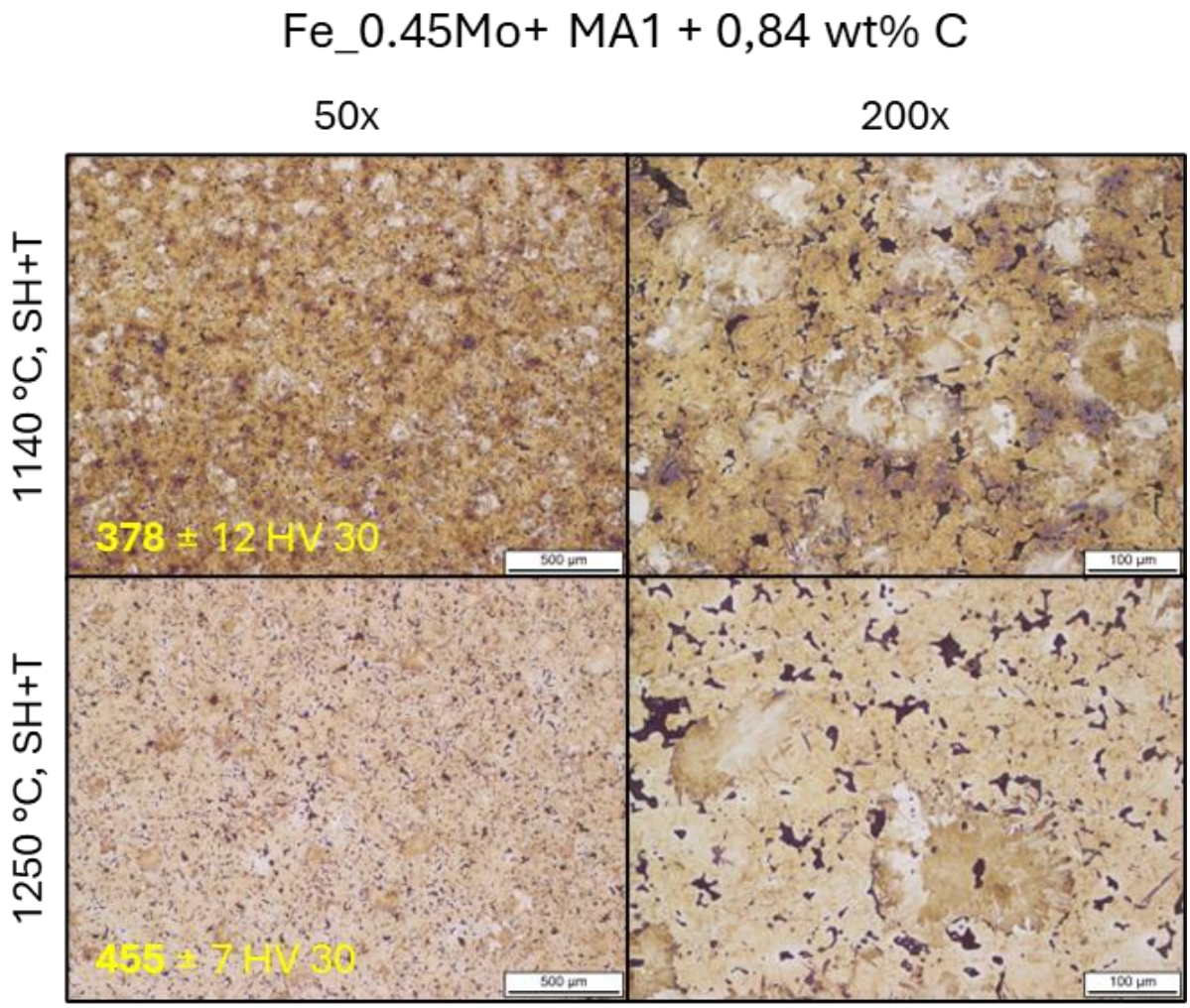

Figure 47: Nital-etched microstructures of the sinter hardened and tempered samples with Fe_0.45Mo + MA1

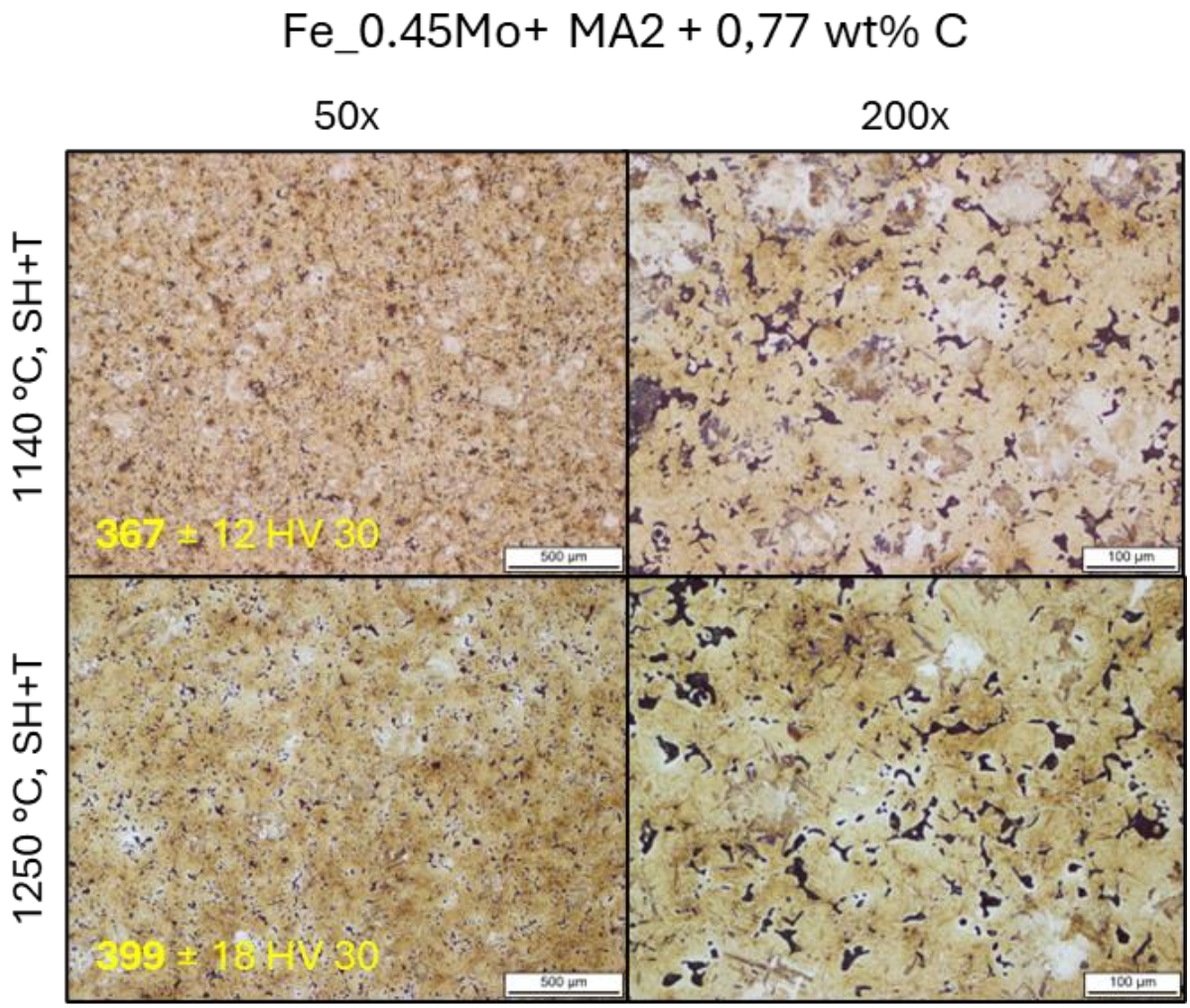

Figure 48: Nital-etched microstructures of the sinter hardened and tempered samples with Fe_0.45Mo + MA1

4.3.2 Mechanical properties

The green density for the Mo-pre-alloyed samples was measured geometrically, the sintered density was determined via the Archimedes method. From each sample number all 3 individual samples were measured. For each sample 5 indentations were measured in the middle of the embedded surface for the HV30 value. The values of the green and sintered density, dimensional change, impact energy and HV30 for the Mo-pre-alloyed samples are listed in Table 13.

Table 13: Mechanical properties of the samples with Fe_0.45Mo as base powder

Sample number	Sample description	Density / g/cm³		Dimensional change / %	Impact energy / J/cm²	HV 30
		green	sintered			
As1	Fe_0.45Mo, MA1, 1140 °C, SH + T	**6,95** ± 0,01	**7,03** ± 0,05	**-0,02** ± 0,01	**6** ± 1	**378** ± 12
As2	Fe_0.45Mo, MA1, 1250 °C, SH + T	**6,96** ± 0,01	**7,02** ± 0,02	**-0,17** ± 0,03	**13** ± 7	**455** ± 7
As3	Fe_0.45Mo, MA2, 1140 °C, SH + T	**6,92** ± 0,01	**7,01** ± 0,05	**-0,18** ± 0,03	**10** ± 5	**367** ± 12
As4	Fe_0.45Mo, MA2, 1250 °C, SH + T	**6,93** ± 0,01	**7,00** ± 0,03	**-0,19** ± 0,02	**11** ± 7	**399** ± 18

The sintered densities correspond to a relative density of 88,9-89,3 % compared to pure Fe. This would correlate to a porosity of ~10,7-11,1%.

Between the measurement of the prepressed samples and the Mo-pre-alloyed samples the Charpy impact testing machine and the hardness testing machine were moved and not calibrated. Therefore, the values for impact energy and hardness were not directly compared to each other. Generally, the values for impact energy must be viewed with caution.

Due to the high scattering and general lowness of the impact energy values, a second set of samples was produced similar to the ones described in Table 13 and the impact energy of those samples was measured. The resulting values and comparison are shown in Table 14.

Table 14: Comparison of the impact energy of the samples with Fe_0.45Mo as base powder

Sample number	Impact energy / J/cm²				
	Round 1		Round 2		Average of all samples
	value	average	value	average	
As1, 1140 °C, MA1	4,1	**6** ± 1	7,2	**9** ± 4	**7** ± 3
	7,0		6,8		
	5,4		13,4		
As2, 1250 °C, MA1	18,3	**13** ± 7	4,8	**8** ± 6	**11** ± 6
	5,6		4,1		
	16,1		14,1		
As3, 1140 °C, MA2	13,3	**10** ± 5	7,7	**7** ± 1	**8** ± 4
	4,9		5,9		
	12,4		6,1		
As4, 1250 °C, MA2	19,0	**11** ± 7	6,9	**10** ± 3	**10** ± 5
	6,5		9,3		
	7,6		12,5		

Since the second round of samples showed comparably scattering and low values the Charpy impact testing machine was retested with already used samples. Fractured pieces of the pre-pressed samples that were long enough to measure were chosen and measured again. 10 fracture pieces were measured, and the resulting values were compared to the initially obtained values. The results are shown in Table 15

Table 15: Remeasurements of the impact energy of pre-pressed samples

Sample	Impact energy / J/cm²		Deviation / %	Average deviation / %
	Inital	Fractured piece		
1	8,7	10	+15	**-23** ± 30
2	29,4	13,5	-54	
3	24,5	16	-35	
4	13	17,5	+35	
5	16,5	7	-58	
6	23,2	15	-35	
7	24,9	15	-40	
8	10	9,5	-5	
9	12	7	-42	
10	29,5	25	-15	

On average the vales for impact energy could be remeasured to **-23** ± 30 %. This is lower than the initial values. It needs to be considered that the samples were produced and fractured several months before the remeasurement. The samples showed oxidation on the surface, but surface oxides should not affect the impact energy as the sinter contacts are essential. As already mentioned, the Charpy impact testing machine was moved and not calibrated which could be a factor for the low impact energy values and the high scattering.

In Figure 49 the densities for the Mo-pre-alloyed samples are compared. The green densities were measured geometrically and the sintered densities after sinter hardening and tempering via Archimedes method. All samples experienced densification compared to the green density. The samples sintered at 1140 °C showed a slightly higher density than the samples sintered at 1250 °C, but the differences are below 0,05 g/cm^3. After sinter hardening and tempering all samples experienced shrinkage. The sample with MA1 sintered at 1140 °C only contracted minimally while all other samples significantly contracted ~0,18 %.

Figure 50 compares the hardness and impact energy values of the Mo-pre-alloyed samples. The samples sintered at 1250 °C showed significantly higher hardness values than the samples sintered at 1140 °C. Again, the samples with MA1 showed higher hardness values than the comparable samples with MA2. This can be traced back again to a difference in the nominal C content, which was higher for the samples with MA1, see 4.3.1. While the hardness values are quite promising when considered the significantly lower Mo content compared to the pre-pressed and Mo-admixed samples, the impact energy values are very low, but this might be due to the Charpy impact testing maching. To further investigate the reason for the low impact energies fracture surfaces of the Mo-pre-alloyed samples were analysed by SEM, see 4.3.3.

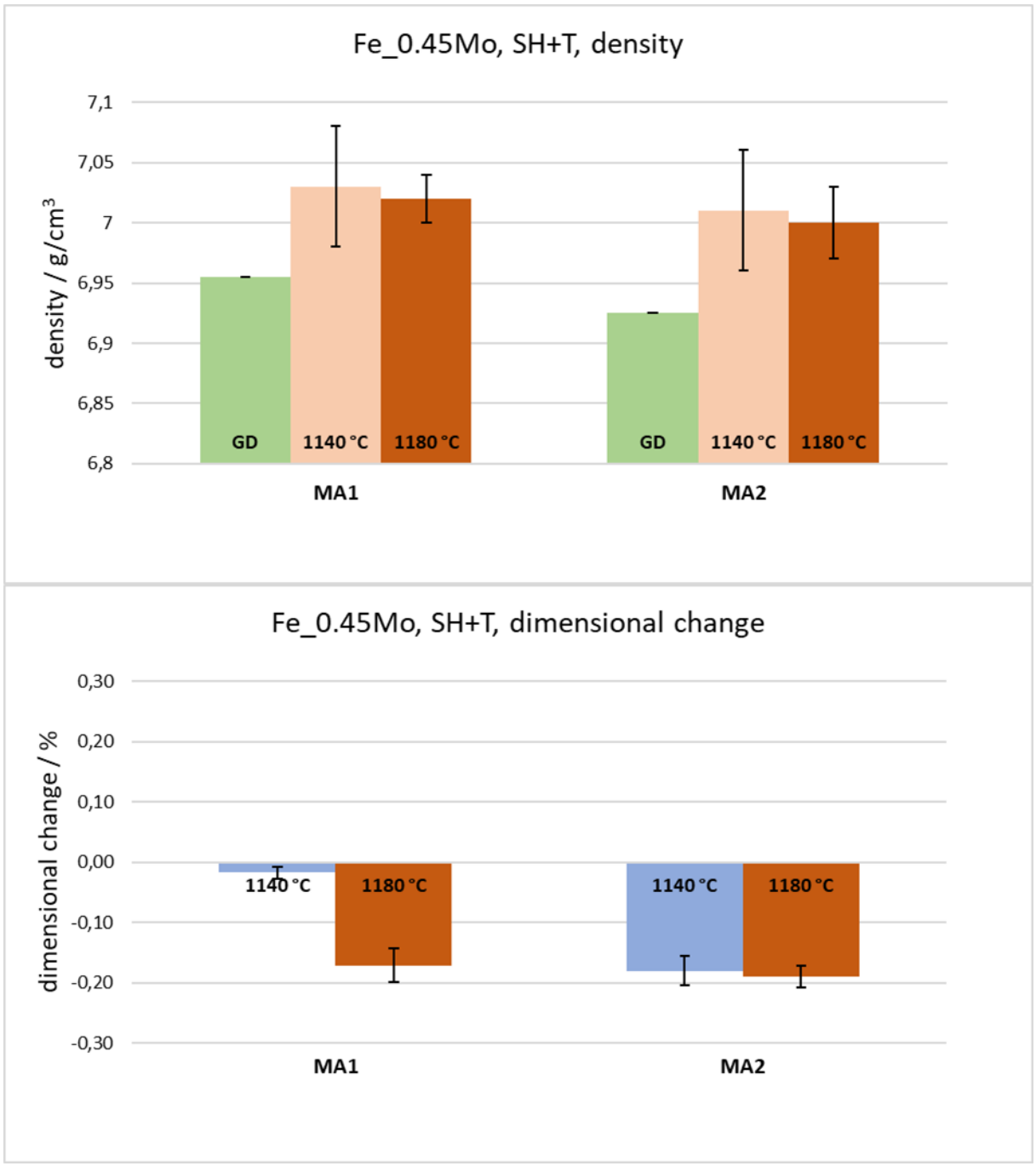

Figure 49: Green and sintered densities of the samples with Fe0.45Mo

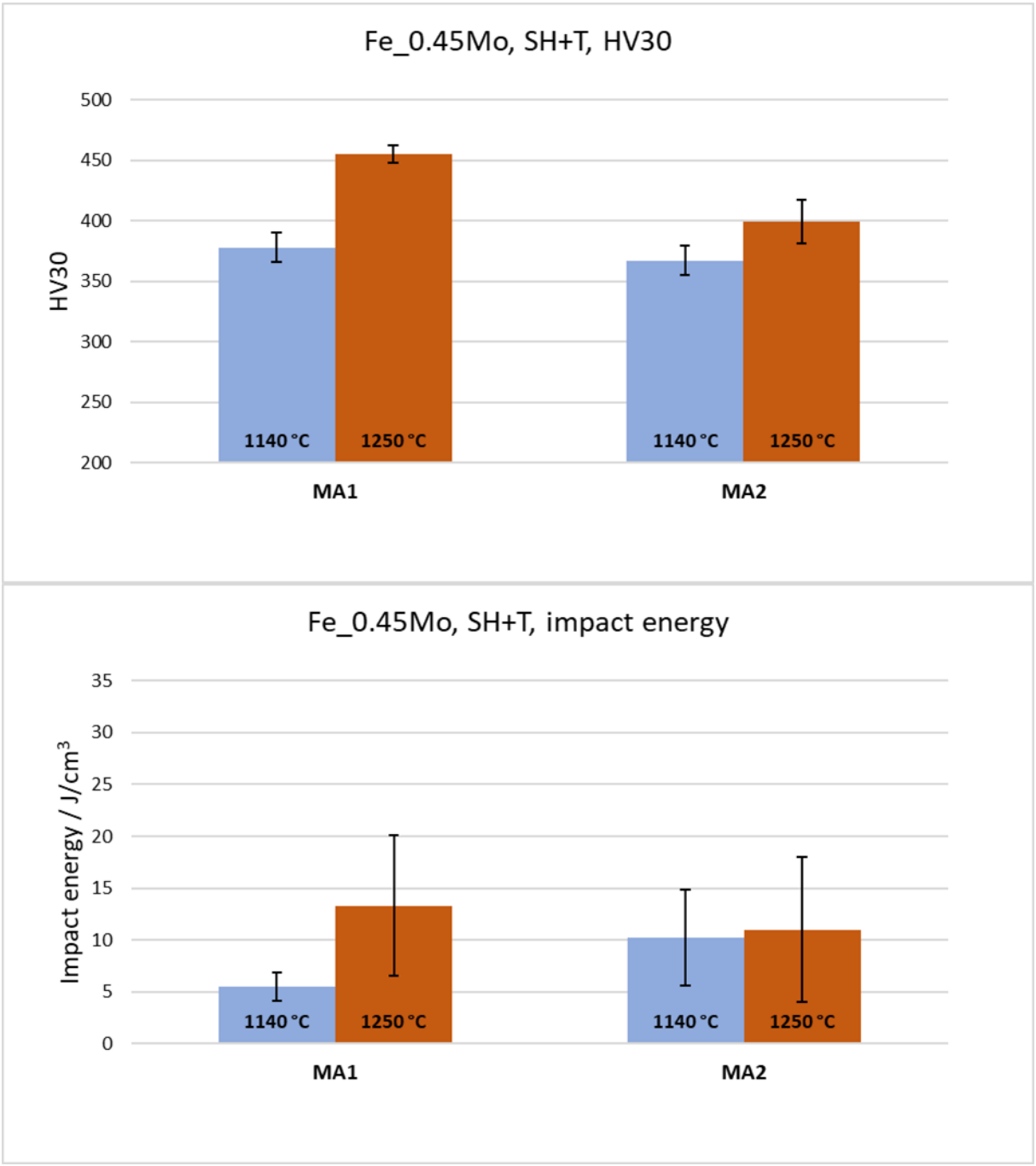

Figure 50: Mechanical properties of the samples with Fe_0.45Mo

4.3.3 SEM

A representative sample with MA2 sintered at 1140 °C was examined by SEM. To see the inhomogeneities as good as possible BSE scans were made of the sample. EDX point analysis was conducted to verify the compositions of the occurring regions. Figure 51 shows the occurring phases, which are the same as in the Mo-admixed samples (see 4.2.3), except for the Mo_2C particles. There were undissolved MA2 particles (~5 wt% Si) in the pores, a light Mn-rich (~1,5-2 wt%) ferrous and a dark Mn-poor (~0,2-0,3 wt%) ferrous phase. There are 2 different kinds of porosity: coarse pores which are also visible in the microscopic pictures of the etched samples and a very fine pores which mainly occur in the dark Mn-poor phase. This fine porosity also slightly occurred in the Mo-admixed samples, see Figure 42 and Figure 44,

but in this sample there was significantly more of it. The very fine pores seem to occur on the grain boundaries as they connect to a grain boundary like structure. An EDX point analysis showed enrichment in Si and O, which could indicate the formation of Si-rich oxides inside the pores. The formation of those oxides is problematic and might be further enhanced by the presence of Mn [48]. The occurrence of a signific amount of those structures in this samples might be an explanation for the low impact energies as they would act as a predetermined breaking point in the material.

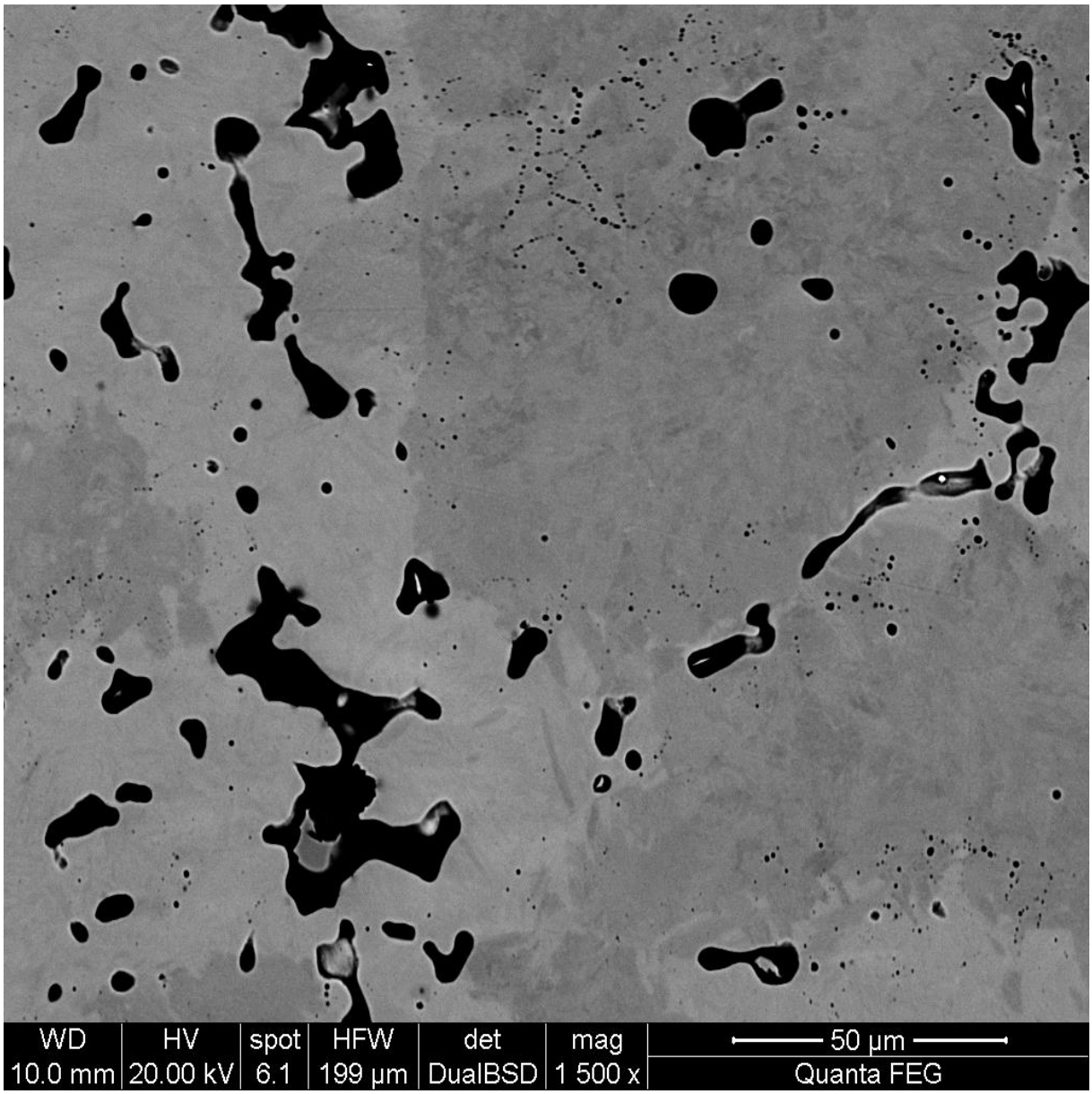

Figure 51: SEM picture in BSE-mode of a polished Mo-pre-alloyed sample with MA2 sintered at 1140 °C, sinter hardened and tempered

To further understand the fracturing mechanism, the fracture surfaces of a Mo-pre-alloyed sample with MA1, sintered at 1140 °C was examined via SEM. This sample was chosen because it showed an extremely low impact energy of 5,4 J/cm^2. As a comparison the fracture surface of a Mo-admixed sample sintered and treated in the same conditions was also examined. The Mo-pre-alloyed sample in Figure 52 showed intergranular decohesion surfaces, which is a

clear indicator for a brittle fracture due to poor connections between grains. Also isolated spherical particles were found in the fracture points which could be oxides.

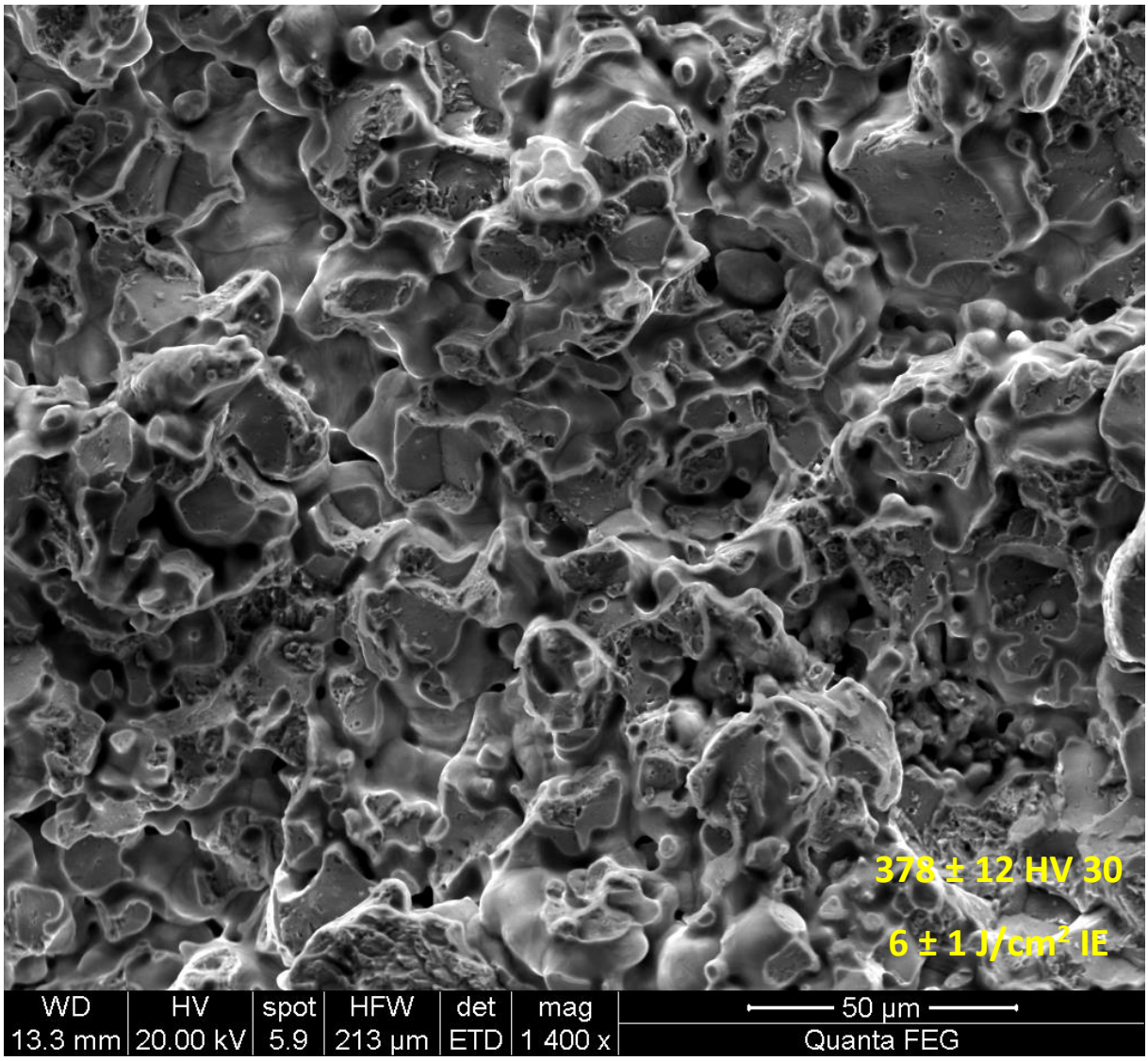

Figure 52: SEM picture of the fracture surface of an Mo-pre-alloyed sample with MA1, sintered at 1140 °C, sinter hardened and tempered

The fracture surface of the Mo-admixed sample for comparison is shown in Figure 53, which shows a transcrystalline fracture surface.

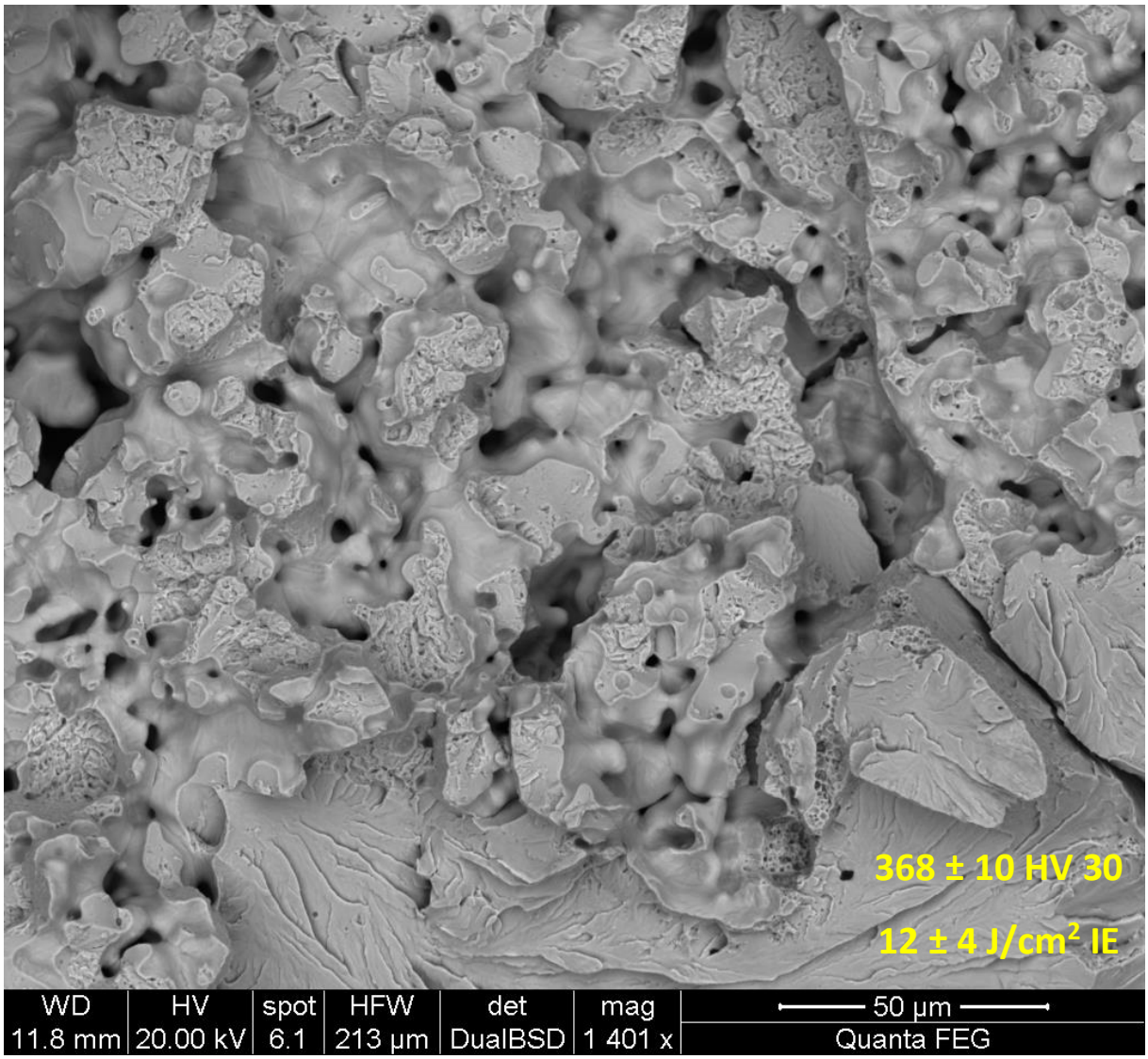

Figure 53: SEM picture of the fracture surface of an Mo-admixed sample with MA1, sintered at 1140 °C, sinter hardened and tempered

The brittle fracture surface and the fine porosity containing Si oxides of the Mo-pre-alloyed samples are in accordance with their inferior impact energies. As to why oxidation occurred in those samples is not clear. The O content of the Fe_0.45Mo powder is 0,08 wt% according to the supplier. This was examined via hot gas extraction O measurement. The measured O content was slightly higher with **0,11 wt%**. This is not an explanation for the inferior impact energies as the base powder for the pre-pressed samples, Fe_0.85Cr_0.15Mo had a significantly higher O content of **0,24 wt%** and those samples had comparably better impact energies. The most probably explanation for the oxidisation of the samples is a leakage during the sintering process and therefore contact with O from the atmosphere.

4.4 Comparison of samples

In Table 16 the mechanical properties (sintered density, impact energy and HV 30) for all Mo-alloyed samples produced/analysed in this work are compared. Also reference values from samples produced with the same MA´s and Fe_0.85Mo as base powder, which were sintered at 1140 °C, were added [89].

The sinter hardened and tempered samples had the best combination of mechanical properties, which was expectable due to the better homogenization of alloying elements. Microstructure examinations showed that the higher the sintering temperature is, the more homogeneous the resulting samples are. Sinter hardening and tempering further enhances homogenization additional to the formation of hard martensite.

The samples with MA2 tended to show higher impact energies than the equivalent samples with MA1. The samples with MA1 seem to lead to higher hardness values although the trend is not as definite as with the impact energies. This seems odd as MA2 has a higher alloying content and therefore should lead to better hardenability and produce samples that are less ductile. In the Mo-admixed and Mo-pre-alloyed samples this can be traced to the difference in C content as discussed in 4.2.1 and 4.3.1, but for the other sample series the C content should be identical. The most probable explanation is the significantly higher O content of MA2 compared to MA1. The more O the “internal getter” alloying elements (Si, Mn) have available, the more of them are oxidised and are no longer available to contribute to the mechanical properties of the steel. As already discussed in 4.1.1 the base powder has a strong influence on the distribution of alloying elements. Also, the O content of the base powder is crucial due to the “internal getter effect” of Mn and Si in the MA´s. One of the biggest influences on the mechanical properties of PM steels in combination with low melting MA´s seems to be C content.

The direct comparison of the pre-pressed samples, where the Mo was pre-alloyed and the Mo-admixed samples show, that the admixed samples have comparable mechanical properties., especially in the sinter hardened and tempered samples. The marginally better mechanical properties could be due to the slight differences in density, the C content and/or the higher Mo content. The samples with Fe_0.45Mo show high hardness values, even outperforming the Mo-admixed samples despite their lower Mo-content. The impact energy values are inferior to all other samples due to grain boundary oxide formation and resulting brittle fracture.

The reference samples with Fe_0.85Mo outperformed the equivalent pre-pressed samples in hardness. As to why those samples were much harder is suspect to speculation. Since the samples are very sensitive to O contact this is probably the biggest source of error for those sample. Also, the exact loading weight of the sintering boats during sintering and sinter hardening is not known. The weight load of samples during those treatments is extremely crucial for the heating rate of the samples and therefore the resulting mechanical properties.

Table 16: Comparison of the mechanical properties of Mo-alloyed samples

		Fe_0.85Mo (0,82 wt% Mo)			Fe + Mo_2C (0,5 wt% Mo)			Fe_0.45Mo (0,43 wt% Mo)			Fe_0.85Mo Reference (0,82 wt% Mo)	
		As sintered										
		Sintered density / g/cm³	Impact energy / J/cm²	HV 30	Sintered density / g/cm³	Impact energy / J/cm²	HV 30	Sintered density / g/cm³	Impact energy / J/cm²	HV 30	Impact energy / J/cm²	HV 30
1140 °C	MA1				7,01 ± 0,02	**11** ± 3	**263** ± 9				**14,0** ± 1,7	**319** ± 9
	MA2				6,96 ± 0,06	**15** ± 2	**268** ± 15				**14,6** ± 1,1	**340** ± 16
1180 °C	MA1				6,94 ± 0,04	**18** ± 2	**270** ± 3					
	MA2				6,97 ± 0,03	**18** ± 2	**254** ± 5					
1250 °C	MA1	7,04 ± 0,02	**23** ± 1	**262** ± 31	6,99 ± 0,01	**18** ± 3	**271** ± 10					
	MA2	7,01 ± 0,02	**24** ± 1	**304** ± 25	7,00 ± 0,03	**17** ± 2	**250** ± 25					
		Sinter hardened										
		Sintered density / g/cm³	Impact energy / J/cm²	HV 30	Sintered density / g/cm³	Impact energy / J/cm²	HV 30	Sintered density / g/cm³	Impact energy / J/cm²	HV 30	Impact energy / J/cm²	HV 30
1140 °C	MA1											**539** ± 12
	MA2											**529** ± 13
1180 °C	MA1											
	MA2											
1250 °C	MA1	7,01 ± 0,01	**22** ± 6	**458** ± 12								
	MA2	7,01 ± 0,01	**23** ± 6	**441** ± 21								
		Sinter hardened + tempered										
		Sintered density / g/cm³	Impact energy / J/cm²	HV 30	Sintered density / g/cm³	Impact energy / J/cm²	HV 30	Sintered density / g/cm³	Impact energy / J/cm²	HV 30	Impact energy / J/cm²	HV 30
1140 °C	MA1	7,05 ± 0,00	**17** ± 4	**417** ± 12	7,01 ± 0,03	**12** ± 4	**368** ± 10	7,03 ± 0,05	**7** ± 3	**378** ± 12		**528** ± 10
	MA2	7,00 ± 0,02	**24** ± 3	**433** ± 4	7,00 ± 0,02	**18** ± 5	**336** ± 4	7,02 ± 0,02	**8** ± 4	**367** ± 12		**492** ± 3
1180 °C	MA1				7,01 ± 0,02	**17** ± 3	**393** ± 7					
	MA2				7,02 ± 0,02	**16** ± 2	**343** ± 9					
1250 °C	MA1	7,02 ± 0,05	**15** ± 5	**405** ± 7	6,99 ± 0,05	**12** ± 1	**443** ± 14	7,01 ± 0,05	**11** ± 6	**455** ± 7		
	MA2	7,02 ± 0,02	**26** ± 6	**424** ± 21	6,93 ± 0,01	**20** ± 6	**361** ± 40	7,00 ± 0,03	**10** ± 5	**399** ± 18		

5 Conclusion and outlook

In this work different Mo-alloyed PM steel samples were produced and sintered. Also, for comparison Cr-pre-alloyed samples were sintered. All samples were produced with a ferrous base powder (pre-alloyed/unalloyed) and two different Mn-Si-MA´s. The main objective was to investigate the possibility of introducing Mo as Mo_2C into a PM steel system with low melting Mn-Si-MA´s.

Pre-pressed samples pre-alloyed with 0,82 wt% Mo and Cr were dewaxed, sintered at different temperatures, sinter hardened and tempered. It was shown that the hardness of the samples could significantly be improved with sinter hardening and the loss in impact energy could be compensated for by tempering without significant loss in hardness. The samples sintered at the higher temperature (1250 °C) showed significantly superior mechanical properties and more homogeneous microstructures than the samples sintered at 1140 °C. The samples pre-alloyed with Mo showed a better combination of mechanical properties than the samples pre-alloyed with Cr. There was no distinct difference between the two different MA´s in the resulting mechanical properties. In samples sintered at 1140 °C undissolved MA particles were found.

Admixing 0,5 wt% Mo as Mo_2C combined with the same MA´s as in the pre-pressed samples and a ferrous base powder produced steel samples that almost matched the properties of the samples that were pre-alloyed with 0,82 wt% Mo. Samples sintered at higher temperatures showed better mechanical properties and more homogeneous microstructures. Sintering temperatures of 1140 and 1180 °C were not sufficient to completely dissolve all components. This was probably further enhanced by the presence of different/higher C contents. In a sample sintered at 1140 °C undissolved MA and Mo_2C particles could be detected via SEM/EDX analysis. Via SEM/EDX analysis it was shown that in the samples sintered at 1250 °C the alloying elements were significantly better distributed than in samples sintered at lower temperatures. The MA with a lower alloying content led to harder samples and the MA with a higher alloying content led to samples with a higher impact energy. This is generally surprising and is most probably attributed to a difference in the C content of both sample mixtures. This is supported by the fact that there was no significant difference in the prepressed samples between the two MA´s, where the C content was identical.

Generally, it can be concluded that the introduction of Mo as Mo_2C was successful. The produced samples showed mechanical properties after sinter hardening and tempering that were comparable to the equivalently sintered and treated samples where the Mo was pre-alloyed. The differences in hardness can most likely be contributed to the more difficult distribution of alloying elements in the Mo-admixed samples. To fairly compare the hardness of all samples the C contents should be measured.

Samples with a pre-alloyed base powder with 0,45 wt% Mo showed promising hardness values after sinter hardening and tempering, but due to grain boundary oxide formation the samples were extremely brittle and therefore not acceptable. As to why those oxides formed is subject to speculation. The most probable explanation is a contamination with O from the atmosphere during sintering or a difference in cooling rates during sinter hardening.

The microstructures and mechanical properties of all investigated samples suggest that only sintering temperatures of 1250 °C led to the complete dissolution of all components in the system and a sufficient homogenization of alloying elements. Dimensional changes in the Mo-admixed samples also suggested a slight densification at 1250 °C compared to 1140 and 1180 °C. Sinter hardening and tempering not only significantly improved the mechanical properties of the investigated samples by martensite formation, but also furthered the homogenization of alloying elements.

For future studies the production of mixtures with different Mo contents admixed would be interesting. As admixing leads to high flexibility, the threshold of Mo content leading to acceptable mechanical properties could be determined by varying the Mo_2C content. To find an optimal C content the effect of the C content should also be studies as the Mo-admixed and Mo-pre-alloyed samples suggest that there is quite a big influence on the mechanical properties. To get a clearer understanding of the MA´s Mo-admixed samples with the exact same C content after sintering could be produced and investigated. Even though the comparison of the pre-pressed samples suggests that there is no substantial difference between the two investigated MA´s. A repetition of the samples with Fe_0.45Mo could be interesting as it seems very unlikely, that the unacceptable mechanical properties are due to the alloying content. The samples are virtually the same in composition compared to the Mo-admixed samples, only the Mo-content is slightly lower (0,43 wt% pre-alloyed and 0,5 wt% admixed). A repetition of those samples with more caution regarding the sintering and sinter hardening process could possibly clarify the obtained results.

6 List of abbreviations

AS	As sintered
BSE	Back-scattered electron
EBS	Ethylene distearylamide
EDX	Energy dispersive X-ray spectroscopy
GD	Green density
HV	Vicker´s hardness
HWC	Hoechst Wachs C
IE	Impact energy
LPS	Liquid phase sintering
MA	Master alloy
MCM	Mo-Cr-Mn
MVM	Mo-V-Mn
PM	Powder metallurgy
SEM	Scanning electron microscope
SH	Sinter hardened
SH+T	Sinter hardened and tempered
UHPWA	Ultra high pressure water atomisation

7 List of figures

8 List of tables

9 References

[1] G. Zapf and K. Dalal, *Introduction of high oxygen affinity elements manganese, chromium, and vanadium in the powder metallurgy of P/M parts*, vol. 10. United States: Metal Powder Industries Federation, 1977.

[2] G. Schlieper and F. Thümmler, 'High strength heat-treatable sintered steels containing manganese, chromium, vanadium and molybdenum', *Powder Metall. Int.*, vol. 11, pp. 172–176, 1979.

[3] P. Beiss, 'Alloy cost optimization of high strength Mn-Cr-Mo steels with kerosene-atomized master alloy', *Adv. Powder Metall. Part. Mater.*, vol. 1(7), pp. 12–20, 2006.

[4] R. De Oro Calderón, E. Bernardo, M. Campos, C. Gierl-Mayer, H. Danninger, and J. M. Torralba, 'Tailoring master alloys for liquid phase sintering: Effect of introducing oxidation-sensitive elements', *Powder Metall.*, vol. 59, no. 1, pp. 31–40, Jan. 2016, doi: 10.1080/00325899.2016.1148897.

[5] S. Banerjee, V. Gemenetzis, and F. Thümmler, 'Liquid Phase Formation During Sintering of Low-Alloy Steels with Carbide-Base Master Alloy Additions', *Powder Metall.*, vol. 23, no. 3, pp. 126–129, Jan. 1980, doi: 10.1179/pom.1980.23.3.126.

[6] M. Campos, J. M. Torralba, R. D. Oro, E. Bernardo, and A. Galán-Salazar, 'New Opportunities for Low Alloy Steels—Master Alloys for Liquid Phase Sintering', *Metals*, vol. 11, no. 1, p. 176, Jan. 2021, doi: 10.3390/met11010176.

[7] H. F. Fischmeister and L.-E. Larsson, 'Fast Diffusion Alloying for Powder Forging using a Liquid-Phase', *Powder Metall.*, vol. 17, no. 33, pp. 227–240, Mar. 1974, doi: 10.1179/pom.1974.17.33.015.

[8] S. Mocarski, D. W. Hall, R. A. Chernenkoff, D. A. Yeager, and C. O. McHugh, 'Master Alloys to Obtain Premixed Hardenable Powder Metallurgy Steels', *Powder Metall.*, vol. 39, no. 2, pp. 130–137, Jan. 1996, doi: 10.1179/pom.1996.39.2.130.

[9] A. N. Klein, R. Oberacker, and F. Thummler, 'Development of New High Strength Si–Mn-Alloyed Sintered Steels', *Mod. Dev. Powder Metall.*, vol. 16, pp. 141–152, 1984.

[10] C. Tojal, T. Gómez-Acebo, and F. Castro, 'Development of PM Stainless Steels with Improved Properties through Liquid Phase Sintering', *Mater. Sci. Forum*, vol. 534–536, pp. 661–664, Jan. 2007, doi: 10.4028/www.scientific.net/MSF.534-536.661.

[11] F. Castro, M. Sarasola, S. Sainz, and T. Gómez-Acebo, 'Processing Routes for Obtaining Novel High Performance Mn-Containing PM Steels', *Mater. Sci. Forum*, vol. 534–536, pp. 705–708, Jan. 2007, doi: 10.4028/www.scientific.net/MSF.534-536.705.

[12] R. Oro, M. Campos, J. M. Torralba, and C. Capdevila, 'Lean alloys in PM: From design to sintering performance', *Powder Metall.*, vol. 55, no. 4, pp. 294–301, Sep. 2012, doi: 10.1179/1743290112Y.0000000016.

[13] 'Copper PRICE Today | Copper Spot Price Chart | Live Price of Copper per Ounce | Markets Insider', markets.businessinsider.com. Accessed: Jun. 13, 2024. [Online]. Available: https://markets.businessinsider.com/commodities/copper-price

[14] 'Nickel PRICE Today | Nickel Spot Price Chart | Live Price of Nickel per Ounce | Markets Insider', markets.businessinsider.com. Accessed: Jun. 13, 2024. [Online]. Available: https://markets.businessinsider.com/commodities/nickel-price

[15] K. E. Daehn, A. Cabrera Serrenho, and J. M. Allwood, 'How Will Copper Contamination Constrain Future Global Steel Recycling?', *Environ. Sci. Technol.*, vol. 51, no. 11, pp. 6599–6606, Jun. 2017, doi: 10.1021/acs.est.7b00997.

[16] E. Forti *et al.*, 'In vitro evaluation of the toxicity induced by nickel soluble and particulate forms in human airway epithelial cells', *Toxicol. In Vitro*, vol. 25, no. 2, pp. 454–461, Mar. 2011, doi: 10.1016/j.tiv.2010.11.013.
[17] *Council Regulation (EC) No 428/2009 of 5 May 2009 setting up a Community regime for the control of exports, transfer, brokering and transit of dual-use items (recast)*, vol. 134. 2009. Accessed: Jun. 13, 2024. [Online]. Available: http://data.europa.eu/eli/reg/2009/428/oj/eng
[18] 'The Role of Critical Minerals in Clean Energy Transitions – Analysis', IEA. Accessed: Jun. 13, 2024. [Online]. Available: https://www.iea.org/reports/the-role-of-critical-minerals-in-clean-energy-transitions
[19] S. Papavinasam, *Corrosion control in the oil and gas industry*. Amsterdam: Elsevier/Gulf Professional, 2014.
[20] 'Molybdenum - Price - Chart - Historical Data - News', Trading Economics. Accessed: Jun. 13, 2024. [Online]. Available: https://tradingeconomics.com/commodity/molybden
[21] *Handbook of Chemistry and Physics*, 67th ed. Boca Raton FL: CRC Press, 1987.
[22] H. Danninger, 'Sintering of Mo alloyed P/M structural steels', *Powder Metall. Int.*, vol. 20, no. 1, pp. 7–11, 1988.
[23] 'ISO 3252:1999(en), Powder metallurgy — Vocabulary'. Accessed: Jun. 10, 2024. [Online]. Available: https://www.iso.org/obp/ui#iso:std:iso:3252:ed-4:v1:en
[24] H. Danninger, R. de Oro Calderon, and C. Gierl-Mayer, 'Powder Metallurgy and Sintered Materials', in *Ullmann's Encyclopedia of Industrial Chemistry*, John Wiley & Sons, Ltd, 2017, pp. 1–57. doi: 10.1002/14356007.a22_105.pub2.
[25] V. Sundaram, 'Novel approaches for achieving full density powder metallurgy steels'.
[26] I. Chang and Y. Zhao, Eds., *Advances in powder metallurgy: properties, processing and applications*. in Woodhead publishing series in metals and surface engineering, no. number 60. Oxford: Woodhead Publishing, 2013.
[27] J. J. Dunkley, 'Metal Powder Atomisation Methods for Modern Manufacturing: Advantages, limitations and new applications for high value powder manufacturing techniques', *Johns. Matthey Technol. Rev.*, vol. 63, no. 3, pp. 226–232, Jul. 2019, doi: 10.1595/205651319X15583434137356.
[28] E. A. Olevsky, 'Theory of sintering: from discrete to continuum', *Mater. Sci. Eng. R Rep.*, vol. 23, no. 2, pp. 41–100, Jun. 1998, doi: 10.1016/S0927-796X(98)00009-6.
[29] H. Danninger, 'Homogenization and Pore Formation during Sintering with Transient Liquid Phase', *Powder Metall. Int.*, vol. 20, no. 1, pp. 20–25, 1988.
[30] R. de Oro Calderon, C. Gierl-Mayer, and H. Danninger, 'Fundamentals of sintering: liquid phase sintering', *Encycl. Mater. Met. Alloys*, vol. 3, pp. 481–492, 2022.
[31] M. Vattur Sundaram *et al.*, 'Enhanced Densification of PM Steels by Liquid Phase Sintering with Boron-Containing Master Alloy', *Metall. Mater. Trans. A*, vol. 49, no. 1, pp. 255–263, Jan. 2018, doi: 10.1007/s11661-017-4383-4.
[32] A. Standards, 'ÖNORM EN 10020:2000 06 01'. Accessed: Jun. 10, 2024. [Online]. Available: https://www.austrian-standards.at/de/shop/onorm-en-10020-2000-06-01~p1327404
[33] G. Krauss, *Steels: heat treatment and processing principles*, 2. print. Materials Park, Ohio: ASM international, 1993.
[34] 'Iron-Carbon Phase Diagram Explained [with Graphs]', Fractory. Accessed: Jun. 19, 2024. [Online]. Available: http://https%253A%252F%252Ffractory.com%252Firon-carbon-phase-diagram%252F

[35] H. K. D. H. Bhadeshia, 'Interpretation of the microstructure of of steels', University of Cambridge. Accessed: Jun. 20, 2024. [Online]. Available: https://www.phase-trans.msm.cam.ac.uk/2008/Steel_Microstructure/SM.html
[36] E. Protopopov, S. Dobrykh, Y. Trofimova, P. Malenko, A. Valter, and A. Protopopov, 'Reflection of strengthening results in values of generalized degrees of metallicity and covalence is principle to new strategy of designing alloys', *Sci. Rep.*, vol. 10, Feb. 2020, doi: 10.1038/s41598-020-58560-z.
[37] X. Wang, H. Zurob, G. Xu, Q. Ye, O. Bouaziz, and D. Embury, 'Influence of Microstructural Length Scale on the Strength and Annealing Behavior of Pearlite, Bainite, and Martensite', *Metall. Mater. Trans. A*, vol. 44, p. 1454, Mar. 2013, doi: 10.1007/s11661-012-1501-1.
[38] M. Maalekian, 'The Effects of Alloying Elements on Steels (I)', *Tech. Univ. Graz*, pp. 17–21, Oct. 2007.
[39] B. Lindsley, C. Schade, and T. Murphy, 'Vanadium and Silicon Alloyed PM Steels', *Hoeganaes Corp.*.
[40] J. R. Davis, *Alloying: understanding the basics*. Ohio: ASM International, 2001.
[41] ASM International, Ed., *ASM handbook*, 10th edition., vol. 3. Materials Park, Ohio: ASM International, 1990.
[42] H. Danninger, G. Frauendienst, K.-D. Streb, and R. Ratzi, 'Dissolution of different graphite grades during sintering of PM steels', *Mater. Chem. Phys.*, vol. 67, no. 1–3, pp. 72–77, Jan. 2001, doi: 10.1016/S0254-0584(00)00422-3.
[43] M. Youseffi, C. S. Wright, and F. M. Jeyacheya, 'Effects of silicon addition and process conditions upon α-phase sintering, sinter hardening, and mechanical properties of Fe-1.5Mo powder', *Powder Metall.*, vol. 45, no. 1, pp. 53–62, Feb. 2002, doi: 10.1179/003258902225001524.
[44] Z. Zhang and R. Sandström, 'Fe–Mn–Si master alloy steel by powder metallurgy processing', *J. Alloys Compd.*, vol. 363, no. 1–2, pp. 199–207, Jan. 2004, doi: 10.1016/S0925-8388(03)00462-6.
[45] M. Youseffi and K. Y. Chong, 'Enhanced sintering and mechanical properties of 316L stainless steel with silicon additions as sintering aid', *Powder Metall.*, vol. 46, no. 1, pp. 30–38, Apr. 2003, doi: 10.1179/003258903225010460.
[46] B. Yang, J. He, G. Zhang, and J. Guo, Eds., *Vanadium: extraction, manufacturing and applications*. Amsterdam Oxford Cambridge, MA: Elsevier, 2021.
[47] Z. Zhang, K. Frisk, A. Salwén, and R. Sandström, 'Mechanical properties of Fe–Mo–Mn–Si–C sintered steels', *Powder Metall.*, vol. 47, no. 3, pp. 239–246, Sep. 2004, doi: 10.1179/003258904225015572.
[48] R. Oro, M. Campos, E. Hryha, J. M. Torralba, and L. Nyborg, 'Surface phenomena during the early stages of sintering in steels modified with Fe–Mn–Si–C master alloys', *Mater. Charact.*, vol. 86, pp. 80–91, Dec. 2013, doi: 10.1016/j.matchar.2013.07.022.
[49] A. Šalak and M. Selecká, *Manganese in powder metallurgy steels*. Cambridge, England: Cambridge International Science Publishing : Springer, 2012.
[50] M. Merwin, 'Low-Carbon Manganese TRIP Steels', *Mater. Sci. Forum*, vol. 539–543, pp. 4327–4332, Mar. 2007, doi: 10.4028/www.scientific.net/MSF.539-543.4327.
[51] A. Šalak and M. Selecká, 'Adverse effect of high purity atmosphere on sintering of manganese steels', *Powder Metall.*, vol. 53, no. 4, pp. 285–294, Dec. 2010, doi: 10.1179/003258910X12707304455185.

[52] A. Šalak and M. Selecká, 'Effect of Manganese Addition and Sintering Conditions on Mechanical Properties of Low Carbon 3Cr Prealloyed Steels', *Mater. Sci. Forum*, vol. 672, pp. 55–58, Jan. 2011, doi: 10.4028/www.scientific.net/MSF.672.55.
[53] C. Gierl-Mayer, R. De Oro Calderon, and H. Danninger, 'The Role of Oxygen Transfer in Sintering of Low Alloy Steel Powder Compacts: A Review of the "Internal Getter" Effect', *JOM*, vol. 68, no. 3, pp. 920–927, Mar. 2016, doi: 10.1007/s11837-016-1819-z.
[54] E. Hryha and L. Nyborg, 'Oxide Transformation in Cr-Mn-Prealloyed Sintered Steels: Thermodynamic and Kinetic Aspects', *Metall. Mater. Trans. A*, vol. 45, no. 4, pp. 1736–1747, Apr. 2014, doi: 10.1007/s11661-013-1969-3.
[55] H. Danninger, R. Pöttschacher, S. Bradac, A. Šalak, and J. Seyrkammer, 'Comparison of Mn, Cr and Mo alloyed sintered steels prepared from elemental powders', *Powder Metall.*, vol. 48, no. 1, pp. 23–32, Mar. 2005, doi: 10.1179/003258905X37567.
[56] H. Hu, G. Xu, M. Zhou, and Q. Yuan, 'Effect of Mo Content on Microstructure and Property of Low-Carbon Bainitic Steels', *Metals*, vol. 6, no. 8, p. 173, Jul. 2016, doi: 10.3390/met6080173.
[57] J. Kong and C. Xie, 'Effect of molybdenum on continuous cooling bainite transformation of low-carbon microalloyed steel', *Mater. Des.*, vol. 27, no. 10, pp. 1169–1173, Jan. 2006, doi: 10.1016/j.matdes.2005.02.006.
[58] R. Wan, F. Sun, L. Zhang, and A. Shan, 'Effects of Mo on high-temperature strength of fire-resistant steel', *Mater. Des.*, vol. 35, pp. 335–341, Mar. 2012, doi: 10.1016/j.matdes.2011.09.009.
[59] H. J. T. Ellingham, 'Reducibility of oxides and sulphides in metallurgical processes', *J. Soc. Chem. Ind.*, vol. 63, no. 5, pp. 125–160, May 1944, doi: 10.1002/jctb.5000630501.
[60] H. Danninger, D. Spoljaric, A. Arakil, and B. Weiss, 'Mo alloyed P/M structural steels prepared by different alloying techniques', *Adv. Powder Metall. Part. Mater.*, vol. 4, p. 13, 1996.
[61] T. Kasuya and N. Yurioka, 'Carbon Equivalent and Multiplying Factor for Hardenability of Steel'.
[62] S. Geroldinger, R. D. Oro Calderon, C. Gierl-Mayer, and H. Danninger, 'Sinter Hardening PM Steels Prepared through Hybrid Alloying', *HTM J. Heat Treat. Mater.*, vol. 76, no. 2, pp. 105–119, Apr. 2021, doi: 10.1515/htm-2020-0007.
[63] A. Šalak, 'Gefüge von manganlegiertem Sinterstahl. Teil 1. Basispulver Verdüsungseisen / Structure of Manganese Alloyed Sintered Steels. Part 1. Base Powder Atomised Iron', *Pract. Metallogr.*, vol. 17, no. 6, pp. 273–280, Jun. 1980, doi: 10.1515/pm-1980-170604.
[64] H. Danninger and C. Gierl, 'Processes in PM steel compacts during the initial stages of sintering', *Mater. Chem. Phys.*, vol. 67, no. 1–3, pp. 49–55, Jan. 2001, doi: 10.1016/S0254-0584(00)00419-3.
[65] H. Abdoos, H. Khorsand, and A. R. Shahani, 'Fatigue behavior of diffusion bonded powder metallurgy steel with heterogeneous microstructure', *Mater. Des.*, vol. 30, no. 4, pp. 1026–1031, Apr. 2009, doi: 10.1016/j.matdes.2008.06.050.
[66] R. Bidulsky, F. S. Gobber, J. Bidulska, M. Ceroni, T. Kvackaj, and M. A. Grande, 'Coated Metal Powders for Laser Powder Bed Fusion (L-PBF) Processing: A Review', *Metals*, vol. 11, no. 11, p. 1831, Nov. 2021, doi: 10.3390/met11111831.
[67] R. Haynes, 'A Study of the Effect of Porosity Content on the Ductility of Sintered Metals', *Powder Metall.*, vol. 20, no. 1, pp. 17–20, Jan. 1977, doi: 10.1179/pom.1977.20.1.17.
[68] R. J. Bourcier, D. A. Koss, R. E. Smelser, and O. Richmond, 'The influence of porosity on the deformation and fracture of alloys', *Acta Metall.*, vol. 34, no. 12, pp. 2443–2453, Dec. 1986, doi: 10.1016/0001-6160(86)90147-1.

[69] *Iron and steel powders for sintered components: Höganäs handbook for sintered components*. Höganäs: Höganäs AB, 2016.
[70] 'Sustainable Gears—Design of Gear Body Modified Powder Metal (PM) Gears | Gear Technology Magazine'. Accessed: Jun. 10, 2024. [Online]. Available: https://www.geartechnology.com/articles/30091-sustainable-gearsdesign-of-gear-body-modified-powder-metal-pm-gears
[71] N. A. Rawashdeh, W. Khraisat, and H. Borgström, 'Pinning Effect of Pores on Grain Growth in Sintered Steel', vol. 11, no. 2, 2017.
[72] L. Albano-Müller, F. Thümmler, and G. Zapf, 'HIGH-STRENGTH SINTERED IRON-BASE ALLOYS BY USING TRANSITION METAL CARBIDES', *Powder Metall.*, vol. 16, no. 32, pp. 236–256, Sep. 1973, doi: 10.1179/pom.1973.16.32.006.
[73] H. Danninger, R. De Oro Calderon, and C. Gierl-Mayer, 'Alloy Systems for Heat Treated Sintered Steels∗', *HTM J. Heat Treat. Mater.*, vol. 74, no. 5, pp. 282–292, Oct. 2019, doi: 10.3139/105.110394.
[74] G. Hoffmann and K. Dalal, 'Development and present situation of low alloyed PM steels using MCM and MVM master alloys', *Powder Met. Int*, vol. 11, no. 4, pp. 177–180, 1979.
[75] N. Eustathopoulos, 'Wetting by Liquid Metals—Application in Materials Processing: The Contribution of the Grenoble Group', *Metals*, vol. 5, no. 1, pp. 350–370, Mar. 2015, doi: 10.3390/met5010350.
[76] R. Oro, M. Jaliliziyaeian, J. Dunkley, C. Gierl-Mayer, and H. Danninger, 'New masteralloys for sintered high strength steels – the attractive route between mixing and prealloying', *Izv. Vuzov Poroshkovaya Metall. Funktsional'nye Pokrytiya Univ. Proc. Powder Metall. And Funct. Coat.*, no. 4, pp. 15–27, Dec. 2018, doi: 10.17073/1997-308X-2018-4-15-27.
[77] 'N,N'-Ethylen-bis(stearamid) - ChemInfo Public', ChemInfo Public. Accessed: Jun. 26, 2024. [Online]. Available: https://recherche.chemikalieninfo.de/public/stoff/7838?dv=18&sv=
[78] A. Standards, 'DIN EN ISO 5754', Austrian Standards. Accessed: Jul. 01, 2024. [Online]. Available: https://www.austrian-standards.at/de/shop/din-en-iso-5754-2023-12~p2821251
[79] M. A. Meyers and K. K. Chawla, *Mechanical behavior of materials*. Upper Saddle River, N.J: Prentice Hall, 1999.
[80] D. Y. Jeong, H. Yu, J. E. Gordon, Y. H. Tang, and John A. Volpe National Transportation Systems Center (U.S.), 'Finite element analysis of unnotched charpy impact tests', Oct. 2008. Accessed: Jul. 23, 2024. [Online]. Available: https://rosap.ntl.bts.gov/view/dot/9900
[81] W. Wagner and A. Pruß, 'The IAPWS Formulation 1995 for the Thermodynamic Properties of Ordinary Water Substance for General and Scientific Use', *J. Phys. Chem. Ref. Data*, vol. 31, no. 2, pp. 387–535, Jun. 2002, doi: 10.1063/1.1461829.
[82] T. Geyer, 'Abbildung cutting surface'.
[83] A. Standards, 'ÖNORM EN ISO 6507-1', Austrian Standards. Accessed: Jul. 01, 2024. [Online]. Available: https://www.austrian-standards.at/de/shop/onorm-en-iso-6507-1-2024-01-01~p2822515
[84] S. L. Flegler, J. W. Heckman, K. L. Klomparens, and S. L. Flegler, *Elektronenmikroskopie: Grundlagen, Methoden, Anwendungen*. Heidelberg Berlin: Spektrum, Akad. Verl, 1995.
[85] A. Šalak, M. Selecká, and R. Bureš, 'MANGANESE IN FERROUS POWDER METALLURGY', *Powder Metall. Prog.*, no. 1, 2001.
[86] E. Bernardo, R. de Oro, M. Campos, and J. M. Torralba, 'Design of Low-Melting Point Compositions Suitable for Transient Liquid Phase Sintering of PM Steels Based on a

Thermodynamic and Kinetic Study', *Metall. Mater. Trans. A*, vol. 45, no. 4, pp. 1748–1760, Apr. 2014, doi: 10.1007/s11661-013-2137-5.

[87] S. W. Geroldinger, 'The master alloy route as an attractive alloying alternative for sintered steels', Thesis, Technische Universität Wien, 2023. Accessed: Jun. 14, 2024. [Online]. Available: https://repositum.tuwien.at/handle/20.500.12708/177089

[88] Horsch A., 'Definition der Gefügebestandteile – Bainit', Arnold Horsch eK Wissensdatenbank. Accessed: Jul. 25, 2024. [Online]. Available: https://wiki.arnold-horsch.de/index.php/Definition_der_Gef%C3%BCgebestandteile

[89] S. Geroldinger *et al.*, 'Rohstoffeffiziente Sinterstähle durch Hybrid-Masteralloylegierungstechnik', 41. Hagener Symposium Pulvermetallurgie 2023, Hagen, Germany, Dec. 2023.